

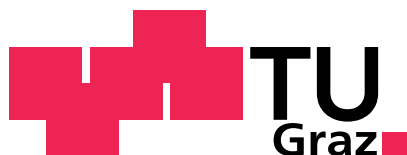
# MASTERTHESIS

## Teflon Soluble Luminophores – A Way to Outstandingly Sensitive Oxygen Sensors

*Christoph Staudinger*

---

Institute of Analytical Chemistry and Food Chemistry  
University of Technology, Graz



Supervisor: Univ.-Prof. Dipl.-Chem. Dr.rer.nat. Ingo Klimant

Graz, January 2014



---

## Abstract

In this thesis  $\text{BF}_2\text{HPhN}$  and  $\text{BF}_2\text{HBAN}$ , two luminophores with phosphorescence lifetimes of several hundred milliseconds, were modified with perfluorooctyl chains to obtain derivatives which are compatible with extremely permeable amorphous perfluorinated matrices (Hyflon® AD 60, Teflon® AF and Cytop®). Sensors made from those components promised to be extraordinarily sensitive because the sensitivity of an oxygen sensor rises with luminescence lifetime and matrix permeability. The obtained dyes ( $\text{BF}_2^-$  and Al-complexes of the modified ligands) were indeed soluble in perfluorinated polymers and retained their spectral properties and very long lifetimes.

Furthermore the produced sensors showed outstandingly high sensitivities which made a standard addition calibration necessary to account for the unavoidable background oxygen contamination. The most sensitive obtained material  $\text{Al}(\text{HBANPF})_3$  in Teflon® AF 1600 was 15 times more sensitive than any previously published oxygen sensor and reached a limit of detection of 5 ppbv under atmospheric pressure.

To demonstrate the suitability for trace measurements the ppmv-level oxygen contaminations in multiple gas bottles were measured. Furthermore a measurement of the oxygen consumption kinetics of glucose oxidase was conducted where the oxygen concentration was traced to concentrations below 1 nM.



---

## Kurzfassung

Im Zuge dieser Arbeit wurden zwei Luminophore, die außergewöhnlich langen Phosphoreszenz-Lebenszeiten im Bereich von mehreren hundert Millisekunden ( $\text{BF}_2\text{HPhN}$  und  $\text{BF}_2\text{HBAN}$ ) aufweisen, mit Perfluorooctyl-Gruppen modifiziert. Die erhaltenen Farbstoffe ( $\text{BF}_2$ - und Al-Komplexe der perfluoralylierten Liganden) waren dadurch in hochpermeablen amorphen perfluorierten Polymeren wie Hyflon® AD 60 oder Teflon® AF löslich. Weiters behielten sie ihre spektralen Eigenschaften und auch ihre Lebenszeiten änderten sich kaum.

Die Sauerstoffsensoren aus diesen Materialien waren wie erwartet extrem sensitiv. Dadurch wurde es auch nötig eine Standardadditionskalibration durchzuführen, bei der die Grundkontamination mit Sauerstoff berücksichtigt werden konnte. Der sensitivste der hergestellte Sensoren,  $\text{Al}(\text{HBANPF})_3$  in Teflon® AF 1600, war 15 mal empfindlicher als der Beste bisher publizierte Spuren-Sauerstoffsensoren und hatte eine Nachweisgrenze von nur 5 ppbv.

Die Eignung der neuen Sensoren zur Messung kleinster Sauerstoffspuren wurde durch Messungen des Sauerstoffgehalts in mehreren Gasflaschen unter Beweis gestellt. Weiters wurde die Kinetik des Sauerstoffverbrauchs von Glukoseoxidase bis unter 1 nM verfolgt.



---

## Statutory Declaration

I declare that I have authored this thesis independently, that I have not used other than the declared sources / resources, and that I have explicitly marked all material which has been quoted either literally or by content from the used sources.

27. January, 2014

Date



Signature



---

## Danksagung

Zuerst möchte ich mich bei Professor Ingo Klimant bedanken, der diese Arbeit erst möglich gemacht hat und mir jederzeit eine große Unterstützung war.

Weiters möchte ich mich bei Sergey Borisov und Philipp Lehner bedanken, die mir während der gesamten Masterarbeit mit ihren Ideen und ihrer Erfahrung zur Seite standen. Ohne ihre Hilfe wäre diese Arbeit nicht möglich gewesen.

Auch bei der gesamten Arbeitsgruppe möchte ich mich für das unglaublich angenehme und freundschaftliche Arbeitsklima bedanken.

Bei meiner Familie möchte ich mich für den Rückhalt während des gesamten Studiums bedanken und natürlich auch für die finanzielle Unterstützung während dieser Zeit.

Zu guter Letzt möchte ich mich bei Birgit bedanken. Dank dir konnte ich eine unglaublich schöne Studienzeit erleben. Wir sind viel gemeinsam gereist und haben viel gesehen und erlebt.

Christoph Staudinger

Graz, January 2014



---

# Contents

<b>1</b>	<b>Introduction</b>	<b>1</b>
<b>2</b>	<b>Theoretical Background</b>	<b>3</b>
2.1	Fundamentals of Luminescence . . . . .	3
2.1.1	Absorption . . . . .	4
2.1.2	Internal Conversion . . . . .	4
2.1.3	Fluorescence . . . . .	5
2.1.4	Intersystem Crossing . . . . .	5
2.1.5	Phosphorescence . . . . .	5
2.1.6	Reverse Intersystem Crossing . . . . .	6
2.1.7	Delayed Fluorescence . . . . .	6
2.1.8	Lifetimes . . . . .	6
2.1.9	Quantum Yields . . . . .	6
2.1.10	Quenching by Oxygen . . . . .	7
2.1.11	Stern-Volmer Kinetics . . . . .	7
2.1.12	Two-Site Model . . . . .	8
2.2	Optical Oxygen Sensors . . . . .	8
2.2.1	Advantages of Optical Oxygen Sensors . . . . .	9
2.2.2	Applications of Optical Oxygen Sensors . . . . .	9
2.3	Tuning the Sensitivity . . . . .	10
2.3.1	Luminescence Lifetime . . . . .	10
2.3.2	Matrix Permeability . . . . .	10
2.4	State of the Art Trace Oxygen Sensors . . . . .	11
2.5	Achieving Maximum Sensitivity . . . . .	12
2.5.1	Amorphous Perfluorinated Polymers . . . . .	12
2.5.2	BF <sub>2</sub> -Chelates of $\beta$ -diketonates . . . . .	13
2.6	Perfluoroalkylation . . . . .	16
<b>3</b>	<b>Experimental</b>	<b>17</b>
3.1	Methods . . . . .	17
3.1.1	Sensor Preparation . . . . .	17

---

3.1.2	Chemical Dye Characterisation . . . . .	17
3.1.3	Optical Dye Characterisation . . . . .	17
3.1.4	Lifetime Measurements . . . . .	18
3.1.5	Calibration . . . . .	19
3.1.6	Glucose Oxidase Measurement . . . . .	19
3.1.7	Trace measurements in gasses . . . . .	19
3.1.8	Model . . . . .	20
3.2	Materials . . . . .	21
3.3	Synthesis . . . . .	24
3.3.1	Synthesis of HPhNPF . . . . .	24
3.3.2	Synthesis of HBANPF . . . . .	24
3.3.3	Synthesis of BF <sub>2</sub> HPhNPF . . . . .	24
3.3.4	Synthesis of BF <sub>2</sub> HBANPF . . . . .	25
3.3.5	Synthesis of Al(HPhNPF) <sub>3</sub> . . . . .	25
3.3.6	Synthesis of Al(HBANPF) <sub>3</sub> . . . . .	25
3.4	Sensor Preparation . . . . .	26
3.4.1	Preparation of the Stock Solutions . . . . .	26
3.4.2	Preparation of Glass Slides . . . . .	26
3.4.3	Preparation of the Sensor “Cocktails” . . . . .	26
3.4.4	Coating . . . . .	26
3.5	Optical Characterization . . . . .	27
3.5.1	Absorption Spectra . . . . .	27
3.5.2	Emission Spectra . . . . .	27
3.5.3	Excitation Spectra . . . . .	27
3.5.4	Luminescence Quantum Yields at Air Saturation . . . . .	28
3.5.5	Anoxic Quantum Yields . . . . .	29
3.5.6	Measurement of the Photochemical Stabilities . . . . .	30
3.5.7	Measurement of the Luminescence Intensity Dependency on Excitation Light . . . . .	31
3.6	Lifetime Measurements with FluoroLog Kinetic Acquisition . . . . .	31
3.6.1	Anoxic Lifetimes . . . . .	32
3.6.2	Anoxic Lifetime Intensity Dependency . . . . .	32
3.6.3	Lifetimes Intensity Dependency at Trace Oxygen Levels . . . . .	32
3.7	Lifetime Measurements with Single Photon Counting . . . . .	34
3.8	Calibration by controlled oxygen consumption of Sodium Ascorbate . . . . .	35
3.9	Intensity Calibrations . . . . .	35
3.9.1	Calibrations of BF <sub>2</sub> HPhN in Polystyrene . . . . .	35
3.9.2	Calibrations of BF <sub>2</sub> HBAN in Polystyrene . . . . .	36

3.9.3	Calibrations of Al(HPhNPF) <sub>3</sub> in Teflon® AF 1600 . . . . .	36
3.9.4	Calibrations of Al(HPhNPF) <sub>3</sub> in Hyflon® AD 60 . . . . .	37
3.9.5	Calibration of Al(HPhNPF) <sub>3</sub> in Hyflon® AD 60 at 5°C and 35°C . . . . .	37
3.9.6	Calibration of Al(HPhNPF) <sub>3</sub> in Hyflon® AD 60 with Higher and Lower Intensities . . . . .	37
3.9.7	Calibrations of Al(HBANPF) <sub>3</sub> in Teflon® AF 1600 . . . . .	38
3.9.8	Calibrations of Al(HBANPF) <sub>3</sub> in Hyflon AD 60 . . . . .	38
3.9.9	Calibrations of Al(HPhNPF) <sub>3</sub> in Cytotop® CTL-809A . . . . .	38
3.9.10	Calibration of Al(HBANPF) <sub>3</sub> in Cytotop® CTL-107MK . . . . .	39
3.10	Lifetime Calibration of Al(HPhNPF) <sub>3</sub> in Hyflon® AD 60 . . . . .	39
3.11	Measurement of Oxygen Traces in Gases . . . . .	40
3.12	Monitoring of Oxygen consumption by Glucose Oxidase with four Sensors . . . . .	40
<b>4</b>	<b>Results and Discussion</b>	<b>43</b>
4.1	Synthesis . . . . .	43
4.1.1	Perfluoroalkylation of HPhN and HBAN . . . . .	43
4.1.2	Synthesis of BF <sub>2</sub> HPhNPF . . . . .	44
4.1.3	Synthesis of BF <sub>2</sub> HBANPF . . . . .	45
4.1.4	Synthesis of the Aluminium-Complexes . . . . .	46
4.1.5	Conclusion . . . . .	48
4.2	Modeling of Non-Linearity Effects . . . . .	49
4.2.1	Triplet Oxygen Depletion . . . . .	49
4.2.2	Chemical Oxygen Consumption . . . . .	51
4.2.3	Triplet-Triplet Annihilation . . . . .	52
4.2.4	Dye Ground State Depletion . . . . .	52
4.2.5	Conclusion . . . . .	53
4.3	Sensor Preparation . . . . .	54
4.4	Photophysical Properties . . . . .	54
4.4.1	Absorption Spectra . . . . .	54
4.4.2	Emission and Excitation Spectra . . . . .	57
4.4.3	Quantum Yields . . . . .	61
4.4.4	Photochemical Stability . . . . .	62
4.4.5	Intensity Dependency of the Luminescence . . . . .	64
4.4.6	Conclusion . . . . .	67
4.5	Lifetime Measurements . . . . .	67
4.5.1	Anoxic Lifetimes . . . . .	67
4.5.2	Anoxic Lifetimes Intensity Dependency . . . . .	69
4.5.3	Lifetimes Intensity Dependency with Oxygen Traces . . . . .	72

4.5.4	TCSPC Lifetimes . . . . .	73
4.5.5	Conclusion . . . . .	75
4.6	Calibration by Controlled Oxygen Consumption of Sodium Ascorbate . . . . .	75
4.7	Calibrations . . . . .	77
4.7.1	BF <sub>2</sub> HPhN and BF <sub>2</sub> HBAN in Polystyrene . . . . .	78
4.7.2	Al(HPhNPF) <sub>3</sub> and Al(HBANPF) <sub>3</sub> in Perfluorinated Matrices . . . . .	79
4.7.3	Temperature Dependency of Al(HPhNPF) <sub>3</sub> in Hyflon® AD 60 . . . . .	81
4.7.4	Intensity Dependency of Al(HPhNPF) <sub>3</sub> in Hyflon® AD 60 . . . . .	82
4.7.5	Calibration Attempt of Al(HBANPF) <sub>3</sub> in Cytosol® CTL-107MK . . . . .	83
4.7.6	Lifetime Calibration of Al(HPhNPF) <sub>3</sub> in Hyflon® AD 60 . . . . .	84
4.7.7	Conclusion . . . . .	85
4.8	Measurement of Oxygen Traces in Gases . . . . .	85
4.9	Monitoring of Oxygen consumption by Glucose Oxidase . . . . .	86
<b>5</b>	<b>Conclusion and Outlook</b>	<b>89</b>
5.1	Outlook . . . . .	89
<b>6</b>	<b>References</b>	<b>91</b>
<b>7</b>	<b>List of Figures</b>	<b>97</b>
<b>8</b>	<b>List of Tables</b>	<b>100</b>
<b>9</b>	<b>Appendix</b>	<b>103</b>
9.1	NMR and Mass Spectra . . . . .	103
9.1.1	HPhNPF . . . . .	103
9.1.2	HBANPF . . . . .	105
9.1.3	BF <sub>2</sub> HBANPF . . . . .	107
9.1.4	Al(HPhNPF) <sub>3</sub> . . . . .	109
9.1.5	Al(HBANPF) <sub>3</sub> . . . . .	111
9.2	Model Equations . . . . .	113
9.3	Quantum Yields . . . . .	115
9.4	Photochemical Stability . . . . .	119
9.5	Lifetime Measurements . . . . .	122
9.6	Measurement of the Luminescence Intensity Dependency on Excitation Light . . . . .	125
9.7	Lifetime Calibration of Al(HPhNPF) <sub>3</sub> in Hyflon® AD 60 . . . . .	125

---

# 1 Introduction

Oxygen is the second most abundant component in the earth's atmosphere and undoubtedly belongs to the most important analytes on earth. Measuring its exact concentration is of great importance for numerous technical applications (e.g. various combustion processes, biotechnological fermentations) and while it is nearly omnipresent in the biosphere its concentration can vary greatly.

Most oxygen sensors are tailored for measurements in the physiological region, however oxygen quantification in trace and ultra trace amounts is essential for many applications as well. These include monitoring of impurities in gases[1], oxygen sensitive processes (e.g. semiconductor industry[2]) and especially biological research.

Ultra trace oxygen sensors are of special relevance in microbiology because it has been shown that some microorganisms can grow aerobically at concentrations far below the Pasteur point [3]. Stolper et al. [4] could even show aerobic growth at oxygen concentrations  $\leq 3$  nM which could imply that aerobic life could have developed before the "Great Oxidation" which happened 2.3 to 2.4 billion years ago.

Furthermore investigation of oxygen minimum zones in the deep sea requires more sensitive oxygen sensors than the currently available ones. Revsbech et al. [5] could determine oxygen concentrations below 2 nM of dissolved oxygen in the oxygen minimum zone off Peru, but determination of the exact oxygen concentration was impossible.

These possible applications illustrate the demand for even better, more sensitive trace oxygen sensors. To achieve this goal we combined luminophores with extremely long living phosphorescence with very permeable perfluorinated matrices to obtain outstandingly sensitive oxygen sensors.



---

## 2 Theoretical Background

### 2.1 Fundamentals of Luminescence

Luminescence is the emission of photons from an organic or anorganic compound during relaxation of an excited electronic state. Luminescence is very sensitive to many environmental influences and is therefore used extensively in miscellaneous sensors for their monitoring [6, pp. 3-4].

As most optical oxygen sensors are based on luminescence, its principles are presented in this section.

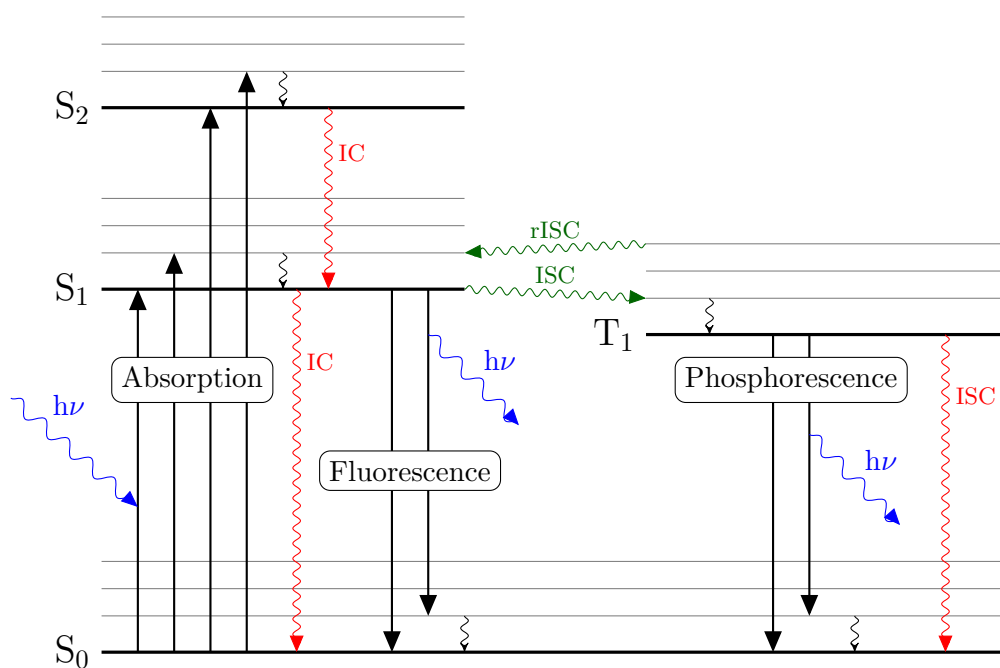


**Figure 2.1:** Jablonski diagram of a phosphorescent dye. Showing all important transitions that can occur between excitation and subsequent de-excitation.

### 2.1.1 Absorption

Among the many possibilities to excite a luminophore, irradiation with light is the most common one. During absorption of a photon an electron is promoted to an energetically higher state in the dye. This electron can go through various transitions before the dye relaxes to its ground state. This absorption of a photon is an extremely fast process and takes place in about  $10^{-15}$  s. [6, pp. 20,30-31]

In case of absorption of visible light the observed transitions are in most cases  $\pi \longrightarrow \pi^*$  or  $n \longrightarrow \pi^*$  because most other transitions (e.g.  $\sigma \longrightarrow \sigma^*$ ,  $n \longrightarrow \sigma^*$ ) occur at higher energies and thus lower wavelengths. The energy for  $\pi \longrightarrow \pi^*$  transitions decreases with greater conjugated  $\pi$ -systems and usually several conjugates bonds are required to reach absorptions in the VIS-region. Furthermore it should be noted that the dye retains its spin multiplicity during excitation. A direct transition from the ground state to the excited triplet state is spin-forbidden. [6, pp. 20-27]

According to the Born-Oppenheimer approximation the movements of electrons are much faster than the movements of the heavy nuclei. Thus the atoms can be considered stationary during the fast ( $10^{-15}$  s) excitation process. Because the atom positions of the vibrationally lowest ground state will not be the equilibrium conformation of the excited state, the molecule will most likely be in an vibrationally excited state after excitation. This is called the Frank-Condon principle. [6, pp. 30-32]

The ability of a dye to absorb light is given by the molar absorption coefficient  $\varepsilon$  as given in the beer-lambert law (eq. 2.1), in which  $A$  is the absorbance of the sample and defined as the decadic logarithm of the light intensity ratio before ( $I_0$ ) and after ( $I$ ) the sample. Furthermore it contains the length of the light path through the sample  $l$  and the concentration of the dye  $c$  [6, pp. 23-27].

$$A = \log \left( \frac{I_0}{I} \right) = \varepsilon \cdot l \cdot c \quad (2.1)$$

### 2.1.2 Internal Conversion

After excitation and before light emission multiple processes can occur. Vibrational relaxation converts the excited states ( $S_1$ ,  $S_2$ ) to their vibrational ground levels. Furthermore internal conversion can occur and transfer higher excited states to the lowest excited state. These processes are not as fast as absorption but still occur in timescales of  $10^{-13}$  s to  $10^{-11}$  s. Internal conversion to the electronic ground state  $S_0$  is also possible but due to the higher energy difference usually slower than between excited states. [6, pp. 34-36]

### 2.1.3 Fluorescence

Fluorescence happens usually after vibrational relaxation and internal conversion to the vibrational ground state of the lowest excited state  $S_1$ . Therefore the emission wavelength is independent of the excitation wavelength.

The fluorescence emission is a very fast process ( $10^{-15}$  s), but the lifetime of the  $S_1$ -state has usually a lifetime of a few nanoseconds before it undergoes this transition.

Due to the energy loss during internal conversion and/or vibrational relaxation the energy of the emitted light is lower than the absorbed light. This difference is called the Stokes shift. Like the absorption the radiative emission also follows the Frank-Condon principle. Therefore the de-excitation usually happens from the vibrational lowest level of the excited state to a higher vibrational level of the electronic ground state. Because the spacing of the vibrational levels is usually similar between excited and ground state this often leads to a mirroring of the absorption peaks. [6, pp. 37-38]

### 2.1.4 Intersystem Crossing

During the lifetime of the excited singlet state  $S_1$  another process can occur: intersystem crossing to the excited triplet state. This transition is spin-forbidden but is possible due to spin-orbit coupling. Spin-orbit coupling is caused by overlapping wavefunctions of the excited states of different multiplicities and usually enhanced by heavy atoms. The reaction speed can be high enough to compete with fluorescence or internal conversion. [6, pp. 30,41]

### 2.1.5 Phosphorescence

Once the excited triplet state  $T_1$  is reached it is very long-lived compared to the singlet states as all its de-excitation paths are spin-forbidden. However in solution usually no radiative de-excitation is visible due to the relatively fast relaxation by collisions with solvent molecules. Only at low temperatures or after embedding in rigid matrices this deactivation slows down sufficiently to make radiative relaxation observable. The lifetimes of these transitions are much higher than those of fluorescence emissions and may even reach several seconds or more.

Because the energies of the triplet state  $T_1$  are lower than those of the singlet state  $S_1$  the wavelengths of phosphorescence emissions are higher than the respective fluorescence emissions. [6, p. 41]

### 2.1.6 Reverse Intersystem Crossing

Besides internal conversion and phosphorescence reverse intersystem crossing is another process that can occur from the  $T_1$  state if the energy difference to the  $S_1$  state is small. Reverse intersystem crossing of the E-type is thermally activated and much more prominent at higher temperatures. Another possibility for reaching the  $S_1$  state is triplet-triplet annihilation (P-type). In this case two excited molecules collide and one is transferred to the  $S_1$  state.[6, pp. 41-42]

### 2.1.7 Delayed Fluorescence

After the repopulation of the excited singlet state  $S_1$  fluorescence, internal conversion or intersystem crossing can occur. The fluorescence emission has the same spectral properties as common prompt fluorescence but has the lifetimes properties of phosphorescence (hence the name delayed fluorescence). As long as there is dye in the excited triplet state there is both reverse intersystem crossing and phosphorescence. Thus both luminescences decay with the same lifetime.

An exception to this is P-type delayed fluorescence which is based upon the triplet-triplet annihilation. Because the kinetics of this reverse intersystem crossing process is of second order in respect to the excited triplet state concentration the P-type delayed fluorescence lifetime is only half the phosphorescence lifetime. [6, p. 42]

### 2.1.8 Lifetimes

All so far discussed lifetimes are only statistical values and only true for a large amount of molecules. The kinetics of the various de-excitation processes are all of first order (except triplet-triplet annihilation) and follow the general equation 2.2. While lifetimes of excited singlet states are in the range of tens of picoseconds to hundreds of nanoseconds, phosphorescence lifetimes are usually much longer ranging from milliseconds to seconds. [6, pp. 42-46]

$$[A] = [A]_0 \cdot e^{-\frac{t}{\tau}} \quad (2.2)$$

### 2.1.9 Quantum Yields

The quantum yield of an emission is the ratio between emitted and absorbed photons and an important parameter for sensor brightness. It can reach up near to unity for fluorescence but is usually lower for phosphorescence. During quenching the quantum yield is reduced together

with the lifetime. If the quenching is only dynamic the ratio of reduction can be the same for both. [6, pp. 46-47]

### 2.1.10 Quenching by Oxygen

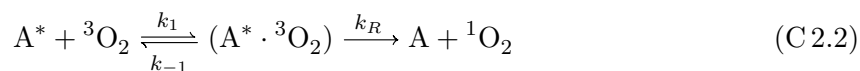
Quenching is the radiationless de-excitation of a fluorophor due to intermolecular interactions. This can happen due to many reasons (collisions, electron transfer, proton transfer, energy transfer and excimer or exciplex formation).

However in this work only quenching through collisions will be considered and especially the quenching by molecular oxygen. Collisions with heavy atoms or paramagnetic molecules (like oxygen) can deactivate an excited dye. During the quenching the triplet oxygen get promoted into the  $^1\Delta$  singlet state and the dye is transferred back to its ground state (see reaction C 2.1). This process reduces both lifetime and quantum yield.



Different mechanisms exist for the excited state quenching. If the quencher is present in a very high concentration the probability is high to find a quencher in reaction distance. If the probability is 1 the system shows simply a diffusion independent first order decay. In all other cases this state has to be considered as concentration dependent static quenching.

If the quencher concentration is low enough that nearly no dye can be quenched immediately, diffusion of the excited dye or the quencher, is necessary and rate limiting for the process. This is called dynamic quenching and an important reaction for luminescent sensor materials. Dynamic quenching can be seen as a two step process (see scheme C 2.2). First the quencher diffuses to the excited dye (or in solution the dye to the quencher) ( $k_1$ ), then they react and yield the de-excited luminophore ( $k_R$ ). Because the reaction is much faster than the diffusion ( $k_R \gg k_1$ ) only the diffusion speed is rate limiting. Thus the process can be seen as pseudo first order in regard to the quencher concentration. [6, pp. 73-76]



### 2.1.11 Stern-Volmer Kinetics

The Stern-Volmer relation (eq. 2.3) describes the change of luminescence intensity ( $I$ ) and lifetime ( $\tau$ ) in dependency on the quencher concentration ( $[Q]$ ) and the quench constant ( $k_q$ ) caused by dynamic quenching and is the theoretical foundation of most optical oxygen sensors.

The combination of the unquenched lifetime ( $\tau_0$ ) and the quench constant ( $k_q$ ) is the Stern-Volmer constant  $K_{SV}$  and a measure for sensor sensitivity. However quenching in a polymer matrix is usually more complex than in solution and the simple Stern-Volmer relation is often not able to describe it accurately [6, pp. 77-78].

$$\frac{I_0}{I} = \frac{\tau_0}{\tau} = 1 + k_q\tau_0[Q] = 1 + K_{SV}[Q] \quad (2.3)$$

### 2.1.12 Two-Site Model

In practical applications deviation from ideal Stern-Volmer kinetics can be seen very often. This can be due to multiple reasons. One very often encountered cause are different regions in the sensor matrix. In those domains the quenching coefficients can be different and thus cause the Stern-Volmer plots to show superimposed non-linear curves. Such systems can be described by introducing a second Stern-Volmer constant  $K_{SV2}$  and a factor for the dye distribution between the regions  $f$  (see eq. 2.4).

$$\frac{I_0}{I} = \frac{1}{\frac{f}{1+K_{SV1}p_{O_2}} + \frac{1-f}{1+K_{SV2}p_{O_2}}} \quad (2.4)$$

This equation has three fit parameters instead of one for the original Stern-Volmer equation and is able to fit the often observed downwards curvature of Stern-Volmer plots. To simplify this model the assumption can be made that quenching is only possible in one of the two domains. This is a rather unrealistic assumption but reduces the fit parameters to two and still yields acceptable fits for many practical applications. [7, 8]

$$\frac{I_0}{I} = \frac{1}{\frac{f}{1+K_{SV1}p_{O_2}} + \frac{1-f}{1}} \quad (2.5)$$

## 2.2 Optical Oxygen Sensors

As the so-called Cambridge definition of a chemical sensor states: "*Chemical sensors are miniaturised devices that can deliver real time and on-line information on the presence of specific compounds or ions in even complex samples.*" [9]

A sensor system usually consists of the analyte, the transduction platform and a signal processing unit which yields the measured analyte concentration. (see fig. 2.2). An optical sensor is defined by its usage of optical transduction techniques (fluorescence, phosphorescence, absorption, etc.) [10].

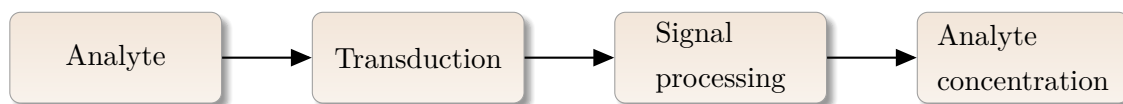


**Figure 2.2:** Functional principle of a sensor [10].

Among optical sensors chemical oxygen sensors are a widely used and well developed field. Their functional principle is often fluorescence or phosphorescence quenching by molecular triplet oxygen ( $^3\text{O}_2$ ). The quenching is often dynamic and follows the Stern-Volmer relation and intensity as well as lifetime measurements can be used to generate the signal. [9–11]

The utilized dye is often contained in a polymer or sol-gel matrix in a film or in (nano)particles. The matrix has many important tasks. It has to be permeable for the analyte while shielding the dye from other environmental influences (e.g. ions). Furthermore it should prevent leaching and thus keep the dye concentration constant. This is especially important for intensity measurements. Moreover even the measurement range can be tuned by the permeability of the matrix. [10, 11]

### 2.2.1 Advantages of Optical Oxygen Sensors

Optical oxygen sensors are but one method among many for oxygen quantification (e.g. Winkler titration or more importantly electrochemical methods like the Clark electrode). [11]

Especially the Clark electrode was the standard oxygen sensor owing to its robustness and reliability. Nevertheless it is continuously replaced by optical oxygen sensors due to their many advantages. They are often relatively inexpensive, can be miniaturized easily, enable remote and nearly noninvasive measurements and especially importantly for oxygen trace measurements: do not consume oxygen during the measurement [11]. Furthermore optical oxygen sensor sensitivities are easily tuneable by choice of dye and polymer and thus are applicable in a very broad range of oxygen concentrations. [12]

These advantages enable applications like measuring in a closed container through an optical window or measurement of intra-cellular oxygen levels with nanoparticles. [13]

### 2.2.2 Applications of Optical Oxygen Sensors

Owing to these excellent properties optical oxygen sensors have been applied in many different fields. They are indispensable tools in medical applications to measure subcutaneous oxygen levels [14] or the glucose concentration via an glucose oxidase layer [15].

Furthermore they are applied in biotechnology to monitor oxygen concentration in bioreactors [16] and in microbiological research for various measurements of intra or extra cellular space. Especially oxygen sensitive nanoparticles (PEBBLES) are indispensable tools for measuring intracellular oxygen levels [17].

Another important field of application for optical oxygen sensors is marine biology because the concentration of dissolved oxygen in seawater is relevant for many biological processes [4, 11].

## 2.3 Tuning the Sensitivity

The mentioned tuneability of the measurement range of oxygen sensors is an important advantage of this system and is realised mainly with two parameters: firstly the luminescence lifetime of the utilized dye and secondly with the permeability of the embedding matrix.

### 2.3.1 Luminescence Lifetime

The excited state lifetime is an important parameter of the Stern-Volmer constant (see eq. 2.6). Therefore rising lifetimes increase the sensitivity directly. This strong influence can be explained by the extended time oxygen molecules have to quench the excited dye. This increases the probability of the quenching and hence the sensitivity to oxygen is greater.

$$K_{SV} = \tau_0 \cdot k_q \quad (2.6)$$

Consequently choosing a dye with an appropriate lifetime for the desired sensitivity is a good first step when designing a new oxygen sensor [11, 12].

Most sensor dyes have unquenched lifetimes in the  $\mu\text{s}$  to few ms range. Only fullerenes [18] and some  $\text{BF}_2$ -chelates [19–21] have been reported with substantially higher lifetimes.

### 2.3.2 Matrix Permeability

Besides the dye lifetime the permeability of the employed matrix is the main parameter to tune the sensitivity. The permeability of a chosen matrix influences the sensitivity in two ways. This is due to the fact that it is a combination of two parameters: the oxygen solubility  $S$  and the diffusion coefficient  $D$  (see eq. 2.7). [22, p. 243]

$$P = S \cdot D \quad (2.7)$$

A higher solubility increases the oxygen concentration in the sensors and hence the sensitivity to the surrounding (measured) oxygen concentration. However it is nearly constant for most polymers and thus can have no major influence on the sensitivity [12].

The second component of the permeability is the diffusion coefficient, which depends to a much greater extent on the utilized matrix. Because the quenching is a diffusion limited process a higher diffusion coefficient leads to a increased quenching constant  $k_q$  and is therefore a major parameter in tuning the sensitivity [12].

Consequently the rule of thumb relation (2.8) can be deducted from equation (2.6), which states that the sensor sensitivity  $S$  is proportional to the luminescence lifetime  $\tau_0$  and the matrix permeability  $P$ .

$$S \propto \tau_0 \cdot P \tag{2.8}$$

A third, less important influence of the matrix is the change of the luminescence lifetime as the it depends on the embedding polymer. But this influence is usually small because as long as the dye is compatible with the matrix and aggregation is avoided the lifetime remains nearly the same in all matrices. [12]

Common utilized polymers for oxygen sensors include polystyrene, polyvinyl chloride, polymethylmethacrylate, siloxane and polytetrafluorethylenes [10]. Especially permeable ,and thus for trace sensors suitable, matrices are polydimethylsiloxane, ormosils and amorphous perfluorinated polymers like Teflon® AF, Hyflon® AD 60 or Cytop®.

## 2.4 State of the Art Trace Oxygen Sensors

The most sensitive state of the art trace oxygen sensors consist of C<sub>70</sub>-fullerens embedded in ethyl cellulose. Nagl et al. [18] reported a C<sub>70</sub>-fulleren in ethyl cellulose sensor with a  $K_{SV}$  of 0.070 ppmv<sup>-1</sup> with a limit of detection of 160 ppbv and Kochmann et al. [23] reported a similar sensor utilizing <sup>13</sup>C<sub>70</sub>-fulleren with a  $K_{SV}$  of 0.042 ppmv<sup>-1</sup> at 25 °C and a limit of detection of 250 ppbv. While these fullerenes have excellent lifetimes of 20 ms to 25 ms they show only low quantum yields of approximately 1% at room temperature (values for C<sub>60</sub>[18]). At elevated temperatures quantum yields of up to 6% are possible, but the lifetime and therefore the sensitivity decreases significantly at higher temperatures. Furthermore the utilized matrix ethyl cellulose shows only a moderate permeability and thus limits the achievable sensitivities.

A different approach to excellent sensitivities is to embed dyes with moderate lifetimes in matrices with excellent permeabilities. Borisov et al. [24] embedded the palladium(II) complex of 5,10,15,20-meso-tetrakis-(2,3,4,5,6-pentafluorophenyl)-porphyrin (PdTFPP) with a lifetime

of around 1 ms in highly permeable silica particles and reached a  $K_{SV}$  value of  $0.0067 \text{ ppmv}^{-1}$  with a limit of detection of 150 ppmv (at  $25^\circ\text{C}$ ).

However until now no sensor material has been developed that combined very high lifetimes in the tens of milliseconds (or above) and matrices with extremely high oxygen permeabilities. Therefore new oxygen sensors that combine both properties could advance the current limits of oxygen detection greatly.

## 2.5 Achieving Maximum Sensitivity

To obtain sensors with extreme oxygen sensitivities clearly both luminescence lifetime and matrix permeability have to be outstandingly high. Consequently  $\text{BF}_2$ -chelates of  $\beta$ -diketone similar ligands with phosphorescence lifetimes in the range of a few hundred ms and extremely permeable perfluorinated matrices were the materials of choice.

### 2.5.1 Amorphous Perfluorinated Polymers

Perfluorinated polymers like Teflon® AF or Hyflon® AD 60 show outstanding permeabilities for oxygen (see table 2.1), which are 20 to 400 times higher than for example the oxygen permeability of polystyrene. An even more permeable matrix would be poly(trimethylsilylpropyne) but due to its contained double bonds it is prone to oxidation and would consume oxygen during measurements. This would result in a decreased oxygen concentration in the sensor during measurements and aging of the matrix.

Another important reason to use perfluorinated polymers like Teflon AF or Hyflon for oxygen trace sensors is their chemical stability. Common dye matrices can react slowly with the excited singlet oxygen which is generated during the measurement. This reaction consumes oxygen

**Table 2.1:** Oxygen permeabilities of selected polymers.

Polymer	Permeability [ $10^{-16} \text{ mol m}^{-1} \text{ s}^{-1} \text{ Pa}^{-1}$ ]	Reference
Polystyrene	8.8	[25]
Cytop®	28	[26]
Hyflon® AD 60	170	[27]
Teflon® AF 1600	1200	[27]
Poly(dimethylsiloxane)	2700	[28]
Teflon® AF 2400	3500	[27]
Poly(trimethylsilylpropyne)	23 000	[29]

during the measurement (or generally during illumination of the sensor) and thus lowers the available oxygen concentration. While this effect is usually negligible in the physiological range it has a drastically higher impact in the trace and ultra trace region where only very small oxygen amounts are available. Furthermore this reaction introduces a light intensity (and measurement frequency) dependency of the signal.

Perfluorinated matrices solve this grave problem because their C-F bonds cannot be oxidized and thus no oxygen consumption is possible and are therefore preferable to any other type of polymer for ultra trace measurements.

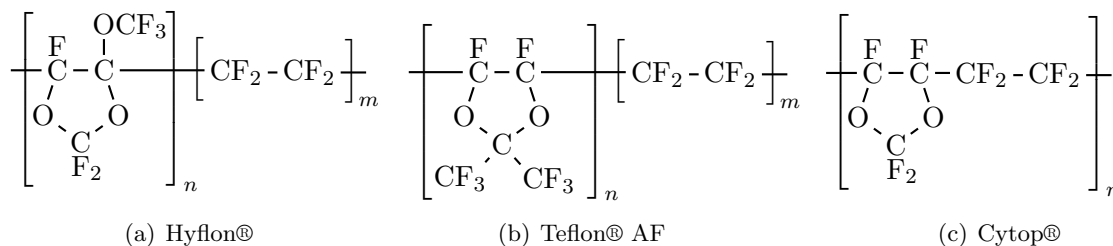


**Figure 2.3:** Structures of the utilized perfluorinated polymers.

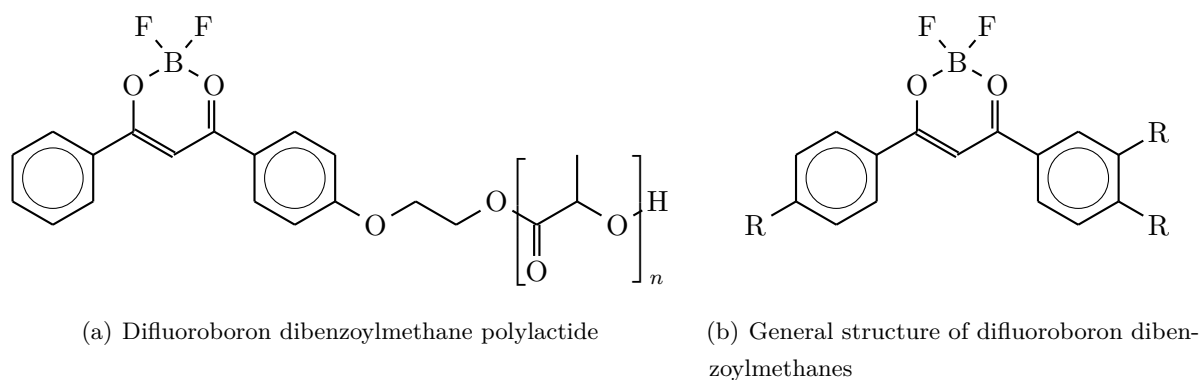
### 2.5.2 BF<sub>2</sub>-Chelates of β-diketonates

BF<sub>2</sub>-chelates of β-diketonates or similar structures are very interesting materials for trace oxygen sensors because they can simultaneously show prompt fluorescence, delayed fluorescence and room temperature phosphorescence [19]. Moreover the phosphorescence and delayed fluorescence emissions show exceptionally long lifetimes.

Zhang et al. [19] showed a difluoroboron dibenzoylmethane polylactide (fig. 2.4(a)) with a phosphorescence lifetime of 170 ms. The main drawback of this compound was a very weak phosphorescence emission. This issue was addressed by Zhang et al. [20] by introducing iodide as heavy atom to increase the spin-orbit coupling and thus the intersystem crossing. The resulting dyes showed considerably increased phosphorescence, but due to the enhanced intersystem crossing the lifetimes dropped down to approximately 4 ms [20].

Xu et al. [21] further investigated this class of compounds (fig. 2.4(b)) by varying substituents and the size of the aromatic system. The synthesized compounds reached phosphorescence lifetimes of up to 614 ms and a bathochromic shift of the phosphorescence emission to approximately 540 nm. But again the phosphorescence quantum yields of the dyes were extremely weak.

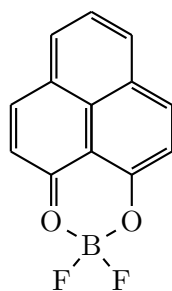
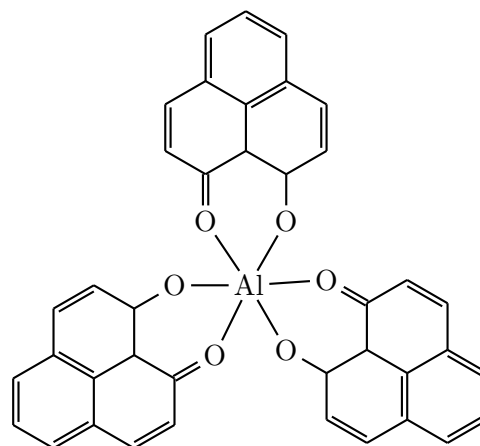
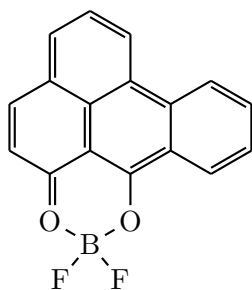
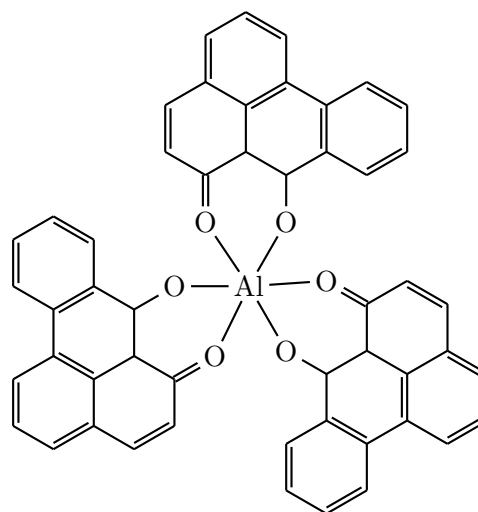
Prior to this work this issue was addressed by Sergey Borisov who synthesized and kindly provided novel BF<sub>2</sub>-chelates with the β-diketonate analogue compounds 9-hydroxy-1*H*-phenalen-1-one (HPhN) and 7-hydroxy-6*H*-benzo[*de*]anthracen-6-one (HBAN) (see fig. 2.5). They exhibited



**Figure 2.4:** Difluoroboron dibenzoylmethanes.

phosphorescence lifetimes of 350 ms and 730 ms and quantum yields of 4.6% and 9.1%, for  $\text{BF}_2\text{HPhN}$  and  $\text{BF}_2\text{HBAN}$ , respectively (measured in this work). Additionally preliminary test indicated that aluminium complexes of these ligands show similar lifetimes and quantum yields.

As mentioned above dyes with such long lifetimes should be able to produce oxygen sensing materials with outstanding sensitivities. However they (and many other dyes) are not compatible with extremely permeable perfluorinated matrices and aggregate readily which renders any sensing material useless. Consequently modification with perfluorooctyl groups was selected to improve the compatibility with those matrices.

(a)  $\text{BF}_2\text{HPhN}$ (b)  $\text{Al}(\text{HPhN})_3$ (c)  $\text{BF}_2\text{HBAN}$ (d)  $\text{Al}(\text{HBAN})_3$ **Figure 2.5:** Formulas of the novel  $\beta$ -diketonates.

## 2.6 Perfluoroalkylation

The most used reagents for introducing perfluoroalkyl groups into molecules are the respective iodides. Multiple reactions have been utilized to attach perfluoroalkyl chains to aromatic compounds, which can be classified into two main groups: radical and catalytic reactions.

The primary used catalyst copper powder has been utilized to substitute aromatic halides (mostly Br and I) with perfluoroalkyl chains in many reactions [30–32]. The proposed reaction mechanism is a insertion of the copper into the perfluoroalkyl-iodide bond with a subsequent reaction with the aromatic halide [33].

However most utilized reactions follow a radical mechanism. Iizuka et al. [34] and Bravo et al. [35] proposed a mechanism where the perfluorooctyl-radical reacts with the aromatic compound and forms a arenium radical. This radical undergoes oxidation to a arenium cation which consequently eliminates a proton. The formation of the most stable arenium-radical intermediate can explain the observed stereoselectivity [35–37]. Many different methods of radical generation have been used for perfluoroalkylation, including high temperature ( $> 250\text{ }^{\circ}\text{C}$ )[38], UV-light and  $\text{TiO}_2$  [34], V-70L (very similar to AIBN, but more reactive) [36], Cu [37], benzoyl peroxide, tert-butyl hydroperoxide, Fe(II) and  $\text{H}_2\text{O}_2$  (Fenton's reagent [39])[35] and many more.

Besides a dramatic increase of solubility in perfluorinated polymers another advantage is a probable significant increase in photochemical stability [40].

---

## 3 Experimental

### 3.1 Methods

#### 3.1.1 Sensor Preparation

All sensors were knife coated on hydrophobically modified glass slides (see section 3.4.2).

The coating was done on a glass plate as support with a 3 mil coating knife. When necessary Mylar®-foils were used as spacers.

#### 3.1.2 Chemical Dye Characterisation

##### NMR

$^1\text{H}$  NMR and COSY spectra were recorded on a 300 MHz instrument from Bruker. A mixture of freon and  $\text{CDCl}_3$  (1:1, v/v) was used for perfluorinated ligands and the respective complexes and chelates.

##### MS

Electron impact (EI, 70eV) and MALDI-TOF mass spectra were recorded on a Waters GCT Premier equipped with direct insertion (DI) and on a Micromass TofSpec 2E, respectively.

#### 3.1.3 Optical Dye Characterisation

##### Absorption Spectra

Absorption spectra were acquired on a Cary 50 UV-VIS spectrophotometer from Varian in 1 cm optical glass cuvettes. Measurements were always corrected by a baseline measurement of

the pure solvent and acquired in the “fast”-mode (equals 1 points per nm). Molar absorption coefficients were calculated with eq. 3.1.

$$\epsilon = \frac{A \cdot M}{c \cdot l} \quad (3.1)$$

With  $\epsilon$  the molar absorption coefficient in  $\text{L mol}^{-1} \text{cm}^{-1}$ , the measured absorption  $A$ , the molar Mass  $M$  in  $\text{g mol}^{-1}$ , the concentration  $c$  in  $\text{mol L}^{-1}$  and the length of the cuvette  $l$  in cm.

### **Emission and Excitation Spectra**

Emission and Excitation spectra were recorded on a FluoroLog® 3 Spectrofluorometer from Horiba Scientific equipped with a R2658 photomultiplier from Hamamatsu. Oxygen-free spectra were measured under a  $25 \text{ g L}^{-1}$  sodium sulfite solution with a small amount cobalt(II) chloride.

### **Quantum Yields**

Quantum yields were measured with a FluoroLog® 3 Spectrofluorometer with a Quanta- $\varphi$  integrating sphere from Horiba Scientific.

### **Photobleaching Stability**

Photobleaching of the dyes was recorded by exposing them to a blue power LED array with a photon flux of  $4000 \mu\text{mol s}^{-1} \text{m}^{-2}$  (Li-250A light meter from Li-COR) and measuring absorbance spectra every 10 min.

## **3.1.4 Lifetime Measurements**

### **Fluorolog Kinetic Acquisition Mode**

The luminescence lifetimes were recorded on a FluoroLog® 3 Spectrofluorometer from Horiba Scientific in kinetic acquisition mode with 0.01 points/s. The obtained decay curves were fitted with a first order exponential decay function.

### **Single Photon Counting**

The single photon counting lifetimes were recorded on a FluoroLog® 3 Spectrofluorometer from Horiba Scientific with a DeltaHub module. The dye was excited with a spectra-LED with an emission maximum of 392 nm and a FWHM of 19 nm.

### 3.1.5 Calibration

#### Calibration by Controlled Oxygen Consumption of Ascorbate

A 30 mL glass vial equipped with a Pd-benzoporphyrine in PS and a Pd-benzoporphyrine in Teflon® AF 1600 sensor was used for this calibration method. The vial was completely filled during the calibration and stirred with a magnetic stirring bar. To avoid oxygen input during the reaction the vial was placed upside down in a sodium sulfite solution. The two sensors were read out with a phase-fluorometric four-channel FireSting O<sub>2</sub> device.

#### Calibration with a Gas Mixer

Two red-y mass flow controllers from Vögtlin instruments were used to mix nitrogen (5.0 or 6.0) and test gas (0.1 % or 20 ppm) to produce a gas stream with the desired oxygen concentration. This stream was led in a measuring cell with a 1.2 cm circular window with a Viton®gasket. The sensor on a glass slide was pressed against this gasket by a teflon wedge. After the measuring cell the gas stream was used to purge the outside of the gasket to reduce contamination by diffusion. All tubes (1/8 inch) and connections (swagelock or upchurch) were made of steel.

### 3.1.6 Glucose Oxidase Measurement

A 25 mL glass vial with a thin metal gasket was equipped with a Pt benzoporphyrin in PS, a Pd benzoporphyrin in PS, a Pd-TPFPP in Hyflon and an Al(HPhNPF)<sub>3</sub> in Hyflon sensor. The polystyrene sensors were read out with a FireSting O<sub>2</sub>, the Pd-TPFPP in Hyflon® AD 60 sensor with a LUMOS and the Al(HPhNPF)<sub>3</sub> sensor with a FluoroLog® 3. During the reaction the vial was completely filled and stirred with a magnetic stirring bar. To avoid oxygen input during the reaction the vial was placed upside down in a sodium sulfite solution.

### 3.1.7 Trace measurements in gasses

Measuring oxygen traces in gasses was done by connecting the bottle directly to the measuring cell. The pressure was set to 0.5 bar and the system purged for 5 min. Then the phosphorescence lifetimes were measured.

### 3.1.8 Model

A mathematical model was developed to simulate and explain non-linear behavior of the trace oxygen sensors. The model is based on a steady-state assumption of all relevant dye and oxygen states ( $S_0$ ,  $S_1$ ,  $T_1$ ,  $O_{2T}$ ,  $O_{2S}$  and  $O_{2C}$ ) during illumination (see equations 3.2 to 3.6). Triplet-triplet annihilation between two excited dye molecules (a second order process) was not considered because it would increase the complexity of the equation system greatly.

$$S_0 : \quad 0 = -[S_0] \cdot k_E \cdot I + [S_1] \cdot (k_F + k_{rF}) + [T_1] \cdot (k_P + k_{rP} + k_q \cdot [O_{2T}]) \quad (3.2)$$

$$S_1 : \quad 0 = [S_1] \cdot k_{isc} - [T_1] \cdot (k_{isc-1} + k_P + k_{rP} + k_q \cdot [O_{2T}]) \quad (3.3)$$

$$T_1 : \quad [C] = [T_1] + [S_0] + [S_1] \quad (3.4)$$

$$O_{2T} : \quad 0 = [O_{2S}] \cdot k_{rO_2} - k_q \cdot [T_1] \cdot O_{2T} \quad (3.5)$$

$$O_{2S} : \quad [O_2] = [O_{2T}] + [O_{2S}] \quad (3.6)$$

$S_0$  . . . . . Dye ground state

$S_1$  . . . . . Dye excited singlet state

$T_1$  . . . . . Dye excited triplet state

$C$  . . . . . Dye concentration

$O_{2T}$  . . . . . Oxygen triplet ground state

$O_{2S}$  . . . . . Oxygen excited singlet state

$O_2$  . . . . . Oxygen concentration

$I$  . . . . . Light Intensity

$k_E$  . . . . . excitation kinetic constant

$k_F$  . . . . . fluorescence kinetic constant

$k_{rF}$  . . . . . kinetic constant for radiationless  $S_0$  relaxation

$k_P$  . . . . . phosphorescence kinetic constant

$k_{rP}$  . . . . . kinetic constant for radiationless  $T_1$  relaxation

$k_q$  . . . . . quench constant

$k_{isc}$  . . . . . intersystem crossing kinetic constant

$k_{isc-1}$  . . . . . reverse intersystem crossing kinetic constant

$k_{rO_2}$  . . . . . kinetic constant for  $O_{2S}$  relaxation

These equations were solved with Wolfram Mathematica® for the concentrations of all dye and oxygen species (see eqs. 9.1 to 9.5 on pages 113 to 114 in the appendix).

With this model extreme values of light intensity, dye concentration,  $T_1$ - and  $O_{2S}$ -lifetime and oxygen consumption speed could be simulated. This simulation was used to determine the influences on the phosphorescence intensity and thus the calibration curves.

## 3.2 Materials

**Table 3.1:** Used Ligands and Dyes.

Ligands and Dyes	Supplier
HPhN <sup>a</sup>	Ramidus
HBAN <sup>b</sup>	TU Graz
BF <sub>2</sub> HPhN	TU Graz
BF <sub>2</sub> HBAN	TU Graz
HPhNPF	synthesized
HBANPF	synthesized
BF <sub>2</sub> HBANPF	synthesized
Al(HPhNPF) <sub>3</sub>	synthesized
Al(HBANPF) <sub>3</sub>	synthesized

<sup>a</sup> 9-hydroxy-1*H*-phenalen-1-one

<sup>b</sup> 7-hydroxy-6*H*-benzo[*de*]anthracen-6-one

**Table 3.2:** Used polymer matrices.

Polymer	Supplier
Polystyrene (MW 250 000)	Scientific Polymer
Teflon® AF 1600	DuPont
Teflon® AF 2400	DuPont
Hyflon® AD 60	Solvay Plastics
Cytop® CTL-809A	AGC Chemicals
Cytop® CTL-107MK	AGC Chemicals

**Table 3.3:** Used gases.

<b>Gas</b>	<b>Supplier</b>
Nitrogen 5.0	Linde Austria
Nitrogen 6.0	Linde Austria
Test gas (0.1 %)	Linde Austria
Ttest gas (20 ppmv)	Linde Austria

**Table 3.4:** Used Solvents.

<b>Solvent</b>		<b>Supplier</b>
<b>Name</b>	<b>Abbreviation</b>	
Dimethylsulfoxide	DMSO	Sigma-Aldrich
1,1,2-Trichloro-1,2,2-trifluoroethane	freon	Sigma-Aldrich
Tetrahydrofuran	THF	VWR
Ethanol	EtOH	Brenntag
Dichloromethane	DCM	Fisher Scientific
Hexan	Hex	VWR
Cyclohexan	Cy	VWR
Octafluorotoluene	OFT	ABCR
Acetone		Brenntag
Chloroform		Carl Roth
Perfluorodecalin		ABCR
Cytop Solvent 100K		AGC Chemicals

**Table 3.5:** Other used chemicals.

Chemical	Supplier
Iron(II)sulfate heptahydrate ( $\text{FeSO}_4 \cdot 7 \text{H}_2\text{O}$ )	Sigma-Aldrich
perfluorooctyl iodide	ABCR
Sodium hydroxide (NaOH)	Carl Roth
Aluminium chloride ( $\text{AlCl}_3$ )	Fluka
Boron trifluoride diethyl etherate ( $\text{BF}_3\text{Et}_2\text{O}$ )	Sigma-Aldrich
Aquaphobe(TM) CF chlorinated fluoroalkylmethylsiloxane AB130304	ABCR
Phenyltrimethoxysilane	ABCR
Sodium ascorbate	Carl Roth
Glucose	Carl Roth
Glucose oxidase (GOx) from aspergillus niger	Sigma-Aldrich
Catalase from bovine liver	Sigma-Aldrich
MES	Sigma-Aldrich
BIS-TRIS	Sigma-Aldrich
Acetic acid	Carl Roth
Hydrochloric acid	VWR

### 3.3 Synthesis

#### 3.3.1 Synthesis of HPhNPF

HPhN (1 g, 5.1 mmol) and  $\text{FeSO}_4 \cdot 7\text{H}_2\text{O}$  (2.5 g, 9.0 mmol) were dissolved in 120 mL DMSO and 40 mL freon in a 200 mL Schlenk flask. The whole reaction was conducted under argon atmosphere. The solution was heated to 40 °C and perfluorooctyl iodide (3.4 mL, 7.03 g, 12.9 mmol) was added. 60 %  $\text{H}_2\text{O}_2$  (1.4 mL, 1.67 g, 49 mmol) was added drop-wise over 5 min. The solution turned red and formed black foam. After 30 min 20 mL freon were added and the foam dissolved. 1 h after the start of the reaction a second portion perfluorooctyl iodide (3.4 mL, 7.03 g, 12.9 mmol) was added and 60 %  $\text{H}_2\text{O}_2$  (1.4 mL, 1.67 g, 49 mmol) was added drop-wise over 5 min. The reaction was continued for 1 h, then the reaction mixture was cooled to room temperature and the DMSO and freon phases were separated. The freon phase was washed 3 times with 36 % hydrochloric acid, once with water and was dried over  $\text{Na}_2\text{SO}_4$ . After removing the solvent 9.3 g reddish-brown oil were obtained. The product was purified on a silica-gel column with hexane and toluene as eluents. Yield: 700 mg (13 %). Rf 0.57 with toluene. NMR and mass spectra can be seen in the appendix on the pages 103 and 104.

NMR spectroscopy:  $\delta_{\text{H}}$  (300 MHz,  $\text{CDCl}_3$ ) 16.75 (1H, s), 8.77 (1H, s), 8.15-8.00 (2H, m), 7.86 (1H, d,  $J$  7.9 Hz), 7.24 (1H, d,  $J$  9.3 Hz).

Mass-spectrum (DI-EI):  $m/z$  1031.98 found, 1031.98 calculated.

#### 3.3.2 Synthesis of HBANPF

HBANPF was prepared with the same procedure as HPhNPF, but with a five-fold excess of perfluorooctyl iodide and after 2 h at 40 °C the reaction mixture was stirred over night at room temperature. Yield 500 mg (23 %) starting from 0.5 g HBAN. Rf 0.69 with hexane/toluene 2/1. NMR and mass spectra can be seen in the appendix on the pages 105 and 106.

NMR spectroscopy:  $\delta_{\text{H}}$  (300 MHz,  $\text{CDCl}_3$ ) 17.01 (1H, s), 8.94 (1H, s), 8.79 (1H, d,  $J$  8.2 Hz), 8.71 (1H, d,  $J$  7.9 Hz), 8.52 (1H, d,  $J$  8.3 Hz), 8.03 (1H, d,  $J$  8.2 Hz), 7.89 (1H, t,  $J$  7.6 Hz), 7.73 (1H, t,  $J$  7.5 Hz).

Mass-spectrum (DI-EI):  $m/z$  1081.9908 found, 1081.9982 calculated.

#### 3.3.3 Synthesis of $\text{BF}_2\text{HPhNPF}$

HPhNPF (100 mg, 97  $\mu\text{mol}$ ) were dissolved in 20 mL water-free THF under Ar atmosphere and  $\text{BF}_3 \cdot \text{Et}_2\text{O}$  (250  $\mu\text{L}$ , 283 mg, 2 mmol) was added. The reaction mixture was stirred for 1 h at 65 °C. The product was unstable and decomposed. No pure product could be isolated.

### 3.3.4 Synthesis of BF<sub>2</sub>HBANPF

HBANPF (700 mg, 0.65 mmol) were dissolved in 80 mL water-free THF and 10 mL freon under Ar atmosphere and BF<sub>3</sub>·Et<sub>2</sub>O (1.23 mL, 1.41 g, 10 mmol) was added. The reaction mixture was stirred for 4 h at 65 °C. After 2 h K<sub>2</sub>CO<sub>3</sub> (70 mg, 0.5 mmol) were added and after 3 h BF<sub>3</sub>·Et<sub>2</sub>O (0.7 mL, 0.805 g, 5.7 mmol) were added. Then the solvent was removed under vacuum and the product was purified on a silica-gel column with hexane and toluene as eluents. Yield: 47 mg (6.4%). R<sub>f</sub> 0.32 with hexane/toluene 1/1. NMR and mass spectra can be seen in the appendix on the pages 107 and 108.

NMR spectroscopy:  $\delta_{\text{H}}$  (300 MHz, CDCl<sub>3</sub>) 8.97 (1H, dd, *J* 7.6 Hz, 1.9 Hz), 8.82 (1H, dd, *J* 7.6 Hz, 1.9 Hz), 8.52-8.42 (1H, m), 8.40 (1H, s), 8.05-7.88 (2H, m), 7.64 (1H, d, *J* 9.8 Hz),  
Mass-spectrum (MALDI): [M+Na]<sup>+</sup>: 1153.0 found, 1153.0 calculated; [M-F]<sup>+</sup>: 1111.0 found, 1111.0 calculated

### 3.3.5 Synthesis of Al(HPhNPF)<sub>3</sub>

HPhNPF (100 mg, 0.097 mmol) were dissolved in 20 mL THF and 20 mL ethanol. NaOH (5.9 mg, 0.15 mmol) and AlCl<sub>3</sub> (3.9 mg, 29  $\mu$ mol) was added and the reaction mixture was stirred for 2.5 h at 40 °C. Then the reaction was stopped and water and freon were added. The phases were separated and the freon phase was washed twice with water. The organic layer was dried over Na<sub>2</sub>SO<sub>4</sub> and evaporated in vacuum. 5 mL THF were added to the raw product and the mixture was placed in the freezer for a few hours. Then the THF phase was removed and new THF was added. The product was washed 7 times with this procedure. Yield: 68.4 mg (74%). NMR and mass spectra can be seen in the appendix on the pages 109 and 110.

NMR spectroscopy:  $\delta_{\text{H}}$  (300 MHz, CDCl<sub>3</sub>) 8.87-8.55 (3H, m), 8.15-7.84 (6H, m), 7.84-7.54 (3H, m), 7.42-7.04 (3H, m),  
Mass-spectrum (MALDI): [M+Na]<sup>+</sup>: 3142.93 found, 3142.90 calculated

### 3.3.6 Synthesis of Al(HBANPF)<sub>3</sub>

Al(HBANPF)<sub>3</sub> was prepared and purified with the same procedure as Al(HPhNPF)<sub>3</sub>. Yield 19.5 mg (31 %) starting from 80 mg HBAN. NMR and mass spectra can be seen in the appendix on the pages 111 and 112.

NMR spectroscopy:  $\delta_{\text{H}}$  (300 MHz, CDCl<sub>3</sub>) 9.2-8.2 (9.9H, m), 8.06 (3H, s), 8.0-7.2 (7.2H, m),  
Mass-spectrum (MALDI): [M]<sup>+</sup>: 3271.11 found, 3270.96 calculated, [M(with one additional C<sub>8</sub>F<sub>17</sub>-Group)]<sup>+</sup>: 3689.02 found, 3688.92 calculated

## 3.4 Sensor Preparation

### 3.4.1 Preparation of the Stock Solutions

The dye stock solutions were prepared by weighing in 1.4 mg, 1.8 mg and 2.2 mg of BF<sub>2</sub>HBANPF, Al(HPhNPF)<sub>3</sub> and Al(HBANPF)<sub>3</sub>, respectively in 3 mL vials. Then they were dissolved in 1.4 g, 1.8 g and 2.2 g octafluorotoluene to obtain 1 mg g<sup>-1</sup> solutions.

### 3.4.2 Preparation of Glass Slides

The slides for Teflon-AF, Hyflon and COOH-ended Cytop® CTL-809A were treated with aquaphobe™ CF chlorinated fluoroalkylmethylsiloxane by applying a thin layer, drying it with a heat gun and washing the slide with acetone.

To prepare the slides for SiOR-ended Cytop® CTL-107MK a diluted Cytop® CTL-107MK solution (1:1 with Cytop solvent 100K) was coated with a 1 mil coating knife on the glass slides. After drying the slide was tempered at 120 °C for 30 minutes.

The slides for the polystyrene sensors were prepared by dipping the clean slides in a mixture of 0.3 mL phenyltrimethoxysilane, 2 mL water, 2 mL acetic acid and 38 mL ethanol for 5 minutes.

### 3.4.3 Preparation of the Sensor “Cocktails”

To prepare the sensor-cocktails the dyes were dosed from 1 mg g<sup>-1</sup> stock solutions. After drying the respective amounts of polymer and solvent were added. BF<sub>2</sub>HPhN and BF<sub>2</sub>HBAN based sensors were prepared with 0.01 % dye content. All other (perfluoroalkylated) dyes were utilized in concentrations of 0.05 % in Teflon AF and Hyflon and with 4.4 % and 5.7 % in Cytop® CTL-809A and Cytop® CTL-107MK, respectively. Polystyrene was dissolved in chloroform with a concentration of 5 %. Hyflon AD 60 and Teflon AF 1600 were dissolved in octafluorotoluene with concentrations of 5 % and 6.6 %, respectively. Teflon AF 2400 was processed as a solution in perfluorodecalin with a content of 2 %. Cytop was used as a commercially available 7.9 % solution in Cytop solvent 100K and 180K for Cytop M and Cytop A, respectively.

### 3.4.4 Coating

The cocktails were knife-coated with a 175 µm spacer. After drying a second layer was coated on top of the first one with a spacer of 275 µm. The obtained sensing layers had thicknesses of 23 µm, 23 µm, 30 µm, 9 µm, 32 µm and 41 µm for polystyrene, Teflon® AF 1600, Hyflon® AD 60, Teflon® AF 2400, Cytop® CTL-107MK and Cytop® CTL-809A respectively.

## 3.5 Optical Characterization

### 3.5.1 Absorption Spectra

Absorption spectra were recorded for all synthesized dyes and ligands to follow the reaction progress and to characterize the pure dyes. All measurements were conducted in DCM.

Absorption coefficients were determined for all dyes by weighing in approximately 0.1 g of the  $1 \text{ mg g}^{-1}$  stock solutions (see section 3.4.1 on page 26) and diluting with DCM directly in the cuvettes. Then the absorption spectrum was recorded. 100 mg, 99 mg and 101 mg solution were used and diluted to 1 mL for  $\text{BF}_2\text{HBANPF}$ ,  $\text{Al}(\text{HBANPF})_3$  and  $\text{Al}(\text{HPhNPF})_3$ , respectively. The molar absorption coefficients of HPhNPF and HBANPF were measured by dissolving 2.9 mg and 40 mg in 5 mL and 60 mL DCM, respectively and diluting them by a factor of ten prior the measurement. Before each measurement a baseline of the pure solvent was recorded.

### 3.5.2 Emission Spectra

Anoxic (in sodium sulfite solution) and oxygenated emission spectra (in water at air saturation) were measured for all dyes in Teflon® AF 1600. Additionally, deoxygenated emission spectra were recorded for all Al-complexes in Hyflon® AD 60 and Cytop® CTL-809A. Additionally a emission spectrum of  $\text{Al}(\text{HBANPF})_3$  in Teflon® AF 2400 was measured. A measurement of  $\text{Al}(\text{HPhNPF})_3$  in polystyrene failed because hardly any emission was visible.

To show the strong temperature dependency of the delayed fluorescence, spectra of  $\text{Al}(\text{HPhNPF})_3$  were measured also at 5 °C and 25 °C. For the FluoroLog® 3 settings during the measurements see table 3.6.

### 3.5.3 Excitation Spectra

Excitation spectra were also measured under anoxic conditions in a sodium sulfite solution. All spectra were recorded in Teflon® AF 1600 at 20 °C at 570 nm emission wavelength. The scanned excitation range was always 350 nm to 550 nm with a increment of 0.2 nm, a excitation slit of 2 nm and a 10 % neutral density filter. The filter transmittance corrected intensity value  $cR$  was between 0 and 0.05. The emission wavelength was set to 570 nm for all dyes with a slit of 8 nm. The spectra were corrected with the wavelength dependency of the lamp intensity and filter transmission.

**Table 3.6:** Measurement settings for the emission spectra.

Dye	Matrix	Exc. [nm]	Exc. slit [nm]	Filter [%]	cR <sup>a</sup>	Emi. [nm]	Emi. slit [nm]
BF <sub>2</sub> HBANPF	Teflon® AF 1600	420	2	10	0.033	435–800	8
Al(HPhNPF) <sub>3</sub>	Teflon® AF 1600	420	2	10	0.033	435–800	8
Al(HPhNPF) <sub>3</sub>	Cytop® CTL-809A	435	2	10	0.033	460–700	12
Al(HPhNPF) <sub>3</sub> <sup>b</sup>	Hyflon® AD 60	435	3	10	0.042	460–470	12
Al(HBANPF) <sub>3</sub>	Teflon® AF 1600	420	2	10	0.033	435–800	8
Al(HBANPF) <sub>3</sub>	Hyflon® AD 60	430	3	10	0.042	460–700	12
Al(HBANPF) <sub>3</sub>	Cytop® CTL-809A	435	2	10	0.033	460–680	9
Al(HBANPF) <sub>3</sub>	Teflon® AF 2400	427	6	5	0.081	450–700	10

The spectra were recorded at 20°.

<sup>a</sup> Value for intensity comparison purposes calculated from the measured  $R$  intensity value and the actual filter transmittance.

<sup>b</sup> Spectra at 5 °C, 20 °C and 35 °C were collected.

### 3.5.4 Luminescence Quantum Yields at Air Saturation

The unmodified BF<sub>2</sub>-chelates (BF<sub>2</sub>HPhN and BF<sub>2</sub>HBAN) and the perfluoroalkylated dyes (BF<sub>2</sub>HBANPF, Al(HPhNPF)<sub>3</sub>, Al(HBANPF)<sub>3</sub>) were measured in concentrations of 0.2 wt% in polystyrene and Teflon® AF 1600, respectively. The excitation wavelength was always 410 nm. For every dye four measurements were conducted: first the absorption background of the integrating sphere was measured by scanning over the excitation wavelength. Then the emission background was recorded. Afterwards several layers of the stained foil were inserted and the dye absorption and emission measured. The absorption experiments were conducted with a 5 % filter for the unmodified dyes and the combination of a 5 % and a 25 % neutral density filter for the perfluoroalkylated dyes. For the FluoroLog® 3 settings during the measurement see table 3.7.

The software FluorEssence from Horiba Scientific was used to calculate the quantum yields. The amount of absorbed light was determined by subtracting the areas of the transmitted excitation light with and without the sample. The emitted light area was calculated by integrating the fluorescence peaks and subtracting the background emission. Because neutral density filters were used for measuring the absorbed light, the obtained absorption values were corrected with the transmittances of the filters (filter factor (FF)). See eq. 3.7 for the calculation of the

**Table 3.7:** Settings for the measurements of the oxygenated quantum yields

Dye	Meas.	Exc. [nm]	Exc. Slit [nm]	Filter [%]	FF <sup>a</sup>	Emi. [nm]	Emi. Slit [nm]
BF <sub>2</sub> HPhN	transm.	410	4	5	37.8	390–430	5
	emission	410	4	–		420–700	5
BF <sub>2</sub> HBAN	transm.	410	4	5	37.8	390–430	5
	emission	410	4	–		420–700	5
BF <sub>2</sub> HBANPF	transm.	410	5	5 + 25	148	390–430	7
	emission	410	5	–		420–700	7
Al(HPhNPF) <sub>3</sub>	transm.	410	5	5 + 25	148	390–430	7
	emission	410	5	–		420–700	7
Al(HBANPF) <sub>3</sub>	transm.	410	5	5 + 25	148	390–430	7
	emission	410	5	–		420–700	7

<sup>a</sup> Filter factor, calculated with the filter transmittances at 410 nm.(2.64 % and 25.4 % for the 5 % and 25 % filters, respectively)

oxygenated prompt fluorescence quantum yields.

$$QY_{pF} = \frac{(A_{transBG} - A_{trans}) \cdot FF}{A_{emi} - A_{emiBG}} \quad (3.7)$$

Where  $QY_{pF}$  is the quantum yield,  $FF$  is the neutral density filter transmittance (at the corresponding wavelength).  $A_{trans}$ ,  $A_{emi}$ ,  $A_{transBG}$  and  $A_{emiBG}$  are the integrated areas of the transmittance and emission spectra and the respective backgrounds. The measured areas and calculated quantum yields can be seen in table 9.1 in the appendix on page 115.

### 3.5.5 Anoxic Quantum Yields

To obtain the oxygen free quantum yields of delayed fluorescence and phosphorescence the necessary areas were determined by measuring the emission spectra at oxygen free and air saturated conditions(see table 3.8 for the FluoroLog® 3 settings and table 9.2 for the obtained areas and used integration ranges). The phosphorescence area  $A_P$  was determined by subtracting the fluorescence peak from the deoxygenated spectrum. This was done by adapting the oxygenated phosphorescence-free emission spectrum to the full height of the combined prompt and delayed fluorescence emissions with the ratio of the intensities  $C$  (eq. 3.8). See table 9.2 in the appendix on page 116 for the calculated areas.

$$I_P = I_{deox} - I_{pF} \cdot C \quad (3.8)$$

$$\text{with } C = \frac{I_{pF+dF}^{peak}}{I_{pF}^{peak}}$$

**Table 3.8:** Measurement settings for the oxygenated and deoxygenated emission spectra.

Dye	Exc. [nm]	Exc. Slit [nm]	R	Filter [%]	cR <sup>a</sup>	Emi. Range [nm]	Emi. Slit [nm]
BF <sub>2</sub> HPhN	425	3	0.71	5	0.023	440–700	10
BF <sub>2</sub> HBAN	434	2	0.30	5	0.011	450–700	10
BF <sub>2</sub> HBANPF	428	3	0.62	5	0.021	440–705	10
Al(HPhNPF) <sub>3</sub>	437	3	0.68	5	0.024	450–700	10
Al(HBANPF) <sub>3</sub>	427	3	0.68	5	0.023	450–700	10

All spectra recorded at 20°.

<sup>a</sup> Value for intensity comparison purposes calculated from the measured *R*-value and the actual filter transmittance.

The areas were set in relation (see eqs. 3.9 to 3.11) and the quantum yields calculated.  $QY_{pF+dF+P}$ ,  $QY_{pF}$ ,  $QY_P$  and  $QY_{dF}$  are the respective quantum yields for fluorescence and phosphorescence, prompt fluorescence, phosphorescence and delayed fluorescence and  $A_{pF+dF+P}$ ,  $A_P$  and  $A_{pF}$  the corresponding areas. See table 9.2 for the calculated quantum yields.

$$QY_{pF+dF+P} = \frac{A_{pF+dF+P}}{A_{pF}} \cdot QY_{pF} \quad (3.9)$$

$$QY_P = \frac{A_P}{A_{pF}} \cdot QY_{pF} \quad (3.10)$$

$$QY_{dF} = QY_{pF+dF+P} - QY_{pF} - QY_P \quad (3.11)$$

### 3.5.6 Measurement of the Photochemical Stabilities

The photochemical stability of the unmodified BF<sub>2</sub>HPhN and BF<sub>2</sub>HBAN-chelates (0.5 wt% in polystyrene) and the perfluoroalkylated Al(HPhNPF)<sub>3</sub> and Al(HBANPF)<sub>3</sub> complexes (0.5 wt% in Teflon® AF 1600) was measured. The foils were attached to the wall of a glass cuvette. Then they were exposed to the light of a focused blue power led, which was run at 7.3 W under ambient atmosphere. This power equals a photon flux of 4000 μmol s<sup>-1</sup> m<sup>-2</sup>. Before the first

exposure and every 10 minutes, the absorption of the foils was recorded from 300 nm to 800 nm in fast acquisition mode. The absorptions of those individual measurements plotted against the illumination time yielded the bleaching curves.

### 3.5.7 Measurement of the Luminescence Intensity Dependency on Excitation Light

The emission spectra of BF<sub>2</sub>HBAN, Al(HPhNPF)<sub>3</sub> and Al(HBANPF)<sub>3</sub> (all 0.05 wt% in Teflon® AF 1600) in a sodium sulfite solution were recorded with different excitation light intensities. To measure in a longer intensity range two different emission slit settings were used. Wide and narrow emission slits were used for low and high excitation energies respectively (see table 3.9). Exact steps in the intensities were obtained by using neutral density filters (no filter, 75 %, 50 %, 25 %, 10 % and 5 % (narrow slit) and 10 %, 5 %, 10 + 75 %, 10 + 50 %, 10 + 25 %, 10 + 5 %, 5 + 75 %, 5 + 50 % and 5 + 25 % (wide slit)) See the calculated *cR*-values in the appendix in table 9.6 on page 125. To combine both ranges into one graph the spectra with a 10 % filter were set in relation and all values with a wide slit converted by this value (eq. 3.12).

$$I_{narrow} = \frac{I_{narrow_{10\%}}}{I_{wide_{10\%}}} \cdot I_{wide} \quad (3.12)$$

**Table 3.9:** FluoroLog® 3 settings for the intensity dependency measurements.

Dye	Excitation [nm]			Emission [nm]		
	Wavelength	Slit	R	Range	Slit High	Slit Low
BF <sub>2</sub> HBANPF	428	9	4.7	448-700	2	8
Al(HPhNPF) <sub>3</sub>	437	9	4.7	460-700	2	8
Al(HBANPF) <sub>3</sub>	427	9	4.8	450-700	2	8

## 3.6 Lifetime Measurements with FluoroLog Kinetic Acquisition

The lifetime measurements with the FluoroLog® 3 were done using the kinetic acquisition mode. The sensor layer was illuminated till it reached a constant phosphorescence (or fluorescence) intensity. Then the shutter was closed and the decreasing luminescence intensities were recorded (with a time resolution of 0.01 points/s and an equally long integration time). The shutter was open for three seconds and then closed for three seconds alternating. This experiment was

repeated multiple times. The decay curves were extracted and fitted with eq. 3.13. Then the obtained decay times were averaged.

$$I = I_{offset} + I_0 \cdot e^{-\frac{t}{\tau}} \quad (3.13)$$

### 3.6.1 Anoxic Lifetimes

The oxygen free lifetimes were measured in a 25 g L<sup>-1</sup> sodium sulfite solution with a small amount of cobalt(II) chloride to catalyse the oxygen consumption. The lifetimes were determined for BF<sub>2</sub>HPhN and BF<sub>2</sub>HBAN in polystyrene, for BF<sub>2</sub>HBANPF in Teflon® AF 1600, for Al(HPhNPF)<sub>3</sub> in Teflon® AF 1600, Hyflon® AD 60, Cytop® CTL-809A and Cytop® CTL-107MK and for Al(HBANPF)<sub>3</sub> in Teflon® AF 1600, Teflon® AF 2400, Hyflon® AD 60 and Cytop® CTL-809A. All measurements were done at 20 °C, except for two measurements of Al(HPhNPF)<sub>3</sub> in Hyflon® AD 60, which were conducted at 5 °C and 35 °C to characterize the temperature behavior of the dye. The utilized dye concentration was always 0.01 wt% and 0.05 wt% for the unmodified and for the perfluoroalkylated dyes, respectively. See table 3.10 for the FluoroLog® 3 settings.

### 3.6.2 Anoxic Lifetime Intensity Dependency

The lifetimes of BF<sub>2</sub>HBANPF, Al(HPhNPF)<sub>3</sub> and Al(HBANPF)<sub>3</sub> (0.05 wt% in Teflon® AF 1600) were measured. For the FluoroLog® 3 settings see table 3.11. The intensity was varied with neutral density filters. 5 + 25 %, 5 %, 10 % and 50 % filters and no filter were used for the measurements. With respective emission slits of 14 nm, 10 nm, 8 nm, 3 nm and 2 nm. Additionally measurements with lower excitation intensities with Al(HPhNPF)<sub>3</sub> in Hyflon® AD 60 with none, a 50 %, a 25 % and a 10 % filter were conducted. The measurement with no filter was done as first and last experiment to ensure constant deoxygenated conditions. The obtained decay curves were fitted with mono-exponential decay functions.

### 3.6.3 Lifetimes Intensity Dependency at Trace Oxygen Levels

The change of the phosphorescence lifetime in presence of small amounts of oxygen (around 1.5 ppmv) of Al(HBANPF)<sub>3</sub> (0.05 wt% in Teflon® AF 1600) was measured in dependency on the excitation light intensity. The used excitation wavelength was 427 nm, the excitation slit was 5 nm ( $R = 1.6$ ), the set emission wavelength was 570 nm and the emission slit was 10 nm. 5 %, 10 %, 25 % and 50 % neutral density filters were used to set the light intensities. Additionally a measurement with a 10 nm excitation slit and 2 nm emission slit ( $R = 4.9$ ) was conducted to obtain values at even higher excitation energies.

**Table 3.10:** Settings for the measurements of the deoxygenated lifetimes.

Dye	Matrix	Exc. [nm]	Slit [nm]	Filter [%]	R	cR <sup>a</sup>	Slit [nm]	Emi. [nm]
BF <sub>2</sub> HPhN	Polystyrene	452	2	10	0.23	0.021	12	544
BF <sub>2</sub> HBAN	Polystyrene	440	2	10	0.22	0.018	12	570
BF <sub>2</sub> HBANPF <sup>b</sup>	Teflon® AF 1600	428	7	10	2.8	0.221	12	567
Al(HPhNPF) <sub>3</sub>	Teflon® AF 1600	435	3	10	0.52	0.042	12	575
Al(HPhNPF) <sub>3</sub> <sup>c</sup>	Hyflon® AD 60	435	3	10	0.50	0.041	12	575
Al(HPhNPF) <sub>3</sub>	Cytop® CTL-809A	435	2	10	0.41	0.033	12	570
Al(HBANPF) <sub>3</sub>	Teflon® AF 1600	435	3	10	0.52	0.042	12	575
Al(HBANPF) <sub>3</sub>	Teflon® AF 2400	427	6	5	2.4	0.081	10	575
Al(HBANPF) <sub>3</sub>	Hyflon® AD 60	430	3	10	0.52	0.042	12	575
Al(HBANPF) <sub>3</sub>	Cytop® CTL-809A	435	2	10	0.41	0.033	12	570
Al(HBANPF) <sub>3</sub> <sup>d</sup>	Cytop® CTL-107MK	430	3	10	0.52	0.041	12	580

The spectra were recorded at 20°.

<sup>a</sup> Value for intensity comparison purposes calculated from the measured  $R$  intensity value and the actual filter transmittances.

<sup>b</sup> Measured in a 10 g L<sup>-1</sup> Na<sub>2</sub>S<sub>2</sub>O<sub>5</sub> solution.

<sup>c</sup> Measured at 5°, 20° and 35°.

<sup>d</sup> Measured in N<sub>2</sub>-atmosphere (purged 1 h). Completely deoxygenated due to the strong chemical oxygen consumption.

**Table 3.11:** FluoroLog® 3 settings for the deoxygenated lifetime intensity dependency measurements

Dye	Exc. [nm]	Exc. Slit [nm]	R	Emi. [nm]	Emi. Slit [nm]
BF <sub>2</sub> HBANPF	426	10	5.6	570	2–14
Al(HPhNPF) <sub>3</sub>	437	10	5.4	570	2–14
Al(HBANPF) <sub>3</sub>	427	10	5.5	570	2–14
Al(HPhNPF) <sub>3</sub> <sup>a</sup>	435	3	0.5	495	12

<sup>a</sup> in Hyflon® AD 60

### 3.7 Lifetime Measurements with Single Photon Counting

The lifetimes of BF<sub>2</sub>HBANPF, Al(HPhNPF)<sub>3</sub> and Al(HBANPF)<sub>3</sub> (all with 0.05 wt% in Teflon® AF 1600) were measured. The foils were submerged in a 25 g L<sup>-1</sup> sodium sulfite solution with catalytic amounts of cobalt chloride. The emitted light was collected at a 90° angle. The high voltage of the photomultiplier was 1450 V and the acquisition window 5.6 s. For the specific emission monochromator settings see table 3.12. The obtained data were fitted with a mono- and a bi-exponential decay function for Al(HPhNPF)<sub>3</sub> and the HBANPF complexes respectively (eq. 3.14 and eq. 3.15). The fitting parameters can be seen in table 3.13.

**Table 3.12:** Single photon counting emission monochromator settings

	Fluorescence		Phosphorescence	
	Emi. [nm]	Slit [nm]	Emi. [nm]	Slit [nm]
BF <sub>2</sub> HBANPF	457	5	567	5
Al(HPhNPF) <sub>3</sub>	485	4	575	4
Al(HBANPF) <sub>3</sub>	485	1	575	3

$$I = I_{offset} + A \cdot e^{-\frac{t}{\tau}} \quad (3.14)$$

$$I = I_{offset} + A \cdot e^{-\frac{t}{\tau_1}} + B \cdot e^{-\frac{t}{\tau_2}} \quad (3.15)$$

**Table 3.13:** Fitting parameters and results of the single photon counting lifetime measurements

Dye		$I_{offset}$	$A_1$	$A_1^{rel}$ [%]	$A_2$	$A_2^{rel}$ [%]	$\tau_1$ [ms]	$\tau_2$ [ms]
BF <sub>2</sub> HBANPF	fluor.	17.1	5557	81.3	2611	18.7	545	266
BF <sub>2</sub> HBANPF	phos.	43.6	18854	88.1	5643	11.9	512	232
Al(HPhNPF) <sub>3</sub>	fluor.	18.3	8021	92.9	1397	7.1	250	110
Al(HPhNPF) <sub>3</sub>	phos.	16.8	23969	100	—	—	251	—
Al(HBANPF) <sub>3</sub>	fluor.	59.8	14818	84.2	9408	15.8	357	106
Al(HBANPF) <sub>3</sub>	phos.	60.5	13011	88.1	6512	11.9	365	99

## 3.8 Calibration by controlled oxygen consumption of Sodium Ascorbate

A 30 mL glass vial was equipped with a Pd-benzoporphyrin in Teflon® AF 1600 and a Pd-benzoporphyrin in polystyrene sensor (glued to the walls with silicone E4). The sensors were read out with a four channel FireSting O<sub>2</sub>. Prior to the measurements the sealing was submerged in a sodium sulfite solution for at least 10 min to remove stored oxygen. During the measurement the cap of the vial was submerged in a sodium sulfite solution. The first calibration point of the Pd-benzoporphyrin in polystyrene and Teflon® AF 1600 sensors was N<sub>2</sub> ( $\phi_0 = 46.518^\circ$  and  $\phi_0 = 49.451^\circ$ , respectively). The second point was air ( $\phi = 5.652^\circ$ ) for the polystyrene sensor and 0.1 % O<sub>2</sub> test gas ( $\phi = 19.627^\circ$ ) for the Teflon® AF 1600 sensor.

The measurement was conducted in a 200 mM MES buffer with pH 5.6 with a sodium ascorbate concentration of 5 g L<sup>-1</sup>. After addition of the sodium ascorbate the vial was closed without air bubbles and stirred with a magnetic stirring bar throughout the reaction. The reaction was stopped after 3.5 h.

## 3.9 Intensity Calibrations

All of the following calibrations were done in a FluoroLog® 3 with kinetic acquisition mode. The phosphorescence emissions of the dyes were used for all calibrations (not the delayed fluorescence). All calibrated sensors were coated on glass slides and measured in the trace measurement cell which was connected only with metal tubes and fittings. The temperature of the measurement cell was controlled with a thermostat which was set to 20 °C for all calibrations except the temperature dependency measurements.

The measuring cell was purged at least 30 min for the zero values, 20 min for the lowest calibration points and 15 min for every other concentration. In the last five minutes of every concentration three kinetic measurements (5 s, 0.1 points/s) with one minute delay after every measurement were conducted. Additionally a fluorescence background under normal atmosphere was recorded in the same way which was deducted from every value. The average values of the last measurement seconds were used for the evaluation.

### 3.9.1 Calibrations of BF<sub>2</sub>HPhN in Polystyrene

The calibrated sensor contained 0.01 wt% dye in polystyrene and had a layer thickness of approximately 23 µm. The excitation and emission monochromators were set to 452 nm wavelength and 2 nm slit and 544 nm wavelength and 12 nm slit respectively (excitation *R*-value of 0.22).

Additionally a 10 % neutral density filter was used on the excitation side (corrected  $cR$  value of 0.020).

The phosphorescence lifetime was measured four times (330 ms, 331 ms, 336 ms and 336 ms)  $\hat{=}$   $333 \pm 4$  ms (deoxygenated:  $(354 \pm 5)$  ms see table 4.3)). To obtain the calibration curve the gas mixer was used to set O<sub>2</sub> concentrations of 0 ppmv, 20 ppmv, 40 ppmv, 60 ppmv, 80 ppmv and 120 ppmv by mixing test gas with 0.1 v% oxygen and nitrogen 5.0. The calibration curve was recorded three times. No lifetime correction of  $I_0$  was used.

### 3.9.2 Calibrations of BF<sub>2</sub>HBAN in Polystyrene

The calibrated sensor contained 0.01 wt% dye in polystyrene and had a layer thickness of approximately 23  $\mu$ m. The excitation and emission monochromators were set to 452 nm wavelength and 2 nm slit and 544 nm wavelength and 12 nm slit respectively (excitation  $R$ -value of 0.22). Additionally a 10 % neutral density filter was used on the excitation side (corrected  $cR$  value of 0.020).

The phosphorescence lifetime was measured six times (683 ms, 686 ms, 696 ms, 680 ms, 688 ms and 699 ms)  $\hat{=}$   $689 \pm 8$  ms (deoxygenated:  $734 \pm 1$  ms see table 4.3 page 68)). To obtain the calibration curve the gas mixer was used to set O<sub>2</sub> concentrations of 0 ppmv, 20 ppmv, 40 ppmv, 60 ppmv, 80 ppmv and 120 ppmv by mixing test gas with 0.1 v% oxygen and nitrogen 5.0. The calibration curve was recorded three times. No lifetime correction of  $I_0$  was used.

### 3.9.3 Calibrations of Al(HPhNPF)<sub>3</sub> in Teflon® AF 1600

The calibrated sensor contained 0.05 wt% dye in Teflon® AF 1600 and had a layer thickness of approximately 23  $\mu$ m. The excitation and emission monochromators were set to 435 nm wavelength and 3 nm slit and 575 nm wavelength and 12 nm slit respectively (excitation  $R$ -value of 0.51). Additionally a 10 % neutral density filter was used on the excitation side (corrected  $cR$  value of 0.041).

The phosphorescence lifetime was measured seven times (135 ms, 133 ms, 128 ms, 125 ms, 131 ms, 133 ms and 129 ms)  $\hat{=}$   $131 \pm 4$  ms (deoxygenated:  $244 \pm 1$  ms see table 4.3)). To obtain the calibration curve the gas mixer was used to set O<sub>2</sub> concentrations of 0 ppmv, 1 ppmv, 2 ppmv, 3 ppmv, 4 ppmv, 5 ppmv and 6 ppmv by mixing test gas with 20.2 ppmv oxygen and nitrogen 5.0. The calibration curve was recorded three times. The deoxygenated intensity  $I_0$  was corrected by the ratio of the measured and the oxygen-free lifetimes ( $\frac{244\text{ms}}{131\text{ms}} = 1.86$ ). Furthermore all concentrations were corrected by the determined contamination of 1.2 ppmv.

### 3.9.4 Calibrations of Al(HPhNPF)<sub>3</sub> in Hyflon® AD 60

The calibrated sensor contained 0.05 wt% dye in Hyflon® AD 60 and had a layer thickness of approximately 30 µm. The excitation and emission monochromators were set to 435 nm wavelength and 3 nm slit and 575 nm wavelength and 12 nm slit respectively (excitation  $R$ -value of 0.50). Additionally a 10 % neutral density filter was used on the excitation side (corrected  $cR$  value of 0.041).

The phosphorescence lifetime was measured five times (215 ms, 210 ms, 210 ms, 216 ms and 203 ms)  $\hat{=}$  211 ± 6 ms (deoxygenated: 253 ± 4 ms see table 4.3)). To obtain the calibration curve the gas mixer was used to set O<sub>2</sub> concentrations of 0 ppmv, 2 ppmv, 4 ppmv, 6 ppmv, 8 ppmv, 10 ppmv and 12 ppmv by mixing test gas with 20.3 ppmv oxygen and nitrogen 5.0. The deoxygenated intensity  $I_0$  was corrected by the ratio of the measured and the oxygen-free lifetimes ( $\frac{253\text{ ms}}{211\text{ ms}} = 1.20$ ). Furthermore all concentrations were corrected by the determined contamination of 0.44 ppmv.

### 3.9.5 Calibration of Al(HPhNPF)<sub>3</sub> in Hyflon® AD 60 at 5°C and 35°C

Calibration curves of Al(HPhNPF)<sub>3</sub> in Hyflon® AD 60 were recorded at 5 °C and 35 °C additionally to the 20 °C measurement. All settings, the excitation intensities and the calibration concentrations were the same as the 20 ms calibration. The measured lifetimes for the  $I_0$ -measurements were 209 ms, 209 ms, 206 ms and 208 ms  $\hat{=}$  208 ± 2 ms (deoxygenated: 283 ± 2 ms) and 215 ms, 219 ms, 220 ms and 217 ms (deoxygenated: 218 ± 3 ms) for 5 °C and 35 °C, respectively. The deoxygenated intensity  $I_0$  was corrected by the ratio of the measured and the oxygen-free lifetimes ( $\frac{253\text{ ms}}{211\text{ ms}} = 1.20$ ). Furthermore all concentrations were corrected by the determined contamination of 0.44 ppmv.

### 3.9.6 Calibration of Al(HPhNPF)<sub>3</sub> in Hyflon® AD 60 with Higher and Lower Intensities

Calibration curves of Al(HPhNPF)<sub>3</sub> in Hyflon® AD 60 were recorded with a 5 and a 25 % neutral density filter (with  $cR$  values of 0.14 and 0.018, respectively (0.041 with the previously used 10 % filter)). All settings and the calibration concentrations were the same as the 10 % filter calibration. The measured lifetimes for the  $I_0$ -measurements were 205 ms, 201 ms, 194 ms, 193 ms and 202 ms  $\hat{=}$  199 ± 6 ms and 221 ms, 223 ms, 223 ms, 224 ms and 223 ms  $\hat{=}$  223 ± 2 ms (deoxygenated: 253 ± 4 ms) for the 5 % and 25 % filters, respectively. The deoxygenated intensities  $I_0$  were corrected by the ratio of the measured and the oxygen-free lifetimes ( $\frac{253\text{ ms}}{199\text{ ms}} = 1.27$ ) and ( $\frac{253\text{ ms}}{223\text{ ms}} = 1.14$ ) for the 5 % and 25 % filters, respectively. Furthermore all concentrations were corrected by the determined contamination of 0.51 ppmv.

### 3.9.7 Calibrations of Al(HBANPF)<sub>3</sub> in Teflon® AF 1600

The calibrated sensor contained 0.05 wt% dye in Teflon® AF 1600 and had a layer thickness of approximately 23 µm. The excitation and emission monochromators were set to 430 nm wavelength and 3 nm slit and 575 nm wavelength and 12 nm slit respectively (excitation  $R$ -value of 0.52). Additionally a 10 % neutral density filter was used on the excitation side (corrected  $cR$  value of 0.042). Then the phosphorescence lifetime was measured three times (168 ms, 171 ms and 170 ms)  $\hat{=}$  170 ± 2 ms (deoxygenated: 353 ± 6 ms see table 4.3)). To obtain the calibration curve the gas mixer was used to set O<sub>2</sub> concentrations of 0 ppmv, 1 ppmv, 2 ppmv, 3 ppmv, 4 ppmv, 5 ppmv and 6 ppmv by mixing test gas with 20.2 ppmv oxygen and nitrogen 5.0. The deoxygenated intensity  $I_0$  was corrected by the ratio of the measured and the oxygen-free lifetimes ( $\frac{353\text{ ms}}{170\text{ ms}} = 2.08$ ). Furthermore all concentrations were corrected by the determined contamination of 1.7 ppmv.

### 3.9.8 Calibrations of Al(HBANPF)<sub>3</sub> in Hyflon® AD 60

The calibrated sensor contained 0.05 wt% dye in Hyflon® AD 60 and had a layer thickness of approximately 30 µm. The excitation and emission monochromators were set to 430 nm wavelength and 3 nm slit and 575 nm wavelength and 12 nm slit respectively (excitation  $R$ -value of 0.52). Additionally a 10 % neutral density filter was used on the excitation side (corrected  $cR$  value of 0.042).

The phosphorescence lifetime was measured three times (270 ms, 272 ms and 265 ms)  $\hat{=}$  269 ± 4 ms (deoxygenated: 394 ± 3 ms see table 4.3)). To obtain the calibration curve the gas mixer was used to set O<sub>2</sub> concentrations of 0 ppmv, 2 ppmv, 4 ppmv, 6 ppmv, 8 ppmv, 10 ppmv and 12 ppmv by mixing test gas with 20.2 ppmv oxygen and nitrogen 5.0. The deoxygenated intensity  $I_0$  was corrected by the ratio of the measured and the oxygen-free lifetimes ( $\frac{394\text{ ms}}{269\text{ ms}} = 1.46$ ). Furthermore all concentrations were corrected by the determined contamination of 1.2 ppmv.

### 3.9.9 Calibrations of Al(HPhNPF)<sub>3</sub> in Cytop® CTL-809A

The calibrated sensor contained 0.05 wt% dye in Cytop® CTL-809A and had a layer thickness of approximately 41 µm. The excitation and emission monochromators were set to 435 nm wavelength and 3 nm slit and 575 nm wavelength and 12 nm slit respectively (excitation  $R$ -value of 0.50). Additionally a 10 % neutral density filter was used on the excitation side (corrected  $cR$  value of 0.041).

The phosphorescence lifetime was measured five times (321 ms, 331 ms, 324 ms, 310 ms and 328 ms)  $\hat{=}$   $323 \pm 9$  ms (deoxygenated:  $339 \pm 10$  ms see table 4.3)). To obtain the calibration curve the gas mixer was used to set O<sub>2</sub> concentrations of 0 ppmv, 10 ppmv, 20 ppmv, 30 ppmv, 40 ppmv, 50 ppmv and 60 ppmv by mixing test gas with 0.1 v% oxygen and nitrogen 5.0. No lifetime correction of  $I_0$  was used.

### 3.9.10 Calibration of Al(HBANPF)<sub>3</sub> in Cytop® CTL-107MK

The calibrated sensor contained 0.05 wt% dye in Cytop® CTL-107MK and had a layer thickness of approximately 32  $\mu$ m. The excitation and emission monochromators were set to 430 nm wavelength and 3 nm slit and 580 nm wavelength and 12 nm slit, respectively (excitation  $R$ -value of 0.52). Additionally a 10 % neutral density filter was used on the excitation side (corrected  $cR$  value of 0.042). The phosphorescence lifetime was measured three times (365 ms, 357 ms and 355 ms  $\hat{=}$   $359 \pm 6$  ms). To obtain the calibration curve the gas mixer was used to set O<sub>2</sub> concentrations of 0 ppmv, 200 ppmv, 400 ppmv, 600 ppmv, 800 ppmv and 1000 ppmv by mixing test gas with 0.1 v% oxygen and nitrogen 5.0. The calibration curve was recorded three times.

Due to the very strong drift of the kinetic intensity curves an evaluation of the calibration was not possible.

The foil was placed for 3 min under a strong UV-lamp to condition the sensors and attempt to saturate the oxidizable groups. Then a new calibration attempt was undertaken with the same settings and concentration, but a excitation slit width of only 2 nm and thus a lower intensity ( $R = 0.22$  and  $cR = 0.018$ ). The drifting was again too strong to evaluate the calibration.

The sensor was again placed under the UV-lamp (20 min total). Then another calibration was tried. The FluoroLog® 3 was set to the settings of the first calibration but the concentrations were set to 0 ppmv, 10 ppmv, 20 ppmv, 30 ppmv, 40 ppmv, 50 ppmv and 60 ppmv. Again it was impossible to evaluate the calibration due to the very high drift.

## 3.10 Lifetime Calibration of Al(HPhNPF)<sub>3</sub> in Hyflon® AD 60

The calibrated sensor contained 0.05 wt% dye in Hyflon® AD 60 and had a layer thickness of approximately 30  $\mu$ m. The excitation and emission monochromators were set to 435 nm wavelength and 3 nm slit and 575 nm wavelength and 12 nm slit respectively (excitation  $R$ -value of 0.50). Additionally a 10 % neutral density filter was used on the excitation side (corrected  $cR$  value of 0.041).

The calibration curve was recorded by mixing test gas with 20.3 ppmv oxygen with nitrogen 6.0 in the range of 0 % to 25 % test gas (0 ppmv to 5.075 ppmv) and a overall flow of 200 mL min<sup>-1</sup>.

The measurements were conducted with kinetic experiments (32 s and a integration time of 0.01 s) and opening or closing the shutter every 3 s. The obtained decay curves were fitted with an exponential decay function and the averages calculated (see table 4.11). They were used together with the deoxygenated lifetime (269 ms) to calculate the  $\tau_0/\tau - 1$  values which were plotted against the set oxygen concentration. With a linear fit  $K_{SV}$  and the y-axis intercept were determined and the oxygen contamination of 0.69 ppmv calculated.

### 3.11 Measurement of Oxygen Traces in Gases

Five different gas bottles (N<sub>2</sub> 5.0 10 L; N<sub>2</sub> 6.0 10 L; CO<sub>2</sub> 100% 10 L, CO<sub>2</sub> 0.2% 10 L and N<sub>2</sub> 5.0 50 L) were connected directly via a steel tube to the measuring cell. The pressure reducer was set to 0.5 bar and the system was purged for 5 min. The lifetimes of a Al(HPhNPF)<sub>3</sub> (0.05 wt% in Hyflon® AD 60) sensor were recorded with the same settings that were used in its lifetime calibration (see section 3.9.8). The calibration parameters were  $\tau_0 = 269$  ms and  $K_{SV} = 0.390$  ppmv<sup>-1</sup>.

### 3.12 Monitoring of Oxygen consumption by Glucose Oxidase with four Sensors

A 25 mL glass vial with a metal seal was equipped with four different oxygen sensors. Two commercially available sensors from PyroScience (a Pd and a Pt benzoporphyrin in polystyrene) coated on Mylar® foils were attached to the glass wall with a Silicone E4 glue and read out with a four channel FireSting O<sub>2</sub> device. A trace Pt-TPFPP in Hyflon® AD 60 sensors was mounted on the bottom of the vial and a ultra-trace Al(HPhNPF)<sub>3</sub> in Hyflon® AD 60 sensor on a glass support, was fixed via two E4 glued edges to the vial. The latter was read-out with a FluoroLog® 3. The polystyrene sensors were calibrated with a two-point calibration in air saturated water and oxygen free sodium sulfite solution. The Pt-TFPP sensor was calibrated with the deoxygenated value and the Al(HPhNPF)<sub>3</sub> sensor after the experiment with a lifetime and intensity measurement.

During the experiment the vial was upside down and the lid submerged in a sodium sulfite solution to avoid contamination by surrounding oxygen. For the measurement 30 mL 20 mM Tris-buffer with pH 7 were mixed with 5 mL of a 10 mg L<sup>-1</sup> glucose oxidase solution (from *Aspergillus niger*) and 1 mL catalase solution (from bovine liver, small amount dissolved in 25 mL water). The solution was mixed and filled in the reaction vial fast without any air bubbles. The reaction was tracked for 580 min with approximately one measurement point per

minute (exc. wavelength = 435 nm , exc. slit = 3 nm, filter = 10 %, emi. wavelength = 575 nm, emi. slit = 12 nm, integration time = 0.5 s, measurement time = 5 s)

To evaluate the  $\text{Al}(\text{HPhNPF})_3$  sensor measurements the phosphorescence intensity and lifetime (180 ms and 187 ms  $\hat{=}$   $184 \pm 5$  ms) (deoxygenated: 253 ms) were determined after 12 h and  $I_0$  calculated ( $I_0 = \frac{\tau_0}{\tau} \cdot I$ ). The average of the first ten measurements was used as the quenched fluorescence background. With these values and the in section 3.9.8 measured  $K_{SV}$  of  $0.418 \text{ ppmv}^{-1}$  the oxygen concentrations were determined. The average of the measurements between 0.5 s to 1.5 s was used.



---

## 4 Results and Discussion

### 4.1 Synthesis

#### 4.1.1 Perfluoroalkylation of HPhN and HBAN

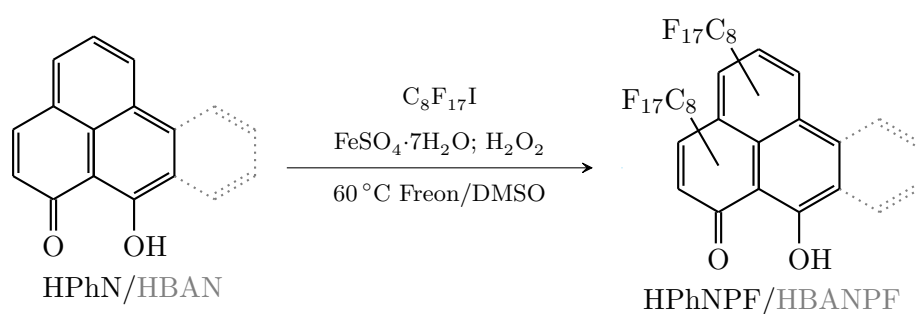


**Figure 4.1:** General reaction scheme for the perfluoroalkylation of HPhN and HBAN

The modification of the dyes with  $\text{C}_8\text{F}_{17}$ -groups was done with quite harsh reaction conditions based on the work of Bravo et al. [35]. The reaction temperature was low with only  $40^\circ\text{C}$  but the mixture of  $\text{FeSO}_4$  and  $\text{H}_2\text{O}_2$  created various radicals (e.g.  $\text{HO}^\cdot$  and  $\text{HOO}^\cdot$ ) [41, 42]. This radical mixture is extremely reactive and is even used for waste water treatment to decompose diverse non-biodegradable organic compounds [43]. In the perfluoroalkylation reaction the radicals are used to generate perfluorooctyl-radicals ( $\text{C}_8\text{F}_{17}^\cdot$ ) which react with the respective ligand (HPhN or HBAN). Radical reactions are quite common for perfluoroalkyl iodides [33] and the stereoselectivity is controlled by the formation of the most stable adducts between perfluoroalkyl-radical and ligand [34]. However both unselective and oxygen-alkylation are possible side-reactions (although O-alkylation was only observed for non-fluorinated alkyl iodides)[36].

The main product of the reactions is the two-fold modified ligand. It could be isolated only in moderate yields of 13 % and 23 % for HPhNPF and HBANPF, respectively. This is probably due to a very broad product spectra which is generated during the reaction. Possible side reactions include (oxidated) decomposition of the ligands, modification on the OH-group and only one-fold perfluoroalkylation. In the case of the bigger  $\text{BF}_2\text{HBANPF}$  ligand threefold modification could be seen in the mass spectra. This side product is very hard to separate

due to the very similar polarity. However the expected optical properties were very alike so no further purification was carried out and the mixture of both varieties was used.

Noteworthy is the fact that the radical reaction was quite selective. Both perfluorooctyl-groups of the isolated products were always attached to the same positions. This could be seen in the  $^1\text{H-NMR}$  (see fig. 9.1 and fig. 9.3 in the appendix on pages 103 and 105) where all found hydrogen atoms had intensities of around 1.0 and two were completely missing. An exact identification of the substituted positions on the ligand was not possible but the structure could be narrowed down with the COSY spectra to five possible structures for HPhNPF and HBANPF (see fig. 4.2).

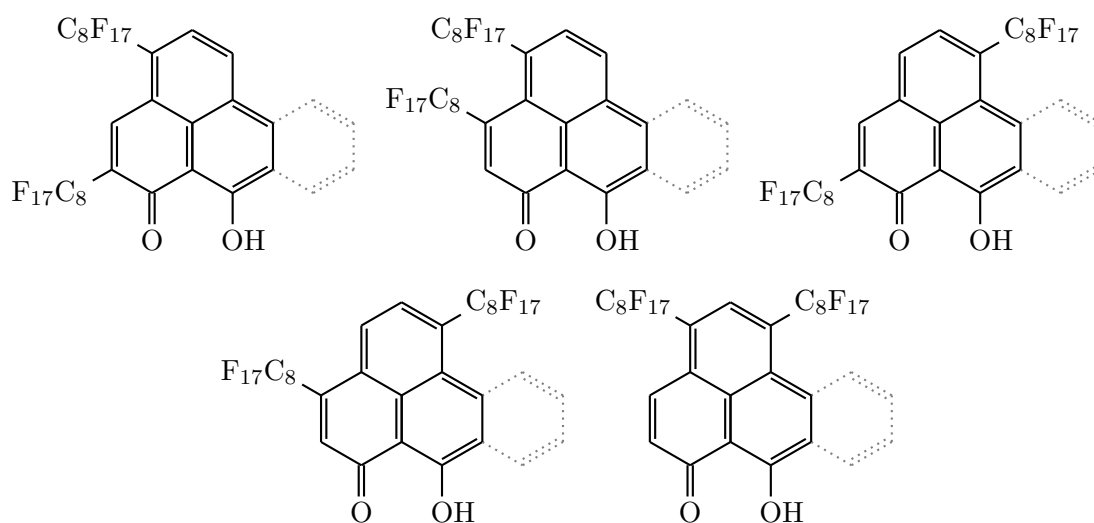


**Figure 4.2:** Possible structures of the synthesized HPhNPF and HBANPF ligands.

The solubility of the ligands in perfluorinated solvents (e.g. freon) increased greatly. Before the modification they were completely insoluble in them and badly soluble in most solvents with low polarity. Afterwards they were readily soluble in perfluorinated solvents and had acceptable solubilities in many other solvents. Therefore it was expected that the derived  $\text{BF}_2$ -chelates (with no OH-groups) and even more so the Al-complexes (also no OH-groups and a nearly globular structure with  $\text{C}_8\text{F}_{17}$ -groups in all directions) would show even better solubility and great compatibility with perfluorinated polymers.

#### 4.1.2 Synthesis of $\text{BF}_2\text{HPhNPF}$

Although the chelate proved to be unstable the formation reaction could be driven to completion with a high  $\text{BF}_3 \cdot \text{Et}_2\text{O}$  excess. The reaction progress was followed with UV-VIS spectroscopy. However during any workup (e.g. extraction, chromatography) it would decompose slowly (see fig. 4.4). The decomposition was especially fast on a aluminium oxide column. The

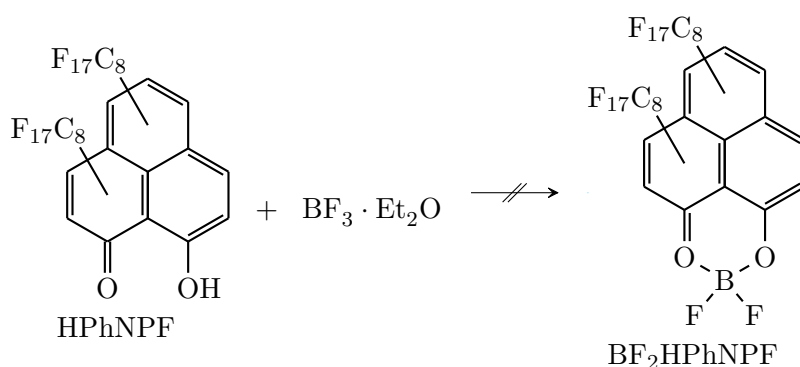


**Figure 4.3:** Reaction scheme of the  $\text{BF}_2$ -chelation of HPhNPF

chelate dissociated fast and the ligand bound itself to the aluminium oxide and could not be eluted. Thus it was impossible to isolate the pure product. It was expected that the chelate would be more stable embedded in a polymer. However more stable dyes were available ( $\text{BF}_2\text{HBANPF}$ ,  $\text{Al}(\text{HPhNPF})_3$  and  $\text{Al}(\text{HBANPF})_3$ ) with longer lifetimes or (at least expected) better compatibility with perfluorinated polymers thus this chelate was not used for further experiments.

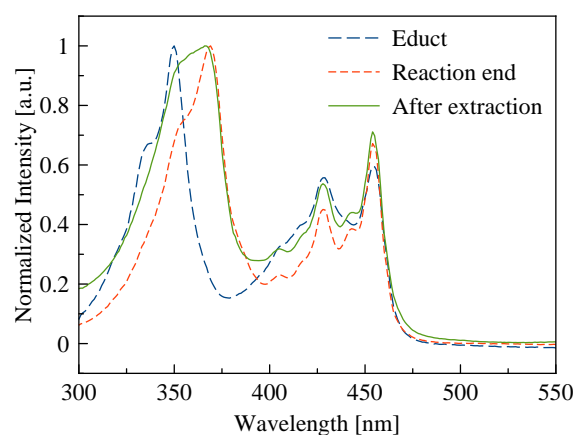


**Figure 4.4:** Normalized absorption indicating partial decomposition of the chelate during work up.

### 4.1.3 Synthesis of $\text{BF}_2\text{HBANPF}$

The synthesis of  $\text{BF}_2\text{HBANPF}$  was quite similar to the  $\text{BF}_2\text{HPhNPF}$  chelation. The reaction could be driven to completion by adding  $\text{BF}_3 \cdot \text{Et}_2\text{O}$  in excess. The main difference was that  $\text{BF}_2\text{HBANPF}$  proved to be more stable. It showed also signs of decomposition during the workup procedures but at a much slower rate. It was possible to concentrate it over with a silica-gel chromatographic column. However some free ligand remained in the product. It

could be eliminated by filtrating the product over a  $\approx 1$  cm high aluminium oxide layer (see fig. 4.6). The main drawback of this method is that it is impossible to elute the bound ligand afterwards. In fact this purification method shows the high affinity of the ligand to aluminium and furthermore proves that the HBANPF  $\text{BF}_2$ -chelate is the more stable one.

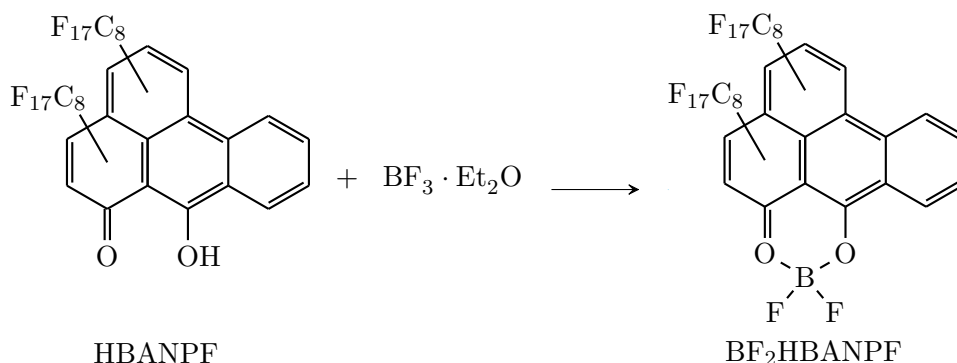


**Figure 4.5:** Reaction scheme of the  $\text{BF}_2$ -chelation of HBANPF

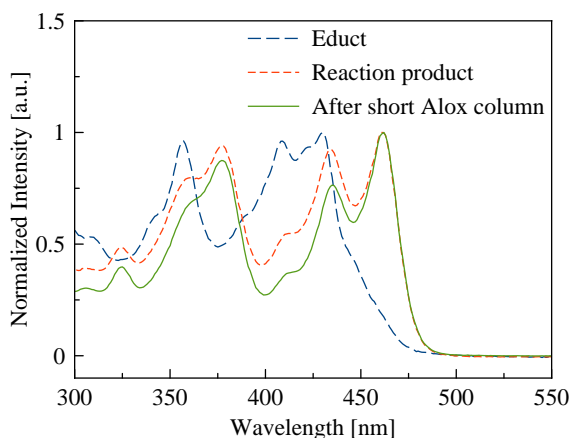


**Figure 4.6:** Normalized absorption spectra showing the spectral change during the reaction and the efficiency of the purification with a short Alox column.

#### 4.1.4 Synthesis of the Aluminium-Complexes

The Al-complexation reaction was similar to the  $\text{BF}_2$ -chelation reactions but imposed some additional problems and properties.

The first problem was that a common solvent for the salts  $\text{AlCl}_3$  and  $\text{NaOH}$  and the highly nonpolar two-fold perfluoroalkylated ligands had to be found. A 1:1:1 mixture of THF, EtOH and freon was utilized for this purpose. The two polar solvents (THF and EtOH) were able to solubilize the salts and due the OH-group the ligands were slightly soluble in them. The fluorinated freon was able to completely dissolve the ligands and the even more demanding

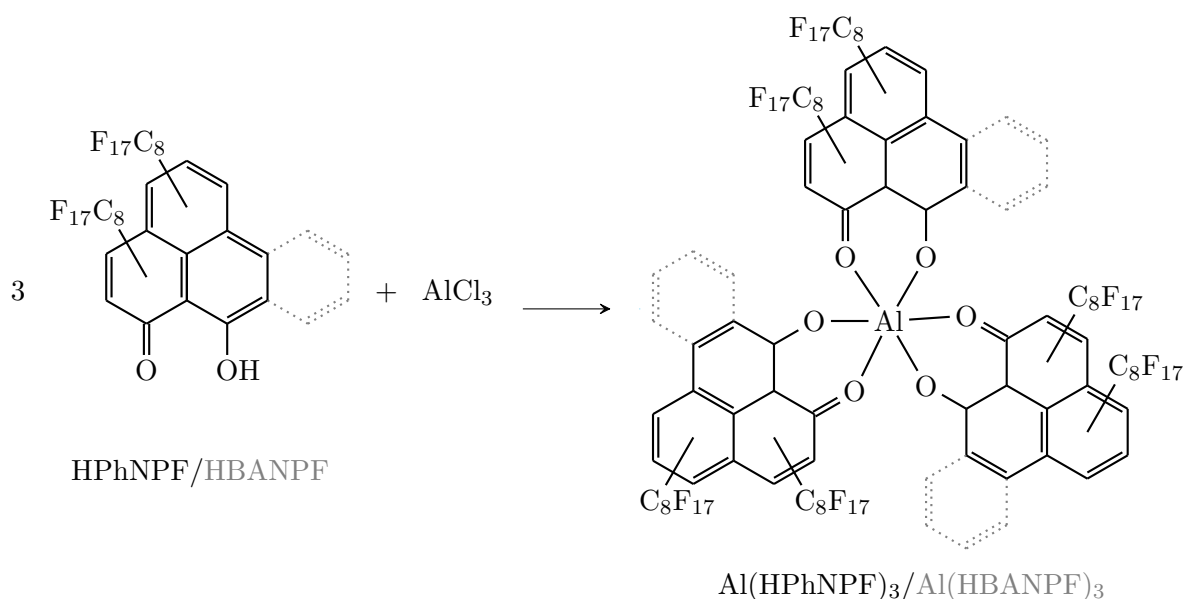


**Figure 4.7:** General reaction scheme for the Al-complex formation with HBANPF and HPhNPF.

complexes. The reaction happened probably mostly in the polar phase where all reactants were at least partly soluble and the entirely nonpolar Al-complexes (nearly globular structures with six perfluorooctyl-groups in all directions, without any accessible polar groups) migrated in the freon phase.

Secondly the stoichiometry of the reaction was 3:1 ligand: $\text{Al}^{3+}$ . Thus the formation of incomplete complex molecules with only one or two ligands was possible. This intermediate product had to be avoided at all costs because it would have decreased the yield drastically. Therefore the cheap  $\text{AlCl}_3$  was used as the limiting component and HPhNPF or HBANPF was added in a 10% excess. This made it also impossible to drive the reaction to completion by adding extra  $\text{AlCl}_3$ . Hence an incomplete conversion had to be accepted rendering the workup procedure much more challenging.

The octahedral structure of the complex and the bidentate nature of the ligands induce four different isomers. Because the formation of isomers could not be avoided, a separation was impossible and similar chemical and optical properties were expected, this mixture of closely related structures was not separated. In the case of  $\text{Al(HBANPF)}_3$  even more different structures were obtained because a small fraction of the used ligand was three-fold perfluoroalkylated. Furthermore, this third  $\text{C}_8\text{F}_{17}$ -chain may be located randomly over all available positions. Therefore a very high number of slightly different  $\text{Al(HBANPF)}_3$  complexes were present in the obtained product. As expected this large amount of structures resulted in very broad  $^1\text{H-NMR}$  peaks where only an estimation of the peak areas and ranges was possible.

The very low polarity, bad solubility in non-fluorinated solvents and possibly the many isomers made a chromatographic purification of the complexes impossible. They were only soluble well in perfluoroalkylated solvents and created very long smearing on TLCs. However the demanding solubility could be used to purify the products. By adding THF to the dry raw product, placing it the freezer at  $-15\text{ }^{\circ}\text{C}$  over night and separating the yellow solvent phase from the brownish precipitate the much more polar ligands (with free OH-groups) could be removed in the THF phase. This procedure was repeated several times and tracked with UV-VIS spectrometry (see fig. 4.8). Despite the multiple isomers the clean product showed narrow absorption peaks, comparable to the spectra of  $\text{BF}_2\text{HPhN}$  and  $\text{BF}_2\text{HBAN}$  which contained no isomers. These spectra indicate that the obtained products may be composed mainly of one stable isomer and/or that all the isomers show very similar optical behavior.

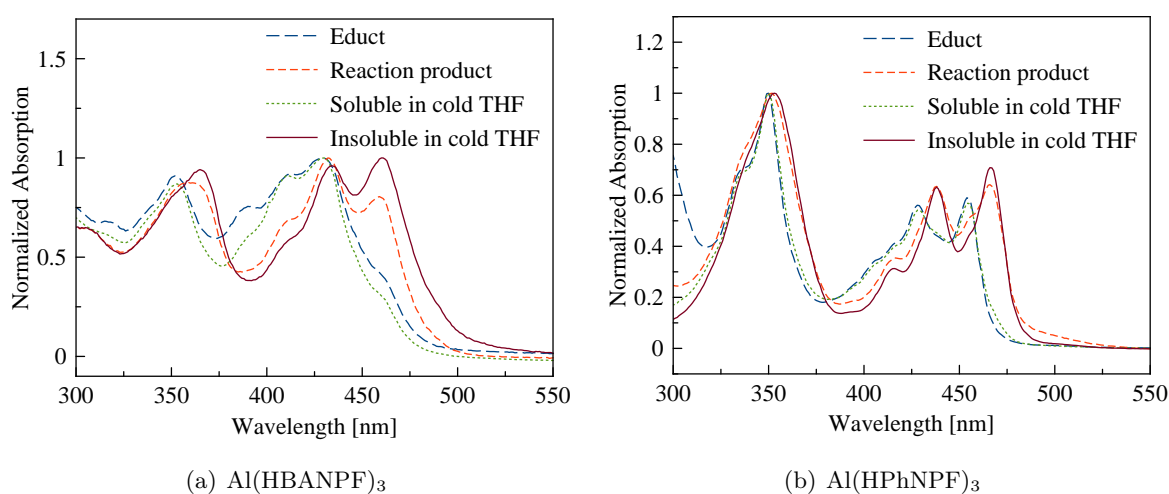


**Figure 4.8:** Absorption spectra of the Al-complexes during the work up procedure. The remaining free ligand is separated by its better solubility in THF.

The obtained mass spectra show the expected masses of the complexes without traces of incomplete complexes with remaining chlorine atoms. In the  $\text{Al}(\text{HBANPF})_3$  mass spectra additional peaks for three-fold perfluoroalkylated ligand can be seen. This additional modification on HBANPF and not on HPhNPF can probably explained by its bigger size with more space for alkyl-chains.

#### 4.1.5 Conclusion

In conclusion it can be said that perfluoroalkylated dyes could be synthesized from both ligands in acceptable yields. The modification appears to reduce the chelate stability, but the  $\text{BF}_2$ -chelate of HBANPF and the Al-complexes of both perfluoroalkylated ligands could be obtained nevertheless.

The synthesized Al-complexes proved much more stable than the  $\text{BF}_2$ -chelates. This makes them much easier to synthesize and process and promises more stable and reliable oxygen sensors. Furthermore these complexes were expected to show better compatibility to perfluorinated polymers due to their very nonpolar nature with six perfluorooctyl-chains in all directions.

The lifetimes of the Al-complexes are generally lower than those of their respective  $\text{BF}_2$  counterparts. However their bigger size increases the collision probability with oxygen molecules and thus is able to more than compensate this slight drawback. Thus they were selected as the primary candidates for the new ultra trace sensor dyes.

## 4.2 Modeling of Non-Linearity Effects

The applied dyes and polymers of the created sensors reach extreme values of luminescence lifetimes and oxygen permeability. Additionally the dyes show effects like pronounced delayed fluorescence and a strong temperature dependency of their properties. To understand this behavior and to simulate it a model was developed that describes most of the dyes' different energetic states and reaction constants of their transitions. Furthermore the model is able to simulate excitation intensities, the dye-oxygen quenching constant, multiple oxygen states and their kinetic constants and the matrix permeability. One limitation of the model is that the triplet-triplet-annihilation between two excited dye molecules was not considered because it is a second order reaction and would have complicated the calculations extremely.

The most important effects that could cause non-linear behavior of oxygen sensors are:

- Dye ground state depletion
- Triplet oxygen depletion
- Chemical oxygen consumption
- Triplet-triplet annihilation of two excited dye molecules

These effects (except TT-annihilation) were investigated and their probabilities and impacts estimated. Moreover measurement conditions and sensor composition were tuned to minimize their effects.

### 4.2.1 Triplet Oxygen Depletion

Only oxygen in its more stable triplet state is able to quench the excited sensor dye molecules and thus generate the measurable signal. However this triplet oxygen is converted to its singlet state during the quenching and has to relax before it can quench again. The time it needs for

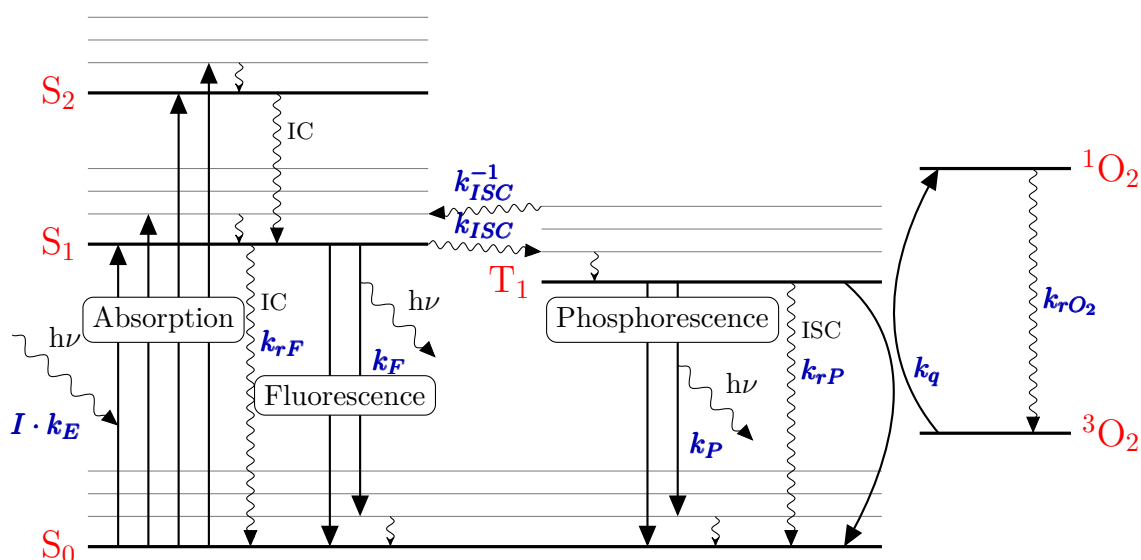
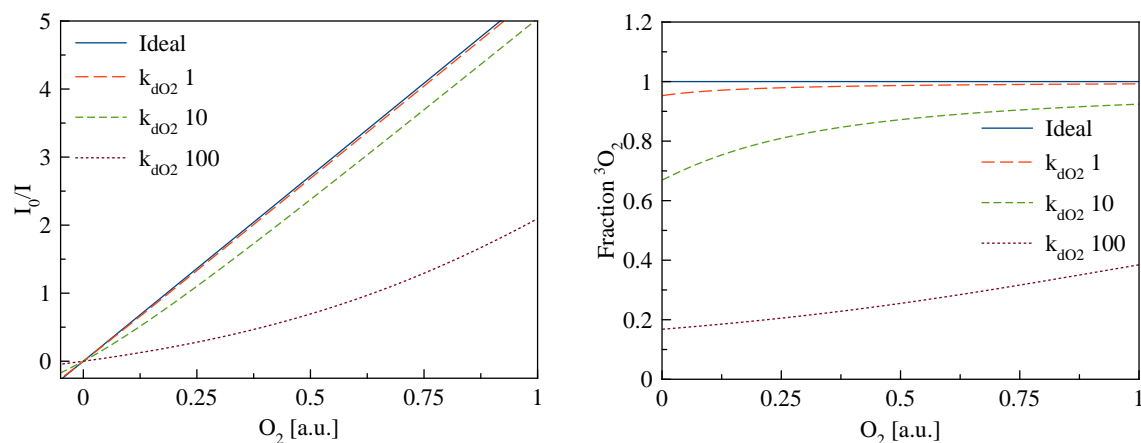


**Figure 4.9:** Jablonski diagram showing all modeled concentrations and kinetic constants.

this relaxation varies greatly. In vacuum the singlet oxygen lifetime is as high as 72 min [44]. However collisions with O-H or C-H bonds relax the singlet state fast [44]. Thus the lifetime is only 4  $\mu$ s in water [45]. In absence of those bonds the lifetimes rise rapidly and reach 68  $\mu$ s in  $D_2O$  [45] and 900  $\mu$ s in  $CCl_4$  [46]. C-F bonds quench the excited oxygen extremely slow (three orders of magnitude slower than C-H or O-C bonds [44]). In perfluorodecalin a singlet oxygen lifetime of even  $309 \pm 20$  ms was found by Afshari et al. [47].

Thus considerably higher triplet oxygen lifetimes are expected in perfluorinated matrices like Teflon AF or Hyflon. Especially at the very low concentrations of ultra trace measurements a significant amount of the present oxygen could be pushed into the singlet state and be thus unavailable for the measurement.

The magnitude of this effect depends on both excitation light intensity and dye concentration. A higher light intensity or dye concentration increases of course the dye excitation and quenching rate and thus the conversion rate of triplet to singlet oxygen.



(a) Calibrations with different triplet  $O_2$  depletions. (b) Percentage of triplet oxygen during the simulated calibrations.

**Figure 4.10:** Simulated calibrations with different levels of triplet  $O_2$  depletion. The upper line is the ideal calibration, the following lines show the influence of tenfold increases of the triplet oxygen lifetimes.

The simulations in fig. 4.10 show the influence of triplet  $O_2$  depletion. It can be clearly seen, that the influence of this effect is much stronger in the lower concentration range of the calibration. This causes the strong deformation of the linear curve.

#### 4.2.2 Chemical Oxygen Consumption

While chemical oxygen consumption is usually not an issue with inert perfluorinated polymers it is quite a big issue for common polymers. It is very similar to triplet oxygen depletion in its behavior. Chemical oxygen consumption also reduces the available amount of oxygen and depends strongly on both light intensity and dye concentration. The chemical oxygen consumption is directly proportional to the generated singlet oxygen. The replenishment rate (via diffusion) is similar to the singlet oxygen decay, a function of the (triplet) oxygen defect. Therefore a graph showing the intensity influence will look very similar to the triplet oxygen depletion plot and distinguishing the effects will very likely be impossible from calibration curves.

Furthermore the chemical oxygen consumption depends on the polymer itself and its susceptibility to oxidation. An important difference to triplet oxygen depletion is that the impact of chemical consumption depends on the layer thickness of the sensor because the diffusion from the environment is the "counter-reaction" to the oxygen consumption. Moreover the effect of the chemical consumption should weaken during the measurements (or a previous conditioning).

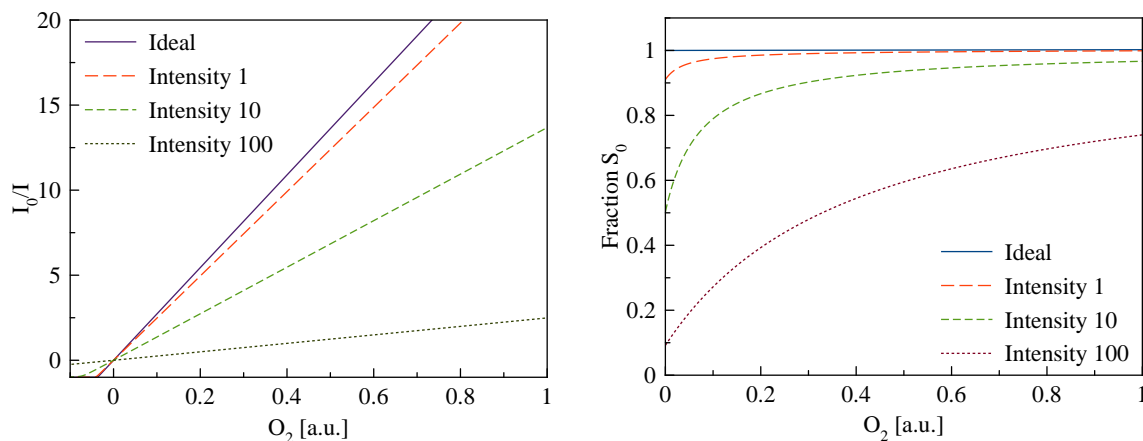
### 4.2.3 Triplet-Triplet Annihilation

Triplet-triplet annihilation is another important process that can influence the performance of an optical oxygen sensor. When two excited dye molecules in triplet state collide it is possible that one gets promoted to the singlet excited state while the other molecule relaxes to the singlet ground state (see reaction C 4.1). This process is spin-allowed. It has a second order dependency on the concentration of the excited dye and thus is greatly influenced by the excitation light intensity and the dye concentration. Because of the second order nature of this reaction it would have extremely increased the complexity of the model equations therefore it was not considered. However the concentration of the dye was kept very low (0.05 wt% dye with MW  $\geq 3000 \text{ g mol}^{-1}$  for the Al-complexes) to avoid this effect and it can be assumed that it played no important role for the synthesized sensor materials.



### 4.2.4 Dye Ground State Depletion

Due to the extremely long luminescence lifetimes of the synthesized dyes ( $>200 \text{ ms}$ ) a significant fraction of the sensor dye can be in the excited triplet state, even at low to moderate excitation intensities. This excited portion of the dye is then, of course, unavailable for absorption of excitation light, thus effectively lowering the amount of absorbed photons which results in decrease of the luminescence intensities. Furthermore, this process does not only diminish the obtained signals, but because its magnitude depends on the excited state lifetimes it also depends on the oxygen concentration. Therefore the lower part of calibrations and especially the  $I_0$ - values are effected much more, which leads to a distortion of the calibration curves. The apparent  $K_{SV}$ -values decrease because the ratios  $\frac{I_0}{I}$  of the calibration points drop due to the lower  $I_0$ . Furthermore, this effect depends strongly on the excitation light intensity and thus causes every calibration to be light intensity dependent.



(a) Calibrations with different ground state depletions. (b) Ground state depletions during the calibrations.

**Figure 4.11:** Simulated calibrations with different levels of ground state depletion. The topmost line is the ideal calibration, the second line shows 10 % depletion and the following lines are based upon a respective increase of intensity by a factor of 10 and have ground state depletions of 50 % and 90 %.

As can be clearly seen in fig. 4.11 the ground state depletion can play a very important role in decreasing the performance of an optical oxygen sensor. Even anoxic depletions of only 10 % show already a visible decrease in sensitivity. Furthermore it can be seen that the dependency on the excitation light becomes drastically stronger at higher intensities. While a tenfold intensity increase from the 10 % depletion line causes 50 % depletion and a calibration with only half the ideal sensitivity a further tenfold increase cuts the simulated  $K_{SV}$ -value down to 10 % of its maximum. Thus it is very important to measure at very low excitation intensities to maximize the sensitivity and minimize the influence of intensity fluctuations. However lifetime calibrations are not affected by ground state depletion because the phosphorescence lifetimes do not depend on the percentage of excited dye.

#### 4.2.5 Conclusion

All the mentioned effects can seriously affect the sensitivity and reliability of any ultra trace oxygen sensor. Especially the chemical oxygen consumption and the triplet oxygen depletion have increasing impact at low concentrations. However also triplet-triplet annihilation and ground state depletion gain influence due to the long lifetimes (and thus high excited state concentrations) which are necessary for extremely sensitive sensor materials.

In the end both excitation intensity and dye concentrations have to be kept as low as possible to minimize the influence of the mentioned effects.

### 4.3 Sensor Preparation

The dye concentration was kept very low in all produced sensor materials. This was done to avoid aggregation and non-linearity effects which depend on the dye concentration. Furthermore the light intensity had to be as low as possible because all important non-linearity effects depend strongly on it. Thus the sensor had to be coated very thick to reach good signal values for the measurements.

The main disadvantage of the thick layers ( $\approx 20\ \mu\text{m}$  to  $40\ \mu\text{m}$ ) was a longer response time of the sensors, but due to the very high permeabilities of the employed polymer matrices the diffusion through the materials should be very fast and the response times good even with very thick layers. For oxidizable polymers thick layers would be impossible for ultra trace sensors because the diffusion speed into the matrix would be slowed down greatly compared to the unhindered chemical oxygen consumption.

To reach such thick layers of  $23\ \mu\text{m}$  to  $41\ \mu\text{m}$  the coating was done in two steps because otherwise the wet layers would become uneven. The first "thin" layer had a wet film strength of  $175\ \mu\text{m}$  and prepared the surface perfectly for the second coating with a wet film strength of around  $250\ \mu\text{m}$ . The glass slides had to be pre-treated with a perfluorinated chloro silane to increase the surface compatibility during the coating and the adhesion between polymer and glass substrate.

Glass slides had to be used because any polymer substrate would have stored a very high amount of oxygen and would have greatly increased the response time of the sensors.

### 4.4 Photophysical Properties

#### 4.4.1 Absorption Spectra

All synthesized dyes and ligands showed similar absorption spectra (see fig. 4.12) with three distinct peaks between  $350\ \text{nm}$  and  $466\ \text{nm}$  and a clear minimum between the first and the second peak. Furthermore all spectra show more or less pronounced shoulders next to the peaks. All three peaks of HBANPF and its derived chelates show molar absorption coefficients of approximately  $10\ 000\ \text{L mol}^{-1}\ \text{cm}^{-1}$  per ligand unit. The absorption spectra of HPhNPF and  $\text{Al}(\text{HPhNPF})_3$  are similar but their peak around  $350\ \text{nm}$  shows a approximately 50% higher extinction coefficient than the two other peaks (see table 4.1).

Generally the absorption coefficients were roughly proportional to the number of ligands. While HBANPF and  $\text{BF}_2\text{HBANPF}$  have approximately the same coefficients, the Al-complex with 3

**Table 4.1:** Molar absorption coefficients of the dyes measured in dichloromethane.

Dye	c [ $\mu\text{mol L}^{-1}$ ]	Wavelength[nm]	$\epsilon$ [ $\text{L mol}^{-1} \text{cm}^{-1}$ ]
HPhNPF	56.2	350	$16 \cdot 10^3$
		429	$9.1 \cdot 10^3$
		454	$9.7 \cdot 10^3$
HBANPF	61.6	357	$8.5 \cdot 10^3$
		408	$8.8 \cdot 10^3$
		430	$9.2 \cdot 10^3$
Al(HPhNPF) <sub>3</sub>	31.7	356	$31 \cdot 10^3$
		438	$20 \cdot 10^3$
		466	$24 \cdot 10^3$
Al(HBANPF) <sub>3</sub>	30.9	364	$25 \cdot 10^3$
		433	$25 \cdot 10^3$
		458	$26 \cdot 10^3$
BF <sub>2</sub> HBANPF	88.4	378	$9.2 \cdot 10^3$
		435	$8.8 \cdot 10^3$
		461	$10 \cdot 10^3$

ligands has nearly three times the absorption. This proportionality is also valid for HPhNPF and Al(HPhNPF)<sub>3</sub>, but less exact.

As expected the first peaks of HBANPF and Al(HBANPF)<sub>3</sub> show a bathochromic shift compared to HPhNPF and Al(HPhNPF)<sub>3</sub> of 7 nm and 8 nm, respectively, due to the larger aromatic system of the ligand and the therefore lower energies of the excited states. However both the second and third peak of HBANPF and its dyes show a hypsochromic shift of 21 nm and 24 nm for HBANPF in respect to HPhNPF and 5 nm and 8 nm for Al(HBANPF)<sub>3</sub> compared to Al(HPhNPF)<sub>3</sub>, despite their extended  $\pi$ -systems. This unexpected shift is especially pronounced in the free ligands but lessens in the complexes. The peaks of all dyes showed distinct bathochromic shifts compared to their free ligands but HBANPF and its complexes to a much higher extent (see fig. 4.12).

Due to the octahedral nature of the aluminium complexes and the bidentate ligands four possible isomers exist for both Al(HPhNPF)<sub>3</sub> and Al(HBANPF)<sub>3</sub>. However very similar optical properties were expected for all isomers and the narrow absorption spectra seem to prove this assumption.

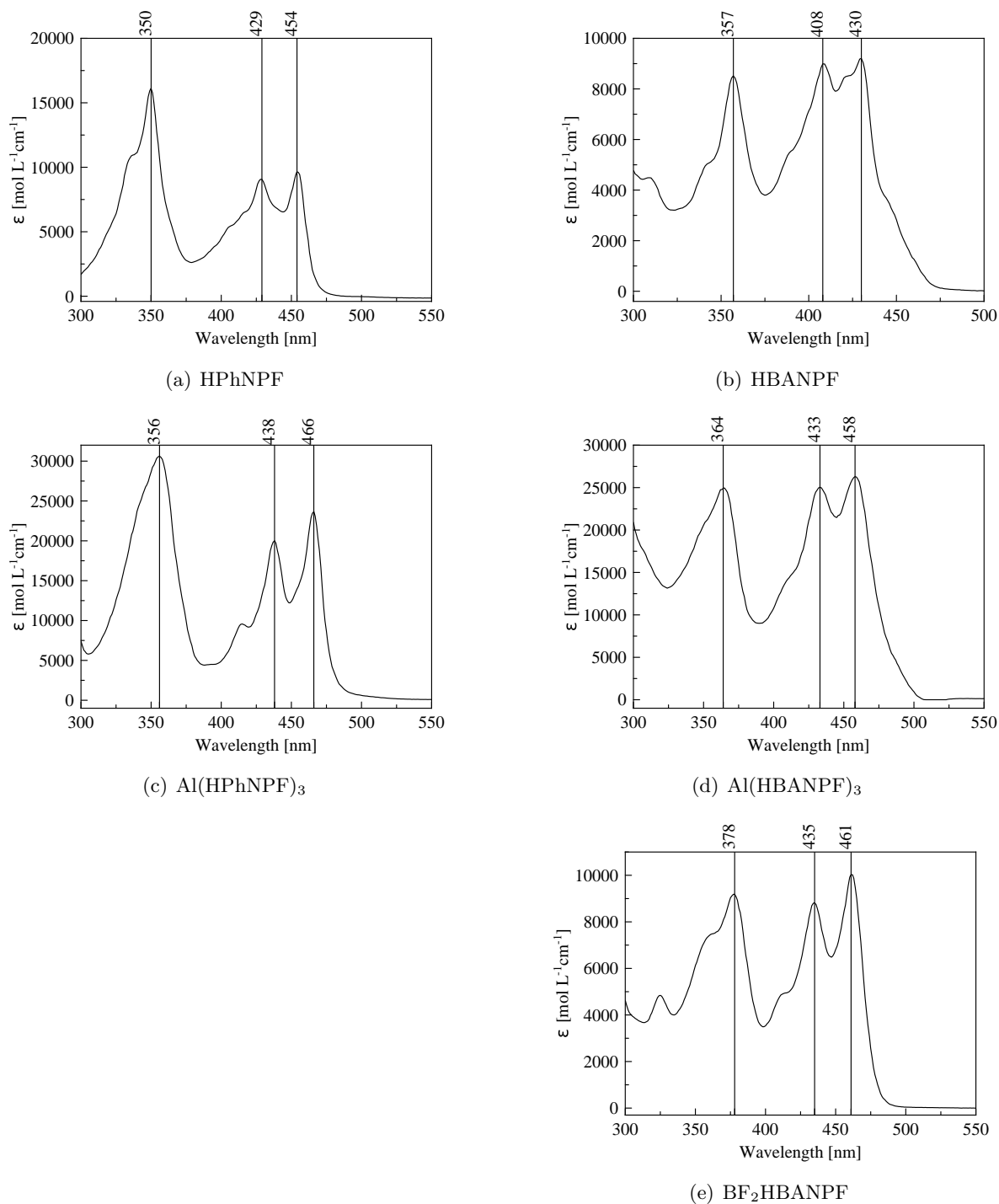


**Figure 4.12:** Absorption spectra of the synthesized dyes and ligands in DCM.

### 4.4.2 Emission and Excitation Spectra

As expected the recorded emission and excitation spectra of the HPhNPF and HBANPF dyes show similar spectra with a broad phosphorescence peak around 570 nm with a distinct shoulder and one or two fluorescence peaks between 450 nm to 500 nm. The excitation spectra for all dyes in Teflon® AF 1600 were very similar to their absorption spectra in dichloromethane.

#### **BF<sub>2</sub>HBANPF**

The excitation spectrum of BF<sub>2</sub>HBANPF in Teflon® AF 1600 (see fig. 4.13) has two well defined peaks at 426 nm and 452 nm. The excitation efficiency drops fast after the lowest energy peak and an excitation above 465 nm is very inefficient. The Stokes shift to the fluorescence maximum (457 nm) is very small with only 5 nm.

While the fluorescence signal is well developed the much more important phosphorescence emission is quite weak. It is still perfectly measurable but the Al-complexes of both HPhNPF and HBANPF show much better signals. Also the delayed fluorescence is very weak compared to Al(HBANPF)<sub>3</sub> and especially Al(HPhNPF)<sub>3</sub>. These weak emissions could be due to a bad compatibility with the used Teflon® AF 1600 matrix. In contrast to Al(HPhNPF)<sub>3</sub> and Al(HBANPF)<sub>3</sub>, which are virtually surrounded with six very nonpolar perfluorooctyl-chains, the BF<sub>2</sub>-chelate has a very polar "head" with two oxygen-boron-bonds. This could lead to a much weaker compatibility and possibly to slight aggregation. Furthermore BF<sub>2</sub>HBANPF has only approximately a third of the molar mass (and extinction coefficient) of the Al-complexes. Thus it is utilized in a three-fold higher molar concentration in a 0.05 wt% sensor which increases the aggregation probability even further. Due to these facts Al(HBANPF)<sub>3</sub> and Al(HPhNPF)<sub>3</sub> seem to be the much more promising dyes for novel ultra trace sensors.

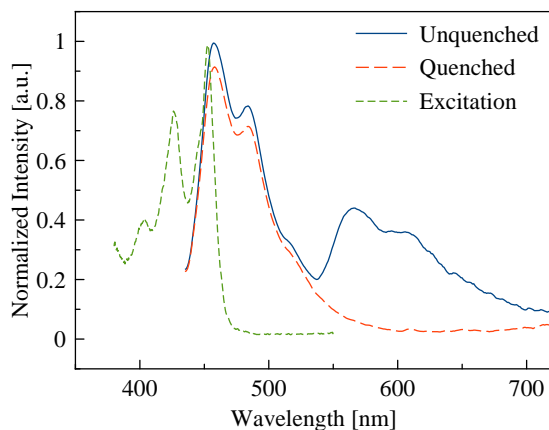


**Figure 4.13:** Excitation (emi: 570 nm) and deoxygenated and oxygenated emission spectra (exc: 420 nm) of  $\text{BF}_2\text{HBANPF}$  in Teflon® AF 1600 at 20 °C.

### $\text{Al}(\text{HBANPF})_3$

$\text{Al}(\text{HBANPF})_3$  in Teflon® AF 1600 (see fig. 4.14) shows a good excitation spectrum with two peaks at 427 nm and 453 nm. These peaks have nearly the same wavelengths as the excitation peaks in  $\text{BF}_2\text{HBANPF}$  but are broader and not as well separated as in both  $\text{Al}(\text{HPhNPF})_3$  and  $\text{Al}(\text{HBANPF})_3$ . Generally all emission and excitation peaks of  $\text{Al}(\text{HBANPF})_3$  appear to be slightly broader compared to the other dyes. This may be due to the fact that the utilized  $\text{Al}(\text{HBANPF})_3$  consists of four isomers due to the octahedral nature of the complex and the bidentate ligand. While this is also true for the  $\text{Al}(\text{HPhNPF})_3$ , HBANPF is much more asymmetric with its larger aromatic system and could thus induce more differences in the complex isomers. Furthermore small amounts of the employed HBANPF ligand are three-fold perfluoroalkylated, which could also cause  $\text{Al}(\text{HBANPF})_3$  molecules with slightly different properties.

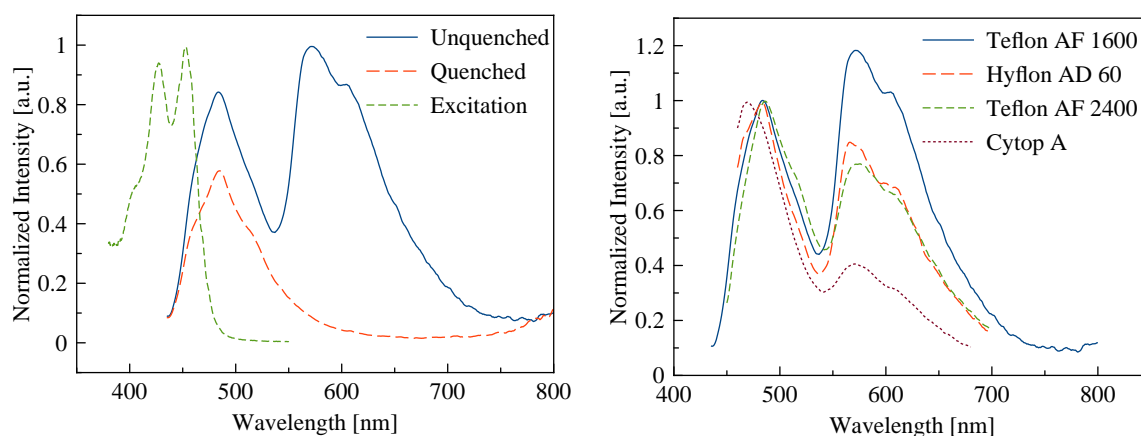
These isomers could also be the reason for the single fluorescence peak of  $\text{Al}(\text{HBANPF})_3$ . While  $\text{BF}_2\text{HBANPF}$  and  $\text{Al}(\text{HPhNPF})_3$  have two distinct fluorescence peaks they have merged in the case of  $\text{Al}(\text{HBANPF})_3$  to one very broad peak. The combination to one peak shifts the fluorescence maximum to lower energies and thus increases the apparent Stokes shift of the dye, which has a value of 31 nm and is much higher compared to  $\text{BF}_2\text{HBANPF}$ .

Both delayed fluorescence and phosphorescence are very pronounced. Under completely deoxygenated conditions the phosphorescence peak is even higher than the fluorescence peak. This is an excellent property for a oxygen sensor with a good signal to noise ratio.

As can be seen in fig. 4.14(b) the phosphorescence intensity depends strongly on the matrix. While the signal is excellent in Teflon® AF 1600 it is still good in Hyflon® AD 60 and Teflon®

AF 2400 but very weak in Cytop® CTL-809A. This may be due to the very rigid structure of Cytop® which could possibly deform the big complex and thus reduce the quantum yield of the dye. Another possible reason for the bad emission in Cytop® CTL-809A could be the utilized high boiling (180 °C) solvent, which dried slowly and possibly enabled the dye to diffuse and aggregate.

While the phosphorescence lifetimes in Hyflon® AD 60 and even Cytop® CTL-809A increased with decreasing luminescence intensities, the lifetime in Teflon® AF 2400 weakened together with the phosphorescence intensity. This was interpreted as a sign of dye aggregation due to the very demanding environment.



(a) Excitation (emi: 570 nm) and emission spectra (exc: 420 nm) in Teflon® AF 1600.

(b) Deoxygenated emission spectra in different polymers normalized to the fluorescence peak.

**Figure 4.14:** Excitation and emission spectra of  $\text{Al}(\text{HBANPF})_3$  at 20 °C.

### $\text{Al}(\text{HPhNPF})_3$

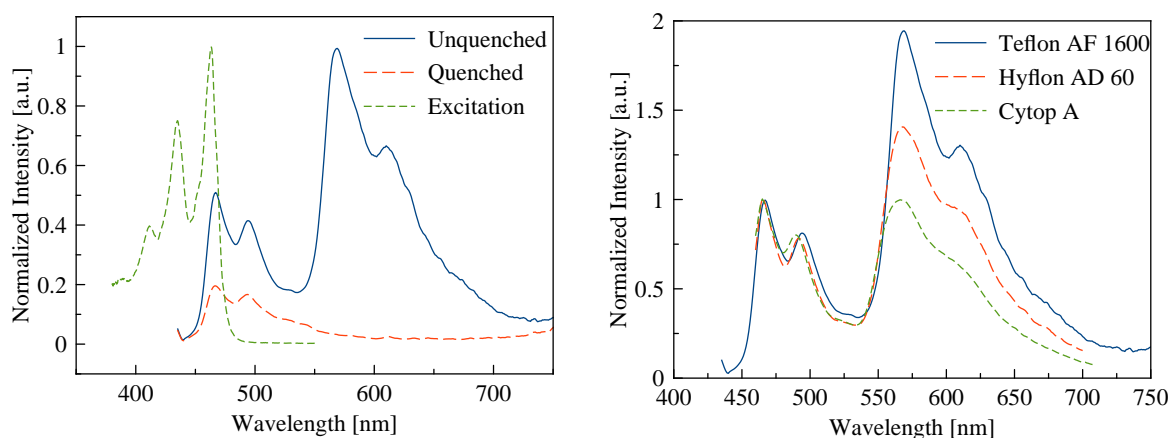
Among the available dyes  $\text{Al}(\text{HPhNPF})_3$  has the best spectral properties. Its two excitation peaks are at 435 nm and 463 nm, respectively. Excitation is possible up to a wavelength of around 470 nm which enables excitation of the dye with common commercially available blue LEDs. The Stokes shift between the excitation and emission peaks is very small with only 4 nm and all peaks are quite narrow.

The phosphorescence intensity is high compared to the fluorescence peak. Thus the fluorescence background is very low and can be easily subtracted. The delayed fluorescence on the other hand is extremely pronounced. Because of its strong temperature dependency (see fig. 4.16) it can be utilized to measure the temperature of the sensor and consequently correct the temperature dependency of the sensor. The delayed fluorescence becomes very strong at

elevated temperatures. Above 50 °C it may even yield the better signals for oxygen monitoring than the phosphorescence. At low temperatures the already strong phosphorescence becomes even stronger and produces an even better signal. This could be an advantage for measurements in the deep sea where usually low temperatures are predominant.

The luminescence intensities of  $\text{Al}(\text{HPhNPF})_3$  depend strongly on the matrix. The phosphorescence intensity is highest in Teflon® AF 1600, still very good in Hyflon® AD 60 and only moderate in Cytop® CTL-809A. While the phosphorescence intensities decreased the excited state lifetimes increased again. This behavior is very similar to  $\text{Al}(\text{HBANPF})_3$ .

All in all  $\text{Al}(\text{HPhNPF})_3$  shows the best spectral properties. It has a good phosphorescence intensity, a very low quenched fluorescence background and can be excited at the longest wavelengths. Furthermore the strong delayed fluorescence can be used for temperature compensation.



(a) Excitation (emi: 570 nm) and emission spectra (exc: 420 nm) in Teflon® AF 1600.

(b) Deoxygenated emission spectra in different polymers normalized to the fluorescence peak.

**Figure 4.15:** Excitation and emission spectra of  $\text{Al}(\text{HPhNPF})_3$  at 20 °C.

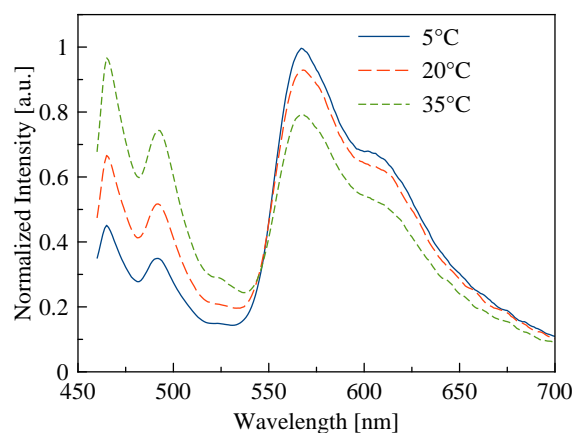


**Figure 4.16:** Deoxygenated emission spectra (exc: 435 nm) of  $\text{Al}(\text{HPhNPF})_3$  in Hyflon® AD 60 at 5 °C, 20 °C and 35 °C.

### 4.4.3 Quantum Yields

The deoxygenated quantum yields could not be measured directly in the quanta- $\varphi$  integrating sphere because it is impossible to deoxygenate it sufficiently. Nevertheless the prompt fluorescence quantum yields which are oxygen independent could be measured with this method and the deoxygenated quantum yields could be calculated from them.

This was done by measuring deoxygenated and oxygenated emission spectra of the dyes, integrating the areas and setting the prompt fluorescence emission in relation to all other emissions. See section 3.5.5 on page 29 for the used procedures and formulas. The obtained areas in the quanta- $\varphi$  integrating sphere can be seen in table 9.1 on page 115 and the measured spectra and their integrated areas can be seen in figs. 9.11 to 9.15 on the pages 117 to 118 and table 9.2 on page 116, respectively.

The obtained quantum yields can be seen in table 4.2 and show acceptable to good values for all dyes, especially when you consider the extremely long lifetimes of all examined dyes. The longer a excited state lives the longer radiationless deactivation processes have time to relax it and can thus reduce the quantum yields drastically.

Especially noteworthy among the values of the unmodified dyes are the quantum yields of  $\text{BF}_2\text{HBAN}$ . It has the longest phosphorescence lifetime of all dyes (734 ms, see table 4.3) and has still more than double the quantum yields of  $\text{BF}_2\text{HPhN}$ . Also of interest is that both unmodified dyes have similar ratios between prompt and delayed fluorescence of around 1:1, while the modified Al-complexes have very different ratios. In both perfluoroalkylated and unmodified dyes the HPhN based systems have much higher phosphorescence than fluorescence intensities. In  $\text{Al}(\text{HPhNPF})_3$  this trend is even stronger than in  $\text{BF}_2\text{HPhN}$ .

**Table 4.2:** Quantum yields of the unmodified and perfluoroalkylated dyes in polystyrene and Teflon® AF 1600, respectively.

Dye	Matrix	Quantum Yield [%]			
		prompt F. <sup>a</sup>	delayed F. <sup>b</sup>	P <sup>b</sup>	Total <sup>b</sup>
BF <sub>2</sub> HPhN	Polystyrene	1.35	1.19	4.6	7.1
BF <sub>2</sub> HBAN	Polystyrene	5.45	4.6	9.1	19.2
BF <sub>2</sub> HBANPF	Teflon® AF 1600	1.45	0.2	1.6	3.3
Al(HPhNPF) <sub>3</sub>	Teflon® AF 1600	0.87	1.3	5.4	7.5
Al(HBANPF) <sub>3</sub>	Teflon® AF 1600	1.97	0.8	3.2	6.0

<sup>a</sup> Measured in integrating sphere.

<sup>b</sup> Calculated from the integration sphere value and the emission spectra.

In case of BF<sub>2</sub>HBANPF the lowest quantum yields were observable. This is probably again due to a bad compatibility of BF<sub>2</sub>HBANPF in Teflon® AF 1600 caused by the polar "head". Again the Al-complexes have superior properties and seem again to be the better choice as sensor dye.

Both Al-complexes show similar quantum yields in Teflon® AF 1600. However while Al(HBANPF)<sub>3</sub> has a slightly higher total quantum yield Al(HPhNPF)<sub>3</sub> has distinctly greater phosphorescence quantum yield and a much lower (oxygen-independent) prompt fluorescence quantum yield which acts as background during measurement. Hence Al(HPhNPF)<sub>3</sub> seems again the slightly better choice as sensor dye.

However all characterized dyes showed quantum yields sufficient for utilization in sensor materials.

#### 4.4.4 Photochemical Stability

The photochemical stability of Al(HPhNPF)<sub>3</sub> and Al(HBANPF)<sub>3</sub> in Teflon® AF 1600, and for comparison purposes for BF<sub>2</sub>HPhN and BF<sub>2</sub>HBAN in polystyrene, were measured to characterize the bleaching of the utilized dyes. The results (see fig. 4.17) show that both Al-complexes have excellent photochemical stability. Over the course of 2 h continuous illumination by a blue power LED both dyes bleached less than 10%. Al(HBANPF)<sub>3</sub> showed less than 5% decomposition.

Considering the facts that this experiment was conducted under normal air saturated atmosphere, whereas the typical application field of the dyes are extremely oxygen depleted environments

and that the excitation intensities will be kept purposefully very low during the measurement to avoid the various non-linearity effects, it can be expected that the dyes will hardly bleach at all during measurements. This high resistance is very important for intensity based calibrations. Otherwise they would drift very fast. Furthermore it enables a pre-conditioning of the sensors under strong light to remove oxidizable compounds (which could lead to chemical oxygen consumption) and other contaminants.

It can generally be said that HBAN-compounds bleached less than their HPhN-counterparts. This is particularly evident in case of the  $\text{BF}_2$ -chelates. Furthermore the perfluoroalkylated Al-complexes showed much better stabilities. This could be due to the  $\text{Al}^{3+}$  central ion, but it is much more likely due to the electron withdrawing perfluorooctyl-groups of the modified ligands. Electron withdrawing groups generally lead to a higher bleaching stability because the oxidation by singlet oxygen, which may be the predominant bleaching mechanism, is much slower on electron poor aromatic systems [48, 49].

The data correlated well to literature. Sun et al. [40] reported a strong increase in bleaching stability of anthracene after attachment of two perfluorooctyl groups. Thus it is very likely that the higher stability is mainly due to the perfluoroalkylation of the ligands.

However not only photochemical bleaching was observed. Dissociation of the  $\text{BF}_2$ -chelates is also visible in the recorded absorption spectra as can be seen in the bleaching curves in the figures 9.16(a) and 9.16(b) in the appendix on page 119. The two tracked absorption peaks decrease with different speeds in case of the  $\text{BF}_2$ -chelates. Dissociation is even more evident in the absorption spectra (figures 9.17(a) and 9.17(b) on page 120).

In contrast to the  $\text{BF}_2$ -chelates the bleaching of the Al-complexes is completely uniform. All peaks decrease with the same rate. This can be seen in the bleaching curves in the figures 9.16(c) and 9.16(d) in the appendix on page 119 and the recorded spectra during the measurement in the figures 9.17(c) and 9.17(d) on page 120.

This observation is another hint that the Al-complexes are much more stable than their  $\text{BF}_2$  counterparts. Even the Al-dyes with the weaker coordinating perfluoroalkylated ligands (due to less electron density) appear to dissociate much harder than the  $\text{BF}_2$ -chelates. Furthermore the dissociation seemed much faster for  $\text{BF}_2\text{HPhN}$  than for  $\text{BF}_2\text{HBAN}$ . This indicates that HBAN is probably the better coordinating ligand and fits to observation that the perfluoroalkylated  $\text{BF}_2\text{HBANPF}$  chelate is still stable but the  $\text{HPhNPF}$  version isn't.

In conclusion it was found out that the perfluorinated aluminium complexes are much more photochemically resistant than their unmodified  $\text{BF}_2$  counterparts and that  $\text{Al}(\text{HBANPF})_3$  is the most stable one. Furthermore the results indicate that the aluminium complexes dissociate much harder and thus are excellent choices as sensor dyes. While  $\text{Al}(\text{HPhNPF})_3$  is not as photochemically stable as  $\text{Al}(\text{HBANPF})_3$  it is more than stable enough for the typical

measurement conditions with a low oxygen content and very low excitation intensities. Both complexes showed excellent photochemical resistances.

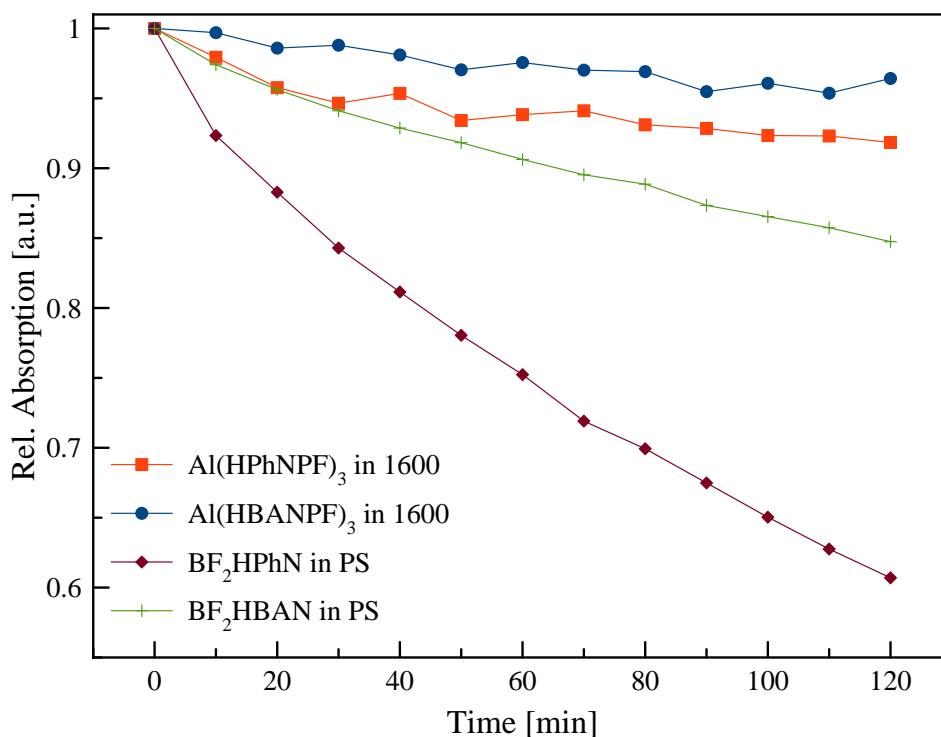


**Figure 4.17:** Bleaching curves of BF<sub>2</sub>HPhN, BF<sub>2</sub>HBAN, Al(HPhNPF)<sub>3</sub> and Al(HBANPF)<sub>3</sub> under intense irradiation of a blue power LED.

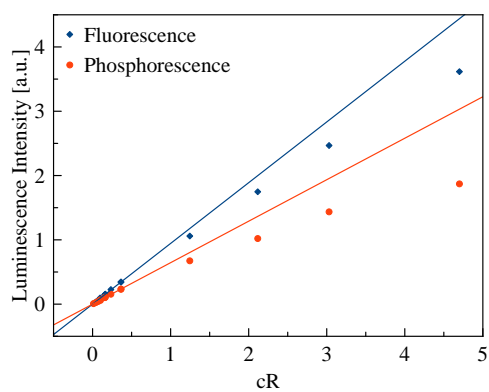
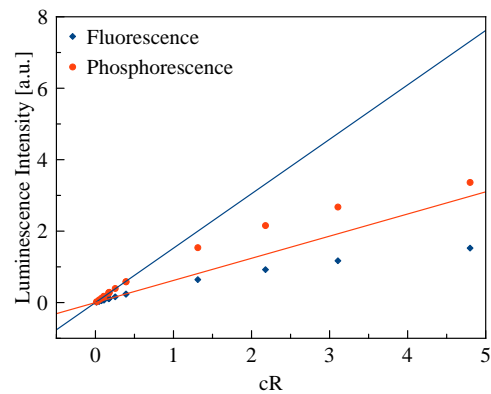
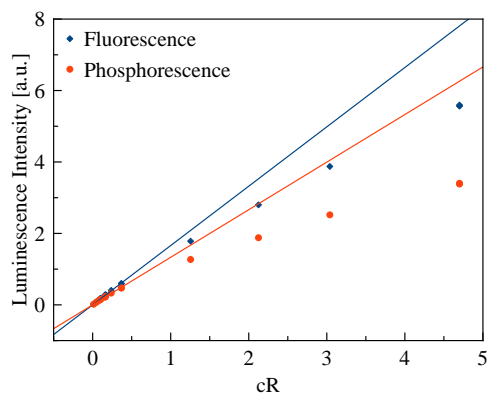
#### 4.4.5 Intensity Dependency of the Luminescence

The emissions of BF<sub>2</sub>HBANPF, Al(HPhNPF)<sub>3</sub> and Al(HBANPF)<sub>3</sub> were measured with different excitation intensities in anoxic sulfite solution and the measured fluorescence and phosphorescence intensities plotted against the excitation intensity (see fig. 4.18). This was done to investigate if ground state depletion is present in the sensor systems and to what extent. The excitation intensities were varied from a  $cR$ -value of 0.0124 to 4.7 (more than two orders of magnitude). The calculated  $cR$ -value is a combination of the internal excitation intensity measurement in the FluoroLog® 3 (measured after the monochromator) and the neutral density filter transmittance at the measured wavelength. This correction is necessary because the filter transmittances are not wavelength-independent and vary strongly especially below 450 nm. To compare the employed light intensities the  $cR$ -value is given for every experiment.

As can be seen in figure 4.18 fluorescence and phosphorescence of the dyes does not rise

proportionally to the excitation energy over the complete range. This is a strong hint for the assumed ground state depletion. Due to the extremely long excited state lifetimes a high portion of the dye can be transferred to and kept in the excited triplet state. Thus the amount of excitable ground state dye decreases and consequently the amount of absorbed and emitted photons. Because the depletion is strongly dependent on lifetime, which in turn is dependent on the surrounding oxygen concentration, the influence of this effect varies over the range of the calibration. It is strongest at low concentrations but contained via the anoxic intensity  $I_0$  in every calibration point.

For all investigated dyes a strong deviation from ideal linear behavior is visible at high light intensities which indicates a strong ground state depletion. However at low to moderate intensities ( $cR < 0.5$ ) the curves appear linear and no significant influence of this effect on the calibration curves is expected. In consequence all calibrations were done at the lowest possible excitation intensities.

(a)  $\text{BF}_2\text{HBANPF}$ (b)  $\text{Al}(\text{HPhNPF})_3$ (c)  $\text{Al}(\text{HBANPF})_3$ 

**Figure 4.18:** Saturation curves of  $\text{BF}_2\text{HBANPF}$ ,  $\text{Al}(\text{HPhNPF})_3$  and  $\text{Al}(\text{HBANPF})_3$  in Teflon® AF 1600. The luminescence intensity is plotted against the corrected excitation intensity  $cR$  together with a linear fit of the lower ( $cR < 0.5$ ) measurement points.

#### 4.4.6 Conclusion

The dyes showed the expected excitation and emission spectra with good to acceptable quantum yields and thus proved the desired compatibility with perfluorinated polymers. While BF<sub>2</sub>HBANPF possesses good values in all the mentioned aspects it was outperformed by both Al-complexes in every regard. This can possibly be explained by a better compatibility of the Al-dyes. Furthermore Al(HPhNPF)<sub>3</sub> and Al(HBANPF)<sub>3</sub> proved their excellent photochemical stabilities. As was expected due to their long lifetimes all dyes showed signs of ground state depletion in the intensity dependency experiments.

### 4.5 Lifetime Measurements

The oxygen-free lifetimes of the dyes could only be measured in a sodium sulfite solution where the surrounding oxygen is consumed fast. To accelerate the consumption and thus obtain more reliable results a small amount of cobalt(II) chloride was added to the solution as a catalyst.

The measured lifetimes of the dyes are extremely long compared to the decay times of commonly utilized oxygen sensing dyes, which are usually in the range of microsecond up to several milliseconds. [11, 50, 51] They are to the best of our knowledge the longest phosphorescence lifetimes of visible light-excitable organic luminophores.

#### 4.5.1 Anoxic Lifetimes

The lifetimes were measured in the kinetic acquisition mode of the FluoroLog® 3 and the obtained decay curves fitted with a mono-exponential decay function. As can be seen in figure 4.19 the decay curves are perfectly mono-exponential. All measurements were repeated multiple times to obtain reliable results. For the obtained results see table 4.3

The measured lifetimes of the different dyes depended strongly on the used matrix. Interestingly the lifetimes of both Al(HPhNPF)<sub>3</sub> and Al(HBANPF)<sub>3</sub> in Cytop® CTL-809A were exceptionally long despite the very weak phosphorescence emission. This could be due to the very rigid nature of this polymer.

The lifetimes of the unmodified BF<sub>2</sub>HBAN is distinctly longer than the lifetime of BF<sub>2</sub>HBANPF in Teflon® AF 1600. This could indicate more or stronger deactivation paths for the modified dyes. An other explanation would be the suspected bad compatibility of BF<sub>2</sub>HBANPF to Teflon® AF 1600, which could lead to aggregation and hence shorter lifetimes.

While the BF<sub>2</sub>-chelates possess the longer lifetimes the Al-complexes are much bigger and thus a higher collision probability with oxygen. Hence the Al-complexes are expected to show similar or higher oxygen sensitivities in sensor materials.

**Table 4.3:** Anoxic lifetimes of the dyes at 20 °C in sodium sulfite solution. For all measured values see table 9.3 on page 122.

Dye	Matrix	Lifetime [ms]
BF <sub>2</sub> HPhN	PS	354 ± 5
BF <sub>2</sub> HBAN	PS	734 ± 1
BF <sub>2</sub> HBANPF	Teflon® AF 1600	443 ± 4
Al(HPhNPF) <sub>3</sub>	Teflon® AF 1600	244 ± 1
Al(HPhNPF) <sub>3</sub>	Hyflon® AD 60	253 ± 4
Al(HPhNPF) <sub>3</sub> <sup>a</sup>	Hyflon® AD 60	284 ± 1
Al(HPhNPF) <sub>3</sub> <sup>b</sup>	Hyflon® AD 60	218 ± 2
Al(HPhNPF) <sub>3</sub>	Cytop® CTL-809A	344 ± 2
Al(HBANPF) <sub>3</sub>	Teflon® AF 1600	343 ± 3
Al(HBANPF) <sub>3</sub>	Teflon® AF 2400	313 ± 5
Al(HBANPF) <sub>3</sub>	Hyflon® AD 60	395 ± 9
Al(HBANPF) <sub>3</sub>	Cytop® CTL-809A	467 ± 4
Al(HBANPF) <sub>3</sub> <sup>c</sup>	Cytop® CTL-107MK	359 ± 6

<sup>a</sup> 5 °C

<sup>b</sup> 35 °C

<sup>c</sup> Measured in N<sub>2</sub>-atmosphere (purged 1 h). Completely deoxygenated due to the strong chemical oxygen consumption.

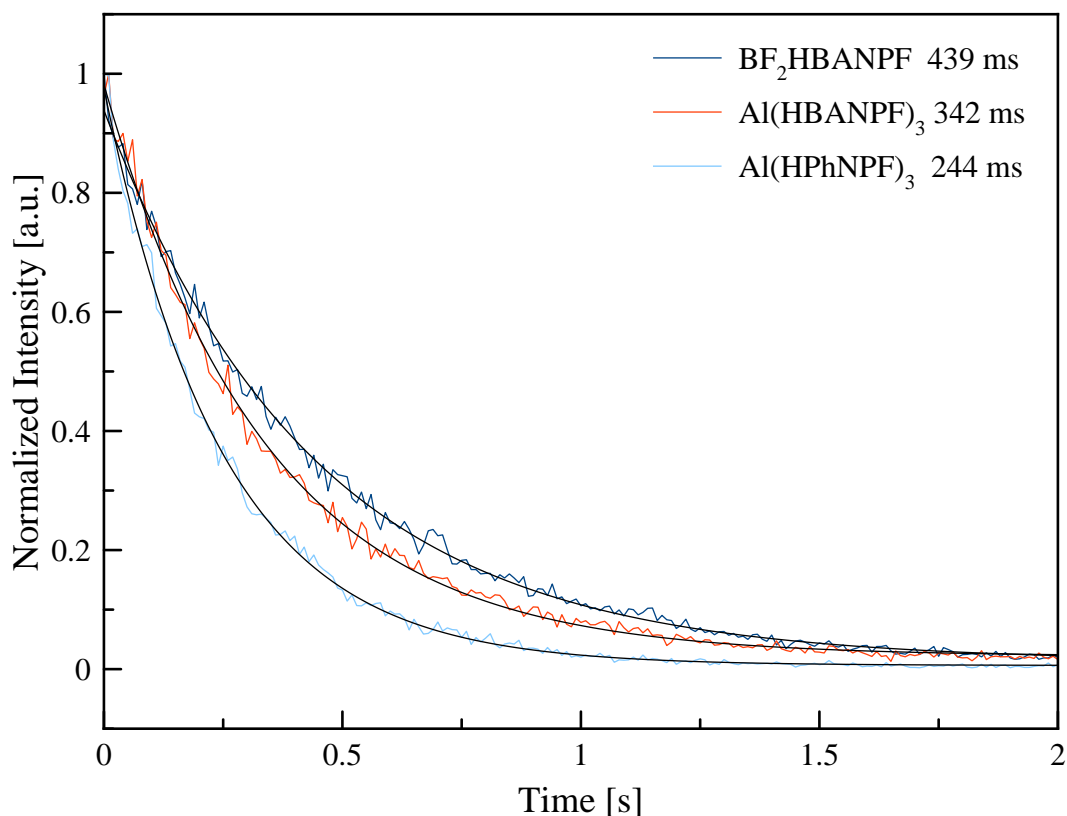


**Figure 4.19:** Exemplary mono-exponential decay fits for  $\text{BF}_2\text{HBANPF}$ ,  $\text{Al}(\text{HPhNPF})_3$  and  $\text{Al}(\text{HBANPF})_3$  in Teflon® AF 1600.

#### 4.5.2 Anoxic Lifetimes Intensity Dependency

To estimate the influence of triplet-triplet annihilation the lifetime dependency on the excitation intensity was measured. This was done under completely deoxygenated conditions to ensure that chemical oxygen consumption or triplet oxygen depletion have no influence on the measurements. For the obtained results see table 4.4 and for exemplary fitting curves see fig. 4.20.

As expected the lifetimes decreased at higher excitation intensities due to triplet-triplet annihilation. However they decreased only very slightly and only at very high excitation intensities. In the intensity range that was chosen based on the luminescence intensity experiments ( $cR$  values below 0.5 (see section 4.4.5)) no significant lifetime dependency could be detected. This indicates that the chosen dye concentrations of 0.05 wt% are sufficiently low to prevent a strong influence of the triplet-triplet annihilation. Nevertheless this experiment confirms that all measurements should be done at the lowest possible excitation intensities.

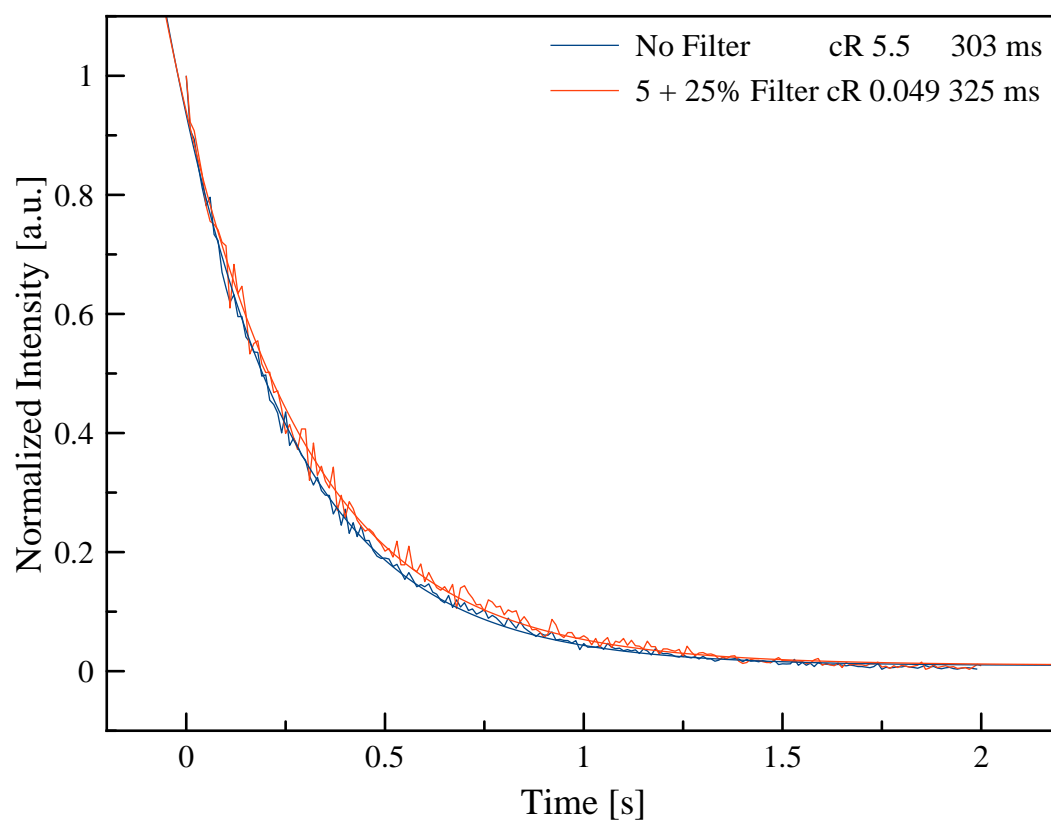


**Figure 4.20:** Mono-exponentially fitted decay curves of  $\text{Al}(\text{HBANPF})_3$  in Teflon® AF 1600 with two different intensities.

**Table 4.4:** Anoxic lifetimes of the dyes in Teflon® AF 1600 at 20 °C in sodium sulfite solution with different excitation intensities. For all measured values see table 9.4 on page 123.

	<b>Filter</b>	<b><math>cR^a</math></b>	<b>Lifetime [ms]</b>
BF <sub>2</sub> HBANPF	–	5.6	432 ± 5
	50	2.5	436 ± 6
	10	0.43	447 ± 6
	5	0.19	447 ± 2
	5 + 25	0.049	453 ± 23
Al(HPhNPF) <sub>3</sub>	–	5.4	243 ± 2
	50	2.5	248 ± 2
	10	0.44	251 ± 1
	5	0.19	250 ± 2
	5 + 25	0.053	246 ± 4
Al(HBANPF) <sub>3</sub>	–	5.5	308 ± 3
	50	2.5	317 ± 3
	10	0.43	328 ± 4
	5	0.18	328 ± 1
	5 + 25	0.049	335 ± 1
Al(HPhNPF) <sub>3</sub> <sup>b</sup>	–	0.50	272 ± 3
	50	0.23	274 ± 2
	25	0.14	270 ± 3
	10	0.041	269 ± 3

<sup>a</sup> Value for intensity comparison purposes calculated from the measured  $R$ -intensity value and the actual filter transmittances.

<sup>b</sup> in Hyflon® AD 60.

### 4.5.3 Lifetimes Intensity Dependency with Oxygen Traces

While the oxygen free intensity dependency measurement was used to estimate the influence of the triplet-triplet annihilation between excited dye molecules, this measurement was used to investigate the influence of either chemical oxygen consumption or triplet oxygen depletion.

The experiment was only performed for Al(HBANPF)<sub>3</sub> in Teflon® AF 1600, but because the investigated effects are dye independent, it is expected to be similar with BF<sub>2</sub>HBANPF and Al(HPhNPF)<sub>3</sub>. The results (see table 4.5) show a much stronger influence of the excitation intensity. In contrast to the deoxygenated measurements the lifetimes rise with higher intensities. For exemplary fitting curves see fig. 4.21.

The measured effect was much higher than the deoxygenated lifetime dependency. Thus it is expected that chemical oxygen consumption or triplet oxygen depletion (or a combination of both) can play an important role in the sensor system. However at the typically utilized excitation intensities the influence is acceptable.

**Table 4.5:** Phosphorescence Lifetimes of Al(HBANPF)<sub>3</sub> (0.05 wt% in Teflon® AF 1600) with  $\approx 1.5$  ppmv O<sub>2</sub> with multiple excitation light intensities. For all measured values see table 9.5 on page 124.

Filter [%]	$cR^a$	Lifetime [ms]
None	4.9	177 ± 4
None	1.6	152 ± 2
50	0.73	145 ± 5
25	0.43	146 ± 2
10	0.13	142 ± 4
5	0.056	146 ± 8

<sup>a</sup> Value for intensity comparison purposes calculated from the measured  $R$ -intensity value and the actual filter transmittances.

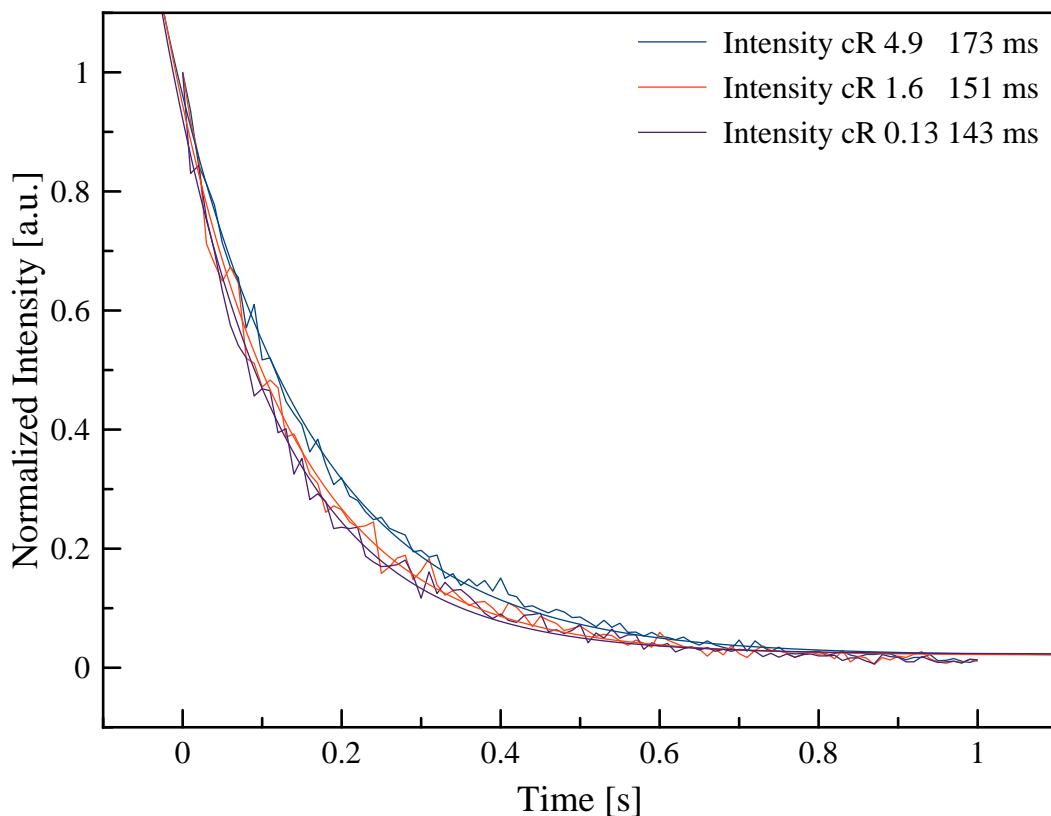


**Figure 4.21:** Mono-exponentially fitted decay curves of  $\text{Al}(\text{HBANPF})_3$  in Teflon® AF 1600 at three different intensities with traces of oxygen.

#### 4.5.4 TCSPC Lifetimes

Additionally to the kinetic acquisition measurements lifetimes of the dyes in Teflon® AF 1600 were determined with time correlated single photon counting. The measurements were conducted at the phosphorescence and, additionally, at the fluorescence peak. The much more exact measurements obtained similar lifetimes for all characterized dyes. Furthermore it was found out that the decay curves of  $\text{Al}(\text{HBANPF})_3$  and  $\text{BF}_2\text{HBANPF}$  do not decay mono exponentially, but have to be fitted with two exponential functions. This could be due to the impurities of three-fold modified ligand. The measured lifetimes and relative amplitudes can be seen in table 4.6. For the plotted measurements with the fit curves see fig. 4.22 on page 74.

For all characterized dyes the delayed fluorescence and phosphorescence lifetimes were approximately identical. This behavior was expected due to the fact that both emissions start from the excited triplet state of the dyes.

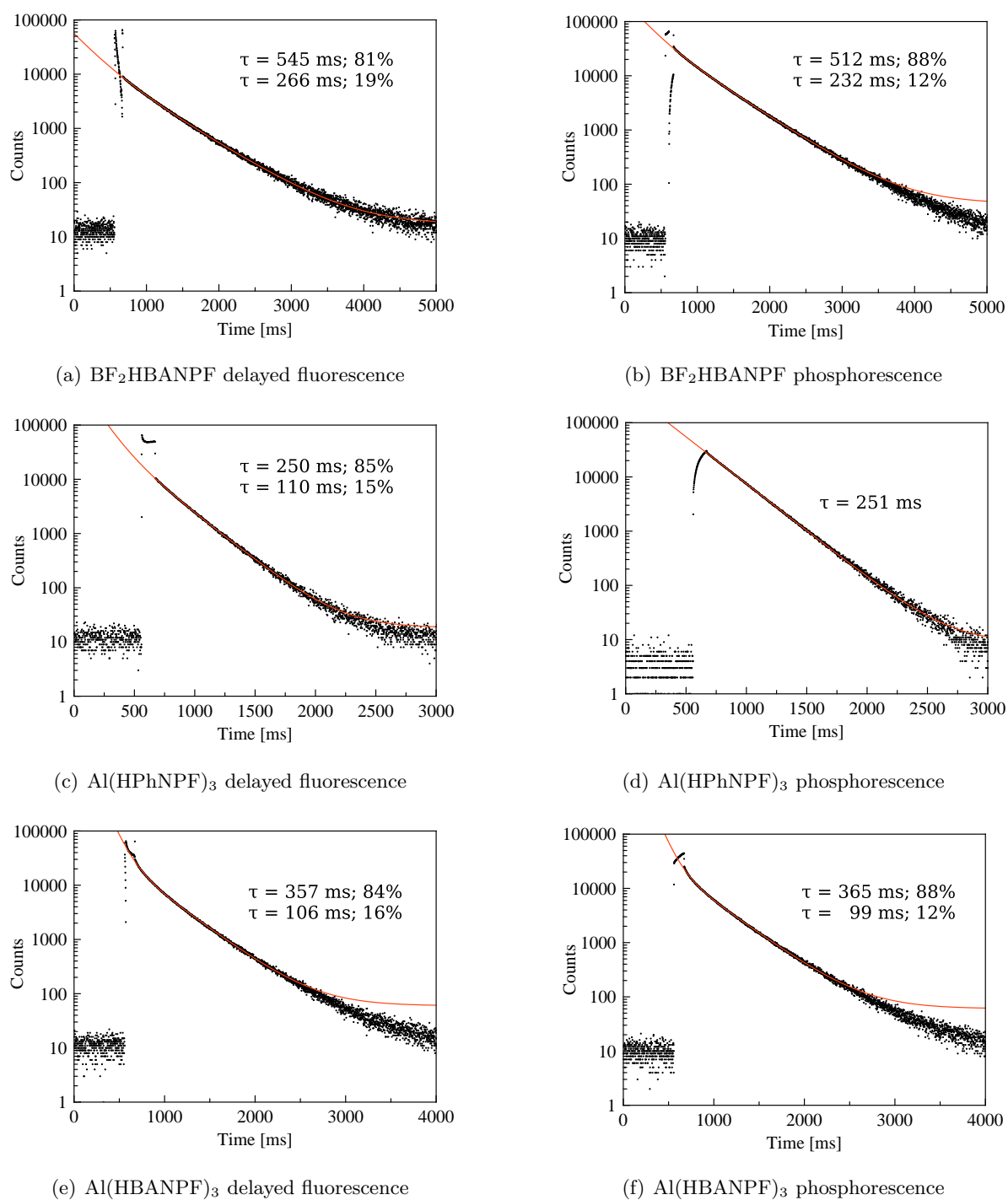


**Figure 4.22:** Single photon counting measurements of the lifetimes of  $\text{BF}_2\text{HBANPF}$ ,  $\text{Al}(\text{HPhNPF})_3$  and  $\text{Al}(\text{HBANPF})_3$  with 0.05 wt% in Teflon<sup>®</sup> AF 1600. Recorded at room temperature.

**Table 4.6:** Lifetimes and relative amplitudes of the dyes (0.05 wt% in Teflon® AF 1600). Measured with time correlated single photon counting.

Dye	Peak	Rel. Amplitude [%]	Lifetime [ms]
BF <sub>2</sub> HBANPF	fluor.	81	545
		19	266
	phos.	88	512
		12	232
Al(HPhNPF) <sub>3</sub>	fluor.	85	250
		15	110
	phos.	100	251
Al(HBANPF) <sub>3</sub>	fluor.	84	357
		16	106
	phos.	88	365
		12	99

#### 4.5.5 Conclusion

In conclusion it can be said that the characterized dyes show outstandingly long phosphorescence lifetimes (on par with their unmodified counterparts), which makes them excellent dyes for extremely sensitive oxygen sensors. The small intensity dependency on the deoxygenated lifetimes proves that triplet-triplet annihilation is no problem at the employed dye concentrations and excitation intensities. On the other hand the much higher lifetime dependency on excitation light with oxygen traces indicates that chemical oxygen consumption (unlikely in a perfluorinated polymer) or triplet oxygen depletion may play a role for the sensor materials.

## 4.6 Calibration by Controlled Oxygen Consumption of Sodium Ascorbate

To calibrate the extremely sensitive oxygen sensors different approaches were investigated. The first one was a controlled consumption of oxygen in a closed container by sodium ascorbate. This reaction was selected because it was slow enough to be tracked (in contrast to sodium sulfite) and it was reported to be of pseudo-first order.[52] To use this system for the sensor calibration it was planned to measure the kinetic constants in the upper range of the curve and use them to predict the oxygen concentration in the immeasurable region. The calculated oxygen values would then be used to calibrate the ultra trace sensors.

In order to test this system the reaction was tracked with two known sensors (Pd-benzoporphyrin in polystyrene and Teflon® AF 1600) and the oxygen consumption was recorded. However multiple problems emerged.

One problem is that the reaction speed depends on the pH of the solution and had to be kept stable over the whole measurement. However this difficulty was addressed with a buffer of pH 5.4.

Another problem was the extreme sensitivity of the measurements to ambient light. As can be seen in fig. 4.23(b) the weak electric lighting in the measurement room was strong enough to deviate the measured signal by more than 50%. Even the influence of the measurement intensity (and frequency) could clearly be seen in the measurements.

Yet another difficulty is the fact that the reaction is catalyzed by many different metal-ions.[53] Thus even small traces of metals could influence the kinetics dramatically.

Most importantly the obtained oxygen consumption curves showed no mono-exponential decay. In figure 4.23(a) the measured curve with two different fits can be seen. One for the whole displayed range and one for a shorter and lower concentration range. It is obvious that both fits deviate strongly from the measured oxygen concentrations. While the kinetics could probably be fitted with a free exponent there is no guarantee that it won't change at lower oxygen concentrations, for example due to diffusion limitations. Moreover the reached oxygen concentrations are much too high. To reach the required concentrations (the most sensitive sensor was calibrated in a range of 1 ppmv to 6 ppmv (two orders of magnitude lower than the concentration at the end of this measurement) the reaction would have to run many hours where no sensor could check the accuracy of the oxygen consumption.

At closer examination it seems unlikely that the oxygen consumption by ascorbate (or any other reagent) follows a first order reaction. Only simple one step reactions can follow first order kinetics perfectly. However the reaction of ascorbate has many reactive intermediates like  $O_2^-$  and  $HO_2$  [54]. Thus a reagent would have to be found that consumes a complete  $O_2$  molecule with one reaction step to obtain a perfectly mono-exponential oxygen consumption. But even then the reaction kinetics could change at low concentrations due to diffusion limitations (see the measured GOx kinetics section 4.9 on page 86).

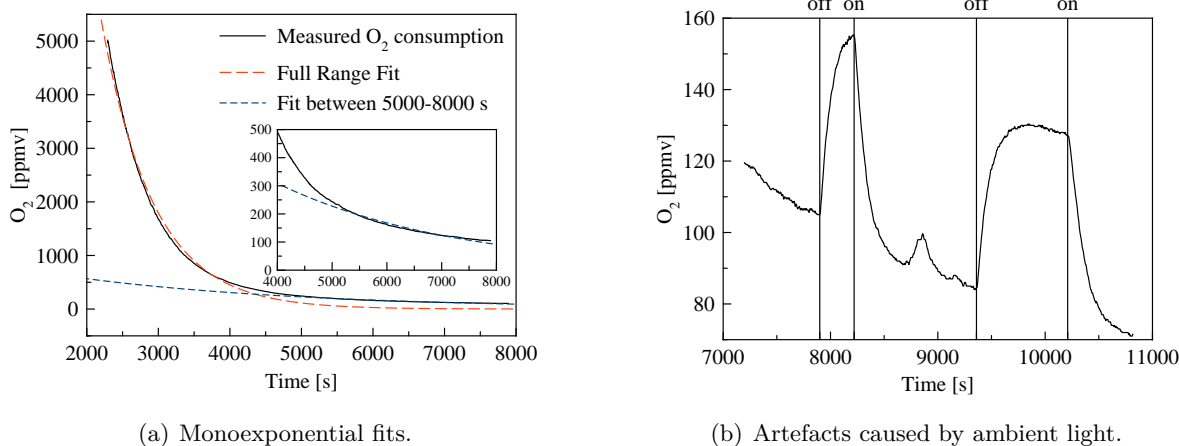


**Figure 4.23:** Measurement curve of the Pd benzoporphyrine in Teflon® AF 1600 sensor during the ascorbate oxygen consumption.

**Table 4.7:** Important unit conversions.

1 ppmv $\hat{=}$	0.101	hPa	(partial pressure)
	1.42	nM	(dissolved oxygen)
	45.5	ng L <sup>-1</sup>	(dissolved oxygen)
	45.5	ppt	(dissolved oxygen)

All values for 20 °C and 1013 hPa total pressure.

## 4.7 Calibrations

The synthesized Al-based dyes were calibrated in different perfluorinated matrices. Among the chosen polymers Teflon® AF 1600 has the highest permeability and Hyflon® AD 60 the second highest. In contrast to them Cytop® CTL-809A has a only slightly higher permeability than polystyrene. For comparison purposes the unmodified dyes were calibrated in polystyrene. The obtained  $K_{SV}$  values can be seen in table 4.8 and the plotted curves in fig. 4.25.

As expected the sensors sensitivity increased with higher permeabilities and dye lifetimes. Teflon® AF 1600 sensors are more sensitive than Hyflon® AD 60 sensors and those in turn are more sensitive than the Cytop® CTL-809A and polystyrene sensors. However the correlation was not as strong as expected. The rule of thumb formula (sensitivity is permeability times lifetime) does obviously no longer apply for these ultra trace sensors.

Not all sensors could be described accurately with the simple Stern-Volmer-equation (4.1). If a fit with this equation was not possible the simplified two-site model equation (4.2) was applied. [8]

$$\frac{\tau_0}{\tau} = \frac{I_0}{I} = K_{SV} \cdot [\text{O}_2] + 1 \quad (4.1)$$

$$\frac{\tau_0}{\tau} = \frac{I_0}{I} = \frac{1}{\frac{f-1}{1} + \frac{f}{K_{SV} \cdot [\text{O}_2] + 1}} \quad (4.2)$$

Because of the outstanding sensitivities of the Al-dyes in the perfluorinated matrices they could not be calibrated easily. Throughout the whole measurements the oxygen background from the used nitrogen and from small leaks was visible. Even while purging with "pure" nitrogen the deoxygenated lifetimes in sulfite solution could not be reached. Thus it was concluded that the calibration had to be done with a standard addition approach.

This standard addition calibration was implemented by measuring the lifetimes in sulfite solution and in nitrogen. Then the intensities under nitrogen and with different additions of test gas were measured. The anoxic intensity  $I_0$  was calculated with the deoxygenated to nitrogen lifetime-ratio (see eq. 4.3) and the calibration points  $\frac{I_0}{I} - 1$  calculated from this value.

$$I_0 = \frac{\tau_{SO_3^{2-}}}{\tau_{N_2}} \cdot I \quad (4.3)$$

These calibration points were plotted and the y-axis intercept and slope ( $= K_{SV}$ ) determined by a linear fit. The oxygen contamination  $dO_2$  was calculated by dividing the intercept  $d$  through the slope  $K_{SV}$  (eq. 4.4) and applied to all concentrations.

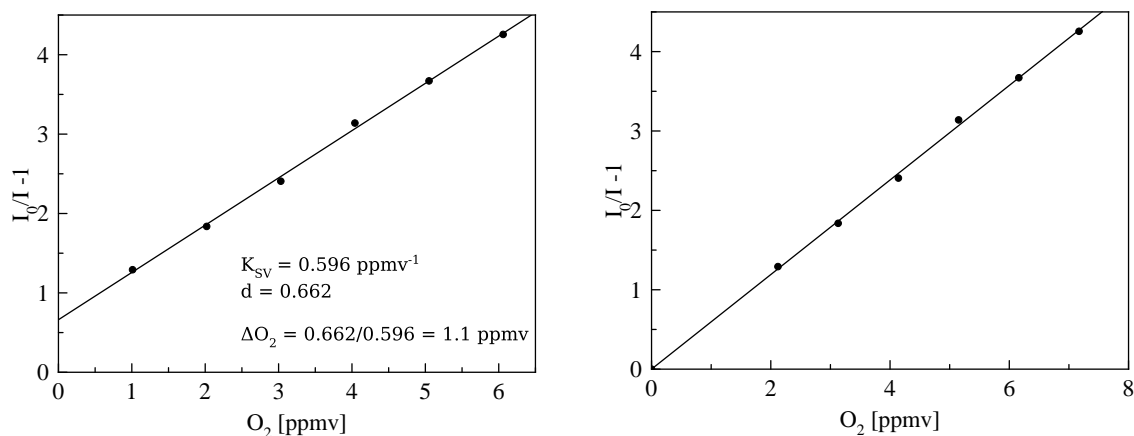
$$\Delta O_2 = \frac{d}{K_{SV}} \quad (4.4)$$

#### 4.7.1 BF<sub>2</sub>HPhN and BF<sub>2</sub>HBAN in Polystyrene

The sensor composed of the unmodified dyes in polystyrene showed the extraordinary influence of the phosphorescence lifetime of the sensor dye. Despite the only moderate permeability of the polymer the sensors showed extraordinary sensitivities.

The significance of the lifetime is also visible in the sensitivity difference between the two dyes. BF<sub>2</sub>HBAN is twice as sensitive as BF<sub>2</sub>HPhN and has twice the phosphorescence lifetime. However both sensor materials (with  $K_{SV}$  values of 0.0566 ppmv<sup>-1</sup> and 0.117 ppmv<sup>-1</sup> for BF<sub>2</sub>HPhN and BF<sub>2</sub>HBAN, respectively) are extremely sensitive. BF<sub>2</sub>HBAN in polystyrene is even more sensitive than the previously published record holding oxygen sensor, which has a  $K_{SV}$  of 0.070 ppmv<sup>-1</sup> [18].

Both calibrations were evaluated without the standard addition method, but with the simplified two-site model fit.



(a) Calculation of the oxygen contamination.

(b) After addition of the determined oxygen background contamination.

**Figure 4.24:** Example of the standard addition calibration. Al(HBANPF)<sub>3</sub> in Hyflon® AD 60 at 20 °C.

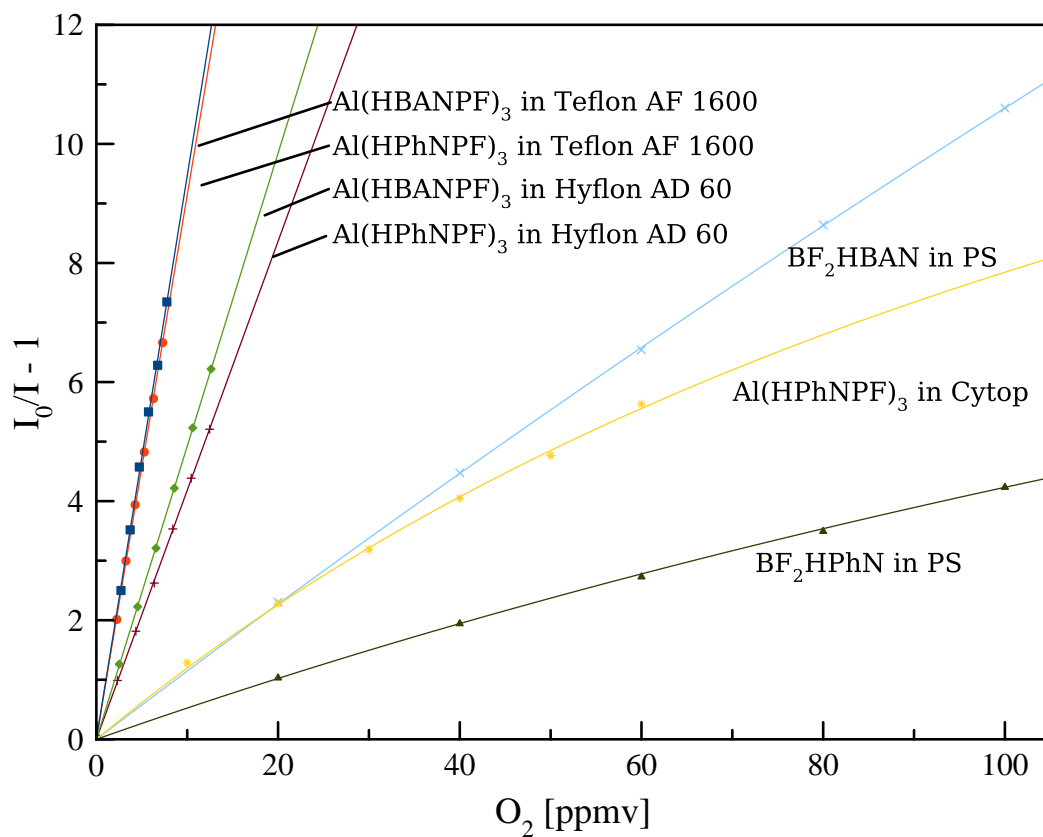
#### 4.7.2 Al(HPhNPF)<sub>3</sub> and Al(HBANPF)<sub>3</sub> in Perfluorinated Matrices

The outstanding sensitivities of the polystyrene sensors were even outperformed by the sensors made of the highly permeable perfluorinated polymers. Because the unmodified dyes are completely insoluble in them and would aggregate readily the perfluoroalkylated dyes were synthesized and utilized.

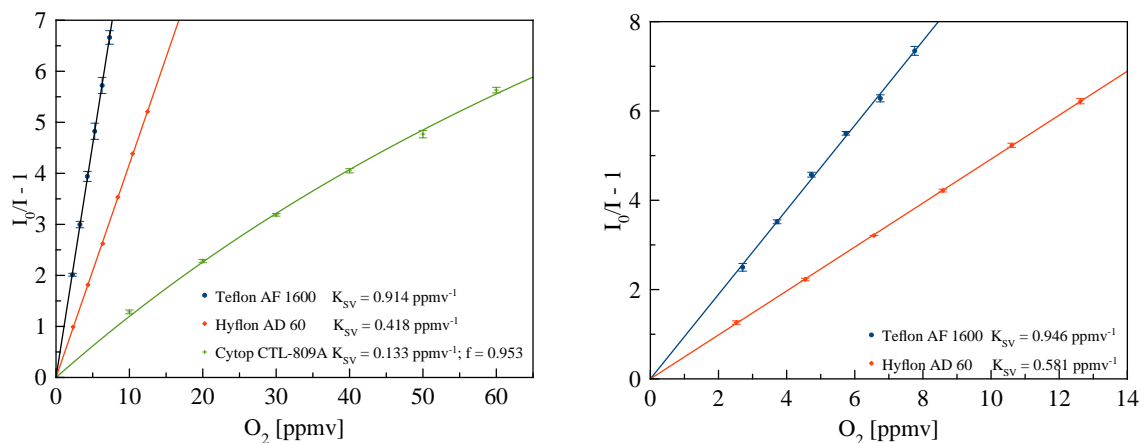
The solubility of both Al(HPhNPF)<sub>3</sub> and Al(HBANPF)<sub>3</sub> was excellent in the perfluorinated polymers. Only BF<sub>2</sub>HBANPF appeared to aggregate in them, which was asserted based on the mediocre lifetime and emission spectrum of this dye in Teflon® AF 1600 (see sections 4.4.2 and 4.5.1). Thus it was not used for sensor materials.

As expected (based on the longer lifetime) Al(HBANPF)<sub>3</sub> yielded the more sensitive oxygen sensors. The difference was, however, not very long and the Al(HPhNPF)<sub>3</sub> sensor yielded overall better signals with much less fluorescence background (see section 4.4.3).

All in all Al(HBANPF)<sub>3</sub> in Teflon® AF 1600 was the most sensitive sensor with a  $K_{SV}$  of  $0.946 \text{ ppmv}^{-1}$  which is nearly 20 times more sensitive than the record holding previously reported sensor (<sup>13</sup>C<sub>70</sub> in Ethyl cellulose), which has a  $K_{SV}$  of  $0.052 \text{ ppmv}^{-1}$  and a limit of detection of 230 ppbv. [23] The new Al(HBANPF)<sub>3</sub> in Teflon® AF 1600 sensing material reaches a limit of detection of 5 ppbv (corresponding to a 0.5 % decrease of intensity). Additionally the quantum yields of the new sensor material are better and it is applicable below room temperature. Despite the slightly lower sensitivity Al(HPhNPF)<sub>3</sub> is an excellent alternative to Al(HBANPF)<sub>3</sub> due to its better signal and background.



(a) All intensity calibrations at 20 °C

(b) Calibrations of Al(HPhNPF)<sub>3</sub> in different matrices. (c) Calibrations of Al(HPhNPF)<sub>3</sub> in different matrices.**Figure 4.25:** Measured calibration curves at 20 °C

**Table 4.8:** Measured  $K_{SV}$  values of the calibrated dyes at 20 °C.

Dye	Matrix	$cR$	$\tau_0$ [ms]	$K_{SV}$ [ppmv <sup>-1</sup> ]
BF <sub>2</sub> HPhN	PS	0.020	354	0.0566 <sup>a</sup>
BF <sub>2</sub> HBAN	PS	0.020	734	0.117 <sup>a</sup>
Al(HPhNPF) <sub>3</sub>	Teflon® AF 1600	0.041	244	0.914
Al(HPhNPF) <sub>3</sub>	Hyflon® AD 60	0.041	253	0.418
Al(HPhNPF) <sub>3</sub>	Cytop® CTL-809A	0.041	467	0.133 <sup>a</sup>
Al(HPhNPF) <sub>3</sub>	Hyflon® AD 60	0.041	269	0.390 <sup>b</sup>
Al(HBANPF) <sub>3</sub>	Teflon® AF 1600	0.042	343	0.946
Al(HBANPF) <sub>3</sub>	Hyflon® AD 60	0.042	395	0.581

The permeabilities for the utilized polymers are  $8.8 \times 10^{-16}$ [25],  $28.3 \times 10^{-16}$ [26],  $170 \times 10^{-16}$ [27] and  $1200 \times 10^{-16}$ [27] mol m<sup>-1</sup> s<sup>-1</sup> Pa<sup>-1</sup> for Polystyrene, Cytop® CTL-809A, Hyflon® AD 60 and Teflon® AF 1600, respectively.

<sup>a</sup> Fitted with a simplified two-site model equation (eq. 4.2). The obtained  $f$ -values were 0.952, 0.992 and 0.953 for BF<sub>2</sub>HPhN, BF<sub>2</sub>HBAN (in PS) and Al(HBANPF)<sub>3</sub> (in Cytop® CTL-809A), respectively

<sup>b</sup> Lifetime calibration.

### 4.7.3 Temperature Dependency of Al(HPhNPF)<sub>3</sub> in Hyflon® AD 60

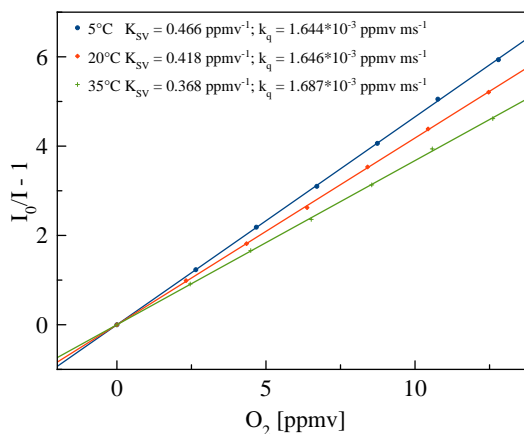
To characterize the temperature dependent behavior of the sensor materials calibrations of Al(HPhNPF)<sub>3</sub> in Hyflon® AD 60 were recorded (see table 4.9 and fig. 4.26). Interestingly the sensitivity decreased with rising temperature, indicating that the decreasing lifetimes outweighs the increasing oxygen diffusion speed in the sensor.

This can be explained by the high temperature dependency of the strong delayed fluorescence of the dye. At elevated temperatures the reverse intersystem-crossing to the excited singlet state is much faster. This results in an increase of the fluorescence emission (see fig. 4.16 in section 4.4.2) but strengthens a relaxation mechanism and thus shortens the lifetimes (see table 4.3 in section 4.5.1) and hence the reduced sensitivity. The bimolecular quenching constants ( $k_q$ ) were calculated at the different temperatures (see eq. 4.5) and show a slight increase with rising temperature (see table 4.9) due to the faster oxygen diffusion. However this effect is not able to compensate the decreasing lifetimes.

$$k_q = \frac{K_{SV}}{\tau_0} \quad (4.5)$$

**Table 4.9:**  $K_{SV}$ -values and calculated quenching constants  $k_q$  for Al(HPhNPF)<sub>3</sub> in Teflon® AF 1600 at 5 °C, 20 °C and 35 °C

Temperature [°C]	$K_{SV}$ [ppmv <sup>-1</sup> ]	Lifetime [ms]	$k_Q$ [ppmv <sup>-1</sup> s <sup>-1</sup> ]
5	0.466	284	1.64
20	0.418	253	1.65
35	0.368	218	1.69

**Figure 4.26:** Temperature dependency of the Al(HPhNPF)<sub>3</sub> in Hyflon® AD 60 calibration.

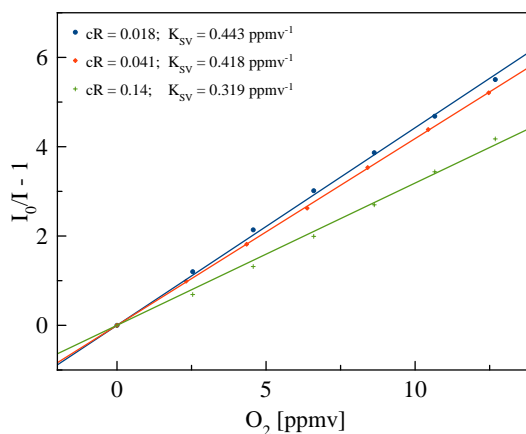
#### 4.7.4 Intensity Dependency of Al(HPhNPF)<sub>3</sub> in Hyflon® AD 60

Apart from temperature, the used excitation intensity was varied as well. Even at the low applied light intensities a noticeable dependency of the calibration was detected (see table 4.10 and fig. 4.27). It is however unclear what causes this dependency, triplet-triplet annihilation between the excited dye molecules seems unlikely because the deoxygenated lifetime measurements (where it should be visible the most) showed no signs of it. Other possibilities are chemical oxygen consumption, triplet oxygen depletion or dye ground state depletion. Whereas chemical oxygen consumption seems unlikely in a perfluorinated polymer and ground state depletion could not be observed at the used intensities in the saturation experiment (see section 4.4.5) triplet oxygen depletion seems a likely possibility.

While the exact reason for this behavior is still uncertain it is mandatory to measure at very low excitation intensities to keep these effects to a minimum and measure with the highest possible sensitivity. Furthermore as it can be seen in figure fig. 4.27 the influence of the intensity seems to be lowest at small excitation intensities as was expected based on the model calculations.

**Table 4.10:**  $K_{SV}$ -values at different excitation intensities for Al(HPhNPF)<sub>3</sub> in Teflon® AF 1600

Intensity $cR$	$K_{SV}$ [ppmv <sup>-1</sup> ]
0.018	0.443
0.041	0.418
0.14	0.319

**Figure 4.27:** Excitation intensity dependency of the Al(HPhNPF)<sub>3</sub> in Hyflon® AD 60 calibration.

#### 4.7.5 Calibration Attempt of Al(HBANPF)<sub>3</sub> in Cytop® CTL-107MK

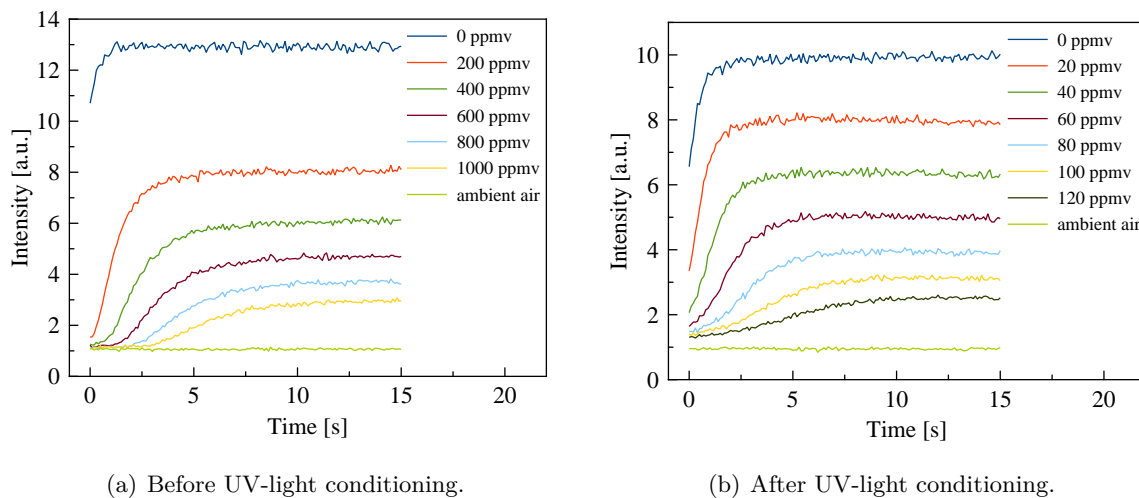
A failed calibration attempt was undertaken for Al(HBANPF)<sub>3</sub> in Cytop® CTL-107MK. This experiment showed that even perfluorinated polymers are not completely safe from chemical oxygen consumption, especially when they are functionalized like Cytop® CTL-107MK.

During the calibration the sensor showed extremely strong chemical oxygen consumption during illumination. This could be seen clearly in the obtained kinetic measurement curves (see fig. 4.28(a)), which show a strong drift from the initial intensity to a oxygen depleted value only controlled by the diffusion speed into the sensor material.

Even after 20 min of conditioning under a UV-lamp in ambient air, where the bigger part of the oxidizable sites of the polymer were saturated, the measurement was impossible due to the remaining oxygen consumption (see fig. 4.28(b)).

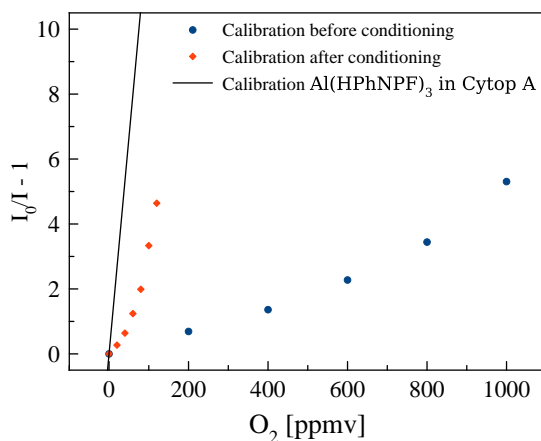
Furthermore both calibration curves (see fig. 4.28(c)) show the typical upwards bending curve of chemical oxygen consumption (see section 4.2). This happens because at higher oxygen concentrations the influence of the consumption isn't as severe as at low concentrations. Thus

the calibration points move closer to the ideal calibration curve (which should be somewhere near the shown calibration curve of  $\text{Al}(\text{HPhNPF})_3$  in Cytop® CTL-809A).



(a) Before UV-light conditioning.

(b) After UV-light conditioning.



(c) Calibration curves. Values taken at 14 s and plotted together with the calibration of  $\text{Al}(\text{HPhNPF})_3$  in Cytop® CTL-809A.

**Figure 4.28:** Kinetic measurements and calibration curves of the failed  $\text{Al}(\text{HBANPF})_3$  in Cytop® CTL-107MK calibration.

#### 4.7.6 Lifetime Calibration of $\text{Al}(\text{HPhNPF})_3$ in Hyflon® AD 60

Additionally to the intensity based calibrations a lifetime calibration of  $\text{Al}(\text{HPhNPF})_3$  in Hyflon® AD 60 was recorded. This calibration has the advantages that it cannot suffer from influences of ground state depletion and that it is transferable to new media with different refractive indices (e.g. liquids). However the kinetic measurement in the FluoroLog® 3 was not as exact as the intensity measurements and only lifetimes above approximately 80 ns could

be measured. Hence the accuracy and range of this calibration was limited. Nevertheless the obtained  $K_{SV}$ -value is approximately the same as for the intensity calibrations.

However with a time correlated single photon counting set-up this measurements could become much easier and much more accurate.

**Table 4.11:** Measured lifetimes and  $\tau_0/\tau - 1$  values of the lifetime calibration. The  $cR$  value was 0.041. For all measured values see table 9.7 on page 125.

$O_2$ [ppmv]	Lifetime [ms]	$\tau_0/\tau - 1$
0	$206 \pm 2$	1.23
1.015	$158 \pm 2$	1.61
2.030	$126 \pm 4$	2.00
3.045	$111 \pm 2$	2.29
4.060	$97 \pm 7$	2.62
5.075	$82 \pm 5$	3.08

#### 4.7.7 Conclusion

The novel sensor materials showed outstanding oxygen sensitivities which are more than on order of magnitude higher than the sensitivity of any previously published sensing material. This was possible by combining the outstanding lifetimes of  $Al(HPhNPF)_3$  and  $Al(HBANPF)_3$  with very permeable perfluorinated matrices.

Despite the very low dye concentrations and light intensities a dependency on the excitation light remains. However it is still unclear which non-linearity effect is responsible for this behavior.

Additionally to the intensity calibrations a lifetime calibration was conducted. While its deviation was significantly higher due to the inapt equipment for lifetime measurements, its overall results fit well to the intensity calibrations.

## 4.8 Measurement of Oxygen Traces in Gases

The measurements of trace oxygen in gases were conducted with a lifetime calibrated  $Al(HPhNPF)_3$  in Hyflon® AD 60 with direct connection of the gas bottles to the measurement cell. This was necessary to minimize the influence of small possible leaks in the lines to and from the gas mixer.

For all measured gases realistic values of oxygen contamination were obtained (see table 4.12). It should be mentioned that the values for both 10 L nitrogen bottles were slightly above their supplier specifications (0.3 ppmv and 3 ppmv for nitrogen 6.0 and 5.0, respectively), but both bottles were connected and disconnected multiple times before the measurements.

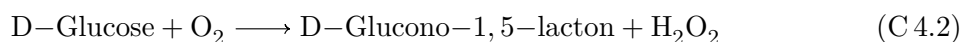
**Table 4.12:** Measured lifetimes and calculated O<sub>2</sub> concentrations of the gas bottles.

Sample	Measurement						Mean	O <sub>2</sub> [ppmv]
	1	2	3	4	5	6		
N <sub>2</sub> 6.0 10L	214	214	212	217	210	213	213	0.67
N <sub>2</sub> 5.0 10L	110	105	113	110	108	113	110	3.7
N <sub>2</sub> 5.0 50L	131	140	137	129	129	135	133	2.6
CO <sub>2</sub> 100 %	109	111	116	113	119	112	113	3.5
CO <sub>2</sub> 0.2 %	68.3	69.7	60.1	71.2	64.3	74.2	68.0	7.6 (>5.7) <sup>a</sup>

<sup>a</sup> 5.7 ppmv is the highest calibration point.

## 4.9 Monitoring of Oxygen consumption by Glucose Oxidase

In this experiment the oxygen consumption by glucose oxidase was tracked over a very broad concentration range. It could be shown that the fabricated sensor materials are suitable to track reactions at extremely low oxygen concentrations. Furthermore the validity of the standard addition calibration was confirmed by the overlapping regions of the multiple sensors. However it should be mentioned that in the overlapping region the Al(HPhNPF)<sub>3</sub> in Hyflon® AD 60 sensor was far above its optimal measurement range. See fig. 4.29 for the obtained data. Catalase was added to the reaction mixture to avoid buildup of hydrogen peroxide.



The sensitivity of the developed sensor was even high enough to observe a change of the reaction kinetics. After 150 min and at an oxygen concentration of 3 nM the reaction followed a first order exponential decay kinetics. This behavior is very likely due to diffusion limitations. The oxygen concentration has become so low that the diffusion to the glucose oxidase is the rate determining step. This observation offers further prove that a calibration by a controlled oxygen consuming reaction is not feasible (see section 4.6).

In conclusion it could be shown that the produced ultra trace oxygen sensors are suitable for measuring at previously unreachable oxygen concentrations.

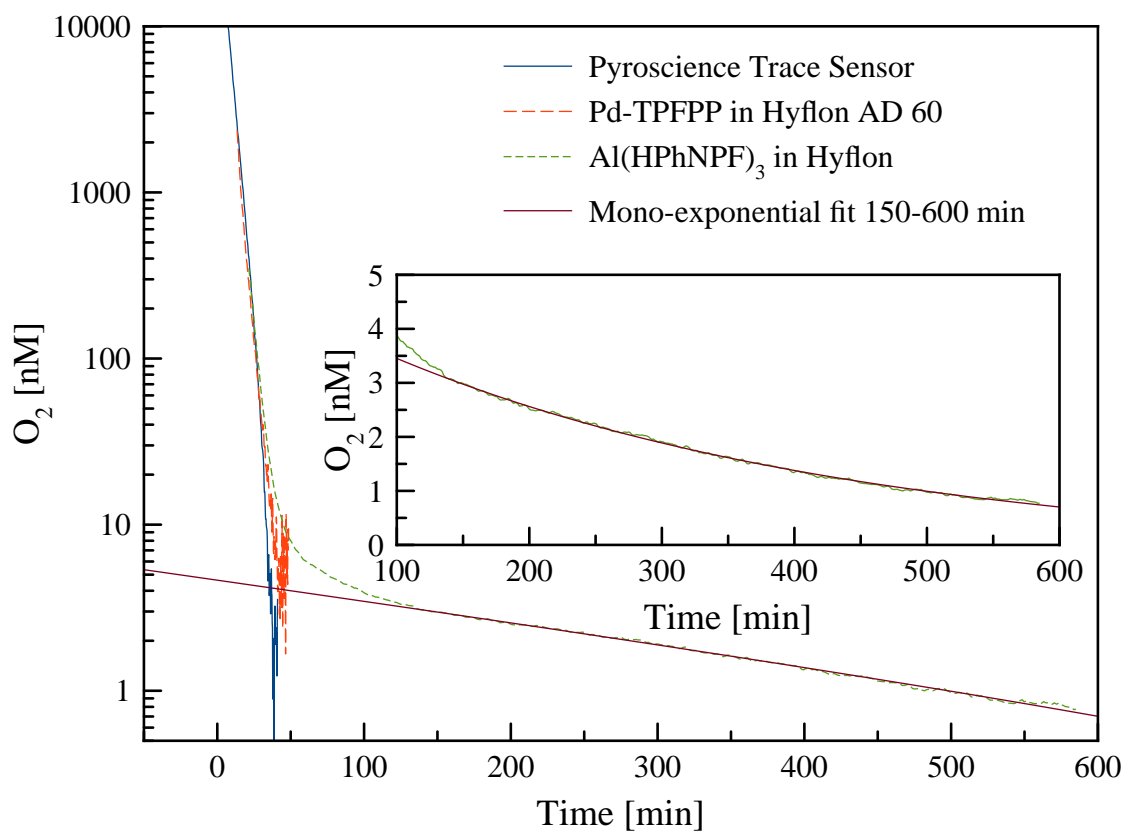


**Figure 4.29:** Measurement curves of three used sensors during the oxygen consumption by glucose oxidase and a mono-exponential fit of the Al(HPhNPF)<sub>3</sub> in Hyflon® AD 60 sensor from 150 min (insert).



---

## 5 Conclusion and Outlook

In conclusion multiple perfluoroalkylated derivatives of  $\text{BF}_2\text{HPhN}$  and  $\text{BF}_2\text{HBAN}$  could be synthesized. The modified ligands carry two perfluoroalkyl-chains each and while the chelates with  $\text{BF}_2$  appeared less stable than the original dyes, the respective Al-complexed showed no signs of dissociation. As expected the solubility in perfluorinated solvents and polymers increased dramatically after the introduction of the perfluoroalkyl-chains and sensor materials with Teflon® AF 1600, Hyflon® AD 60 and Cytop® could be produced. At the same time the novel dyes could retain the good photophysical properties of the unmodified dyes. The Al-complexes reached phosphorescence quantum yields of 5.4% and 3.2% and lifetimes of 240 ms and 340 ms for  $\text{Al}(\text{HPhNPF})_3$  and  $\text{Al}(\text{HBANPF})_3$  in Teflon® AF 1600, respectively.

The sensor materials showed outstandingly high sensitivities and calibration was only possible with a standard addition method, under consideration of the oxygen background contamination. All produced sensor materials showed excellent sensitivities, but  $\text{Al}(\text{HBANPF})_3$  in Teflon® AF 1600 was the most sensitive one with a  $K_{SV}$  of  $0.950 \text{ ppmv}^{-1}$  and a limit of detection of only 5 ppbv, which is 15 times more sensitive than any previously published oxygen sensor.

Furthermore the suitability of the sensor materials for trace measurements was demonstrated by measuring the ppmv-level oxygen contaminations in multiple gas bottles and by measuring the kinetics of glucose oxidase down to dissolved oxygen concentrations below 1 nM.

All in all novel outstandingly sensitive oxygen sensing materials could be produced that are up to 15 times more sensitive than any previously published material. Furthermore their functionality could be demonstrated in two practical measurements.

### 5.1 Outlook

An important remaining issue are the observed non-linearities. Even at very low excitation intensities and dye concentrations the dependency on the excitation light remains an issue. While the developed model is able to qualitatively explain this behavior, it is yet unclear which phenomenon (ground state depletion, triplet-triplet annihilation or triplet oxygen depletion) causes the observed intensity dependence. Furthermore the model is not yet able to quantitatively predict influences on the sensor sensitivity.

However the most important remaining task is to develop or adapt a small read-out system for the novel oxygen sensor materials. While measurements at the FluoroLog® 3 are perfectly possible, practical applications require a much smaller and less expensive measurement setup. A future read-out device could either work based on a ratiometric principle (maybe even referenced by the fluorescence of the dye itself) or based on lifetime measurements. A development of such a device remains the most important challenge.

---

## 6 References

- [1] Markandey M. Tripathi et al. “An optical sensor for multi-species impurity monitoring in hydrogen fuel”. In: *Sensors and Actuators B-Chemical* 171 (Sept. 2012). WOS:000308572700052, pp. 416–422.
- [2] Takeo Nakano, Ken’ichiroh Hoshi, and Shigeru Baba. “Effect of background gas environment on oxygen incorporation in TiN films deposited using UHV reactive magnetron sputtering”. In: *Vacuum* 83.3 (Oct. 15, 2008), pp. 467–469.
- [3] I S Longmuir. “Respiration rate of bacteria as a function of oxygen concentration.” In: *The Biochemical journal* 57.1 (May 1954), pp. 81–87.
- [4] Daniel A. Stolper, Niels Peter Revsbech, and Donald E. Canfield. “Aerobic growth at nanomolar oxygen concentrations”. In: *Proceedings of the National Academy of Sciences* 107.44 (Nov. 2, 2010). PMID: 20974919, pp. 18755–18760.
- [5] Niels Peter Revsbech et al. “Determination of ultra-low oxygen concentrations in oxygen minimum zones by the STOX sensor”. In: *Limnology and Oceanography: Methods* 7 (2009), pp. 371–381.
- [6] Bernard Valeur and Inc John Wiley & Sons. *Molecular Fluorescence*. Weinheim: Wiley-VCH, 2002.
- [7] E. R. Carraway et al. “Photophysics and photochemistry of oxygen sensors based on luminescent transition-metal complexes”. In: *Analytical Chemistry* 63.4 (Feb. 1, 1991), pp. 337–342.
- [8] J. N. Demas, B. A. DeGraff, and Wenying. Xu. “Modeling of Luminescence Quenching-Based Sensors: Comparison of Multisite and Nonlinear Gas Solubility Models”. In: *Analytical Chemistry* 67.8 (Apr. 1, 1995), pp. 1377–1380.
- [9] Otto S. Wolfbeis. “Fiber-Optic Chemical Sensors and Biosensors”. In: *Analytical Chemistry* 78.12 (June 1, 2006), pp. 3859–3874.
- [10] Colette McDonagh, Conor S. Burke, and Brian D. MacCraith. “Optical Chemical Sensors”. In: *Chemical Reviews* 108.2 (Feb. 1, 2008), pp. 400–422.
- [11] Michela Quaranta, Sergey M. Borisov, and Ingo Klimant. “Indicators for optical oxygen sensors”. In: *Bioanalytical Reviews* 4.2 (Dec. 1, 2012), pp. 115–157.

- [12] Andrew Mills. “Controlling the sensitivity of optical oxygen sensors”. In: *Sensors and Actuators B: Chemical* 51 (1998), pp. 60–68.
- [13] Yong-Eun Koo Lee and Raoul Kopelman. “Optical nanoparticle sensors for quantitative intracellular imaging”. In: *Wiley Interdisciplinary Reviews-Nanomedicine and Nanobiotechnology* 1.1 (Feb. 2009). WOS:000276657700011, pp. 98–110.
- [14] Philipp Babilas et al. “Transcutaneous pO<sub>2</sub> imaging during tourniquet-induced forearm ischemia using planar optical oxygen sensors”. In: *Skin Research and Technology* 14.3 (2008), 304–311.
- [15] Alen Pasic et al. “Miniaturized fiber-optic hybrid sensor for continuous glucose monitoring in subcutaneous tissue”. In: *Sensors and Actuators B: Chemical* 122.1 (Mar. 8, 2007), pp. 60–68.
- [16] Xudong Ge et al. “Validation of an optical sensor-based high-throughput bioreactor system for mammalian cell culture”. In: *Journal of Biotechnology* 122.3 (Apr. 10, 2006), pp. 293–306.
- [17] Heather A Clark et al. “Subcellular optochemical nanobiosensors: probes encapsulated by biologically localised embedding (PEBBLEs)”. In: *Sensors and Actuators B: Chemical* 51.1 (Aug. 31, 1998), pp. 12–16.
- [18] Stefan Nagl et al. “Optical Sensing and Imaging of Trace Oxygen with Record Response”. In: *Angewandte Chemie International Edition* 46.13 (2007), 2317–2319.
- [19] Guoqing Zhang et al. “Multi-Emissive Difluoroboron Dibenzoylmethane Polylactide Exhibiting Intense Fluorescence and Oxygen-Sensitive Room-Temperature Phosphorescence”. In: *Journal of the American Chemical Society* 129.29 (July 2007), pp. 8942–8943.
- [20] Guoqing Zhang et al. “A dual-emissive-materials design concept enables tumour hypoxia imaging”. In: *Nature Materials* 8.9 (Aug. 9, 2009), pp. 747–751.
- [21] Songpan Xu et al. “Aromatic Difluoroboron  $\beta$ -Diketonate Complexes: Effects of  $\pi$ -Conjugation and Media on Optical Properties”. In: *Inorganic Chemistry* 52.7 (Apr. 1, 2013), pp. 3597–3610.
- [22] P. Neogi. *Diffusion in Polymers*. CRC Press, Feb. 6, 1996. 338 pp.
- [23] Sven Kochmann et al. “Sensing and Imaging of Oxygen with Parts per Billion Limits of Detection and Based on the Quenching of the Delayed Fluorescence of 13C70 Fullerene in Polymer Hosts”. In: *Analytical Chemistry* 85.3 (Feb. 5, 2013), pp. 1300–1304.
- [24] Sergey M. Borisov, Philipp Lehner, and Ingo Klimant. “Novel optical trace oxygen sensors based on platinum(II) and palladium(II) complexes with 5,10,15,20-meso-tetrakis-(2,3,4,5,6-pentafluorophenyl)-porphyrin covalently immobilized on silica-gel particles”. In: *Analytica Chimica Acta* 690.1 (2011), pp. 108–115.

- 
- [25] *Polymer handbook*. In collab. with J. Brandrup, E. H. Immergut, and Eric A. Grulke. 4th ed. New York: Wiley, 1999. 1 p.
- [26] AGC Chemicals. *Cytop Cataloge*.
- [27] Vincenzo Arcella, Alessandro Ghielmi, and Giulio Tommasi. "High Performance Perfluoropolymer Films and Membranes". In: *Annals of the New York Academy of Sciences* 984.1 (2003), 226–244.
- [28] T. C. Merkel et al. "Gas sorption, diffusion, and permeation in poly(dimethylsiloxane)". In: *Journal of Polymer Science Part B: Polymer Physics* 38.3 (2000), 415–434.
- [29] Toshio Masuda et al. "Poly[1-(trimethylsilyl)-1-propyne]: a new high polymer synthesized with transition-metal catalysts and characterized by extremely high gas permeability". In: *Journal of the American Chemical Society* 105.25 (Nov. 1, 1983), pp. 7473–7474.
- [30] Dave J Adams et al. "Synthesis and coordination chemistry of perfluoroalkyl-derivatised triarylphosphites". In: *Tetrahedron* 58.20 (May 13, 2002), pp. 3827–3834.
- [31] Mohan N. Wadekar et al. "Synthesis of a Polymerizable Fluorosurfactant for the Construction of Stable Nanostructured Proton-Conducting Membranes". In: *The Journal of Organic Chemistry* 75.20 (Oct. 15, 2010), pp. 6814–6819.
- [32] Joep van den Broeke, Berth-Jan Deelman, and Gerard van Koten. "Tetrakis{3,5-bis(perfluorohexyl)phenyl}borate: a highly fluorous anion". In: *Tetrahedron Letters* 42.45 (Nov. 5, 2001), pp. 8085–8087.
- [33] Peter M. Murphy, Christopher S. Baldwin, and Robert C. Buck. "Syntheses utilizing n-perfluoroalkyl iodides [RFI, C<sub>n</sub>F<sub>2n+1</sub>-I] 2000–2010". In: *Journal of Fluorine Chemistry* 138 (June 2012), pp. 3–23.
- [34] Mari Iizuka and Masato Yoshida. "Redox system for perfluoroalkylation of arenes and alpha-methylstyrene derivatives using titanium oxide as photocatalyst". In: *Journal of Fluorine Chemistry* 130.10 (Oct. 2009), pp. 926–932.
- [35] Anna Bravo et al. "New Methods of Free-Radical Perfluoroalkylation of Aromatics and Alkenes. Absolute Rate Constants and Partial Rate Factors for the Homolytic Aromatic Substitution by n-Perfluorobutyl Radical". In: *The Journal of Organic Chemistry* 62.21 (Oct. 1, 1997), pp. 7128–7136.
- [36] Masato Matsugi et al. "Direct perfluoroalkylation of non-activated aromatic C–H bonds of phenols". In: *Tetrahedron Letters* 49.26 (June 23, 2008), pp. 4189–4191.
- [37] Yan Li et al. "Direct Functionalization of Polycyclic Aromatics via Radical Perfluoroalkylation". In: *Organic Letters* 12.10 (May 21, 2010), pp. 2374–2377.
- [38] George V. D. Tiers. "PERFLUOROALKYLATION OF AROMATIC COMPOUNDS". In: *Journal of the American Chemical Society* 82.20 (Oct. 1, 1960), pp. 5513–5513.

- [39] H. J. H. Fenton. “LXXIII.—Oxidation of tartaric acid in presence of iron”. In: *Journal of the Chemical Society, Transactions* 65.0 (1894), pp. 899–910.
- [40] Haoran Sun et al. “Unexpected photostability improvement of aromatics in polyfluorinated solvents”. In: *Chemical Communications* 48.99 (Nov. 19, 2012), pp. 12085–12087.
- [41] Yang Deng and James D. Englehardt. “Treatment of landfill leachate by the Fenton process”. In: *Water Research* 40.20 (Dec. 2006), pp. 3683–3694.
- [42] Chiew Lin Yap, Suyin Gan, and Hoon Kiat Ng. “Fenton based remediation of polycyclic aromatic hydrocarbons-contaminated soils”. In: *Chemosphere* 83.11 (June 2011), pp. 1414–1430.
- [43] Perla Tatiana Almazán-Sánchez et al. “Wastewater treatment of methyl methacrylate (MMA) by Fenton’s reagent and adsorption”. In: *Catalysis Today* 220–222 (Mar. 2014), pp. 39–48.
- [44] Claude Schweitzer and Reinhard Schmidt. “Physical Mechanisms of Generation and Deactivation of Singlet Oxygen”. In: *Chemical Reviews* 103.5 (May 1, 2003), pp. 1685–1758.
- [45] Peter R. Ogilby and Christopher S. Foote. “Chemistry of singlet oxygen. 42. Effect of solvent, solvent isotopic substitution, and temperature on the lifetime of singlet molecular oxygen (1.DELTA.g)”. In: *Journal of the American Chemical Society* 105.11 (June 1, 1983), pp. 3423–3430.
- [46] John R. Hurst, J. D. McDonald, and Gary B. Schuster. “Lifetime of singlet oxygen in solution directly determined by laser spectroscopy”. In: *Journal of the American Chemical Society* 104.7 (Apr. 1, 1982), pp. 2065–2067.
- [47] Ebrahim Afshari and Reinhard Schmidt. “Isotope-dependent quenching of singlet molecular oxygen ( $1\Delta_g$ ) by ground-state oxygen in several perhalogenated solvents”. In: *Chemical Physics Letters* 184.1 (Sept. 20, 1991), pp. 128–132.
- [48] S. M. Borisov et al. “New NIR-emitting complexes of platinum(II) and palladium(II) with fluorinated benzoporphyrins”. In: *Journal of Photochemistry and Photobiology A: Chemistry* 201.2 (2009), pp. 128–135.
- [49] Weekey Wai-San Lee et al. “Halogenated platinum porphyrins as sensing materials for luminescence-based oxygen sensors”. In: *Journal of Materials Chemistry* 3.10 (1993), p. 1031.
- [50] Otto S. Wolfbeis. “Materials for fluorescence-based optical chemical sensors”. In: *Journal of Materials Chemistry* 15.27 (2005), p. 2657.
- [51] Yutaka Amao. “Probes and Polymers for Optical Sensing of Oxygen”. In: *Microchimica Acta* 143.1 (Sept. 1, 2003), pp. 1–12.

- 
- [52] M. H. Eison-Perchonok and T. W. Downes. “Kinetics of Ascorbic Acid Autoxidation as a Function of Dissolved Oxygen Concentration and Temperature”. In: *Journal of Food Science* 47.3 (1982), 765–767.
- [53] M. M. Taqui. Khan and Arthur E. Martell. “Metal ion and metal chelate catalyzed oxidation of ascorbic acid by molecular oxygen. I. Cupric and ferric ion catalyzed oxidation”. In: *Journal of the American Chemical Society* 89.16 (Aug. 1, 1967), pp. 4176–4185.
- [54] Diane E. Cabelli and Benon H. J. Bielski. “Kinetics and mechanism for the oxidation of ascorbic acid/ascorbate by HO<sub>2</sub>/O<sub>2</sub><sup>-</sup> (hydroperoxyl/superoxide) radicals. A pulse radiolysis and stopped-flow photolysis study”. In: *The Journal of Physical Chemistry* 87.10 (May 1, 1983), pp. 1809–1812.



---

## 7 List of Figures

2.1	Jablonski diagramm of a phosphorescent dye. Showing all important transitions that can occur between excitation and subsequent de-excitation. . . . .	3
2.2	Functional principle of a sensor [10]. . . . .	9
2.3	Structures of the utilized perfluorinated polymers. . . . .	13
2.4	Difluoroboron dibenzoylmethanes. . . . .	14
2.5	Formulas of the novel $\beta$ -diketonates. . . . .	15
4.1	General reaction scheme for the perfluoroalkylation of HPhN and HBAN . . . .	43
4.2	Possible structures of the synthesized HPhNPF and HBANPF ligands. . . . .	44
4.3	Reaction scheme of the $\text{BF}_2$ -chelation of HPhNPF . . . . .	45
4.4	Normalized absorption indicating partial decomposition of the chelate during work up. . . . .	45
4.5	Reaction scheme of the $\text{BF}_2$ -chelation of HBANPF . . . . .	46
4.6	Normalized absorption spectra showing the spectral change during the reaction and the efficiency of the purification with a short Alox column. . . . .	46
4.7	General reaction scheme for the Al-complex formation with HBANPF and HPhNPF. . . . .	47
4.8	Absorption spectra of the Al-complexes during the work up procedure. The remaining free ligand is separated by its better solubility in THF. . . . .	48
4.9	Jablonski diagram showing all modeled concentrations and kinetic constants. . . . .	50
4.10	Simulated calibrations with different levels of triplet $\text{O}_2$ depletion. The upper line is the ideal calibration, the following lines show the influence of tenfold increases of the triplet oxygen lifetimes. . . . .	51
4.11	Simulated calibrations with different levels of ground state depletion. The topmost line is the ideal calibration, the second line shows 10 % depletion and the following lines are based upon a respective increase of intensity by a factor of 10 and have ground state depletions of 50 % and 90 %. . . . .	53
4.12	Absorption spectra of the synthesized dyes and ligands in DCM. . . . .	56
4.13	Excitation (emi: 570 nm) and deoxygenated and oxygenated emission spectra (exc: 420 nm) of $\text{BF}_2\text{HBANPF}$ in Teflon® AF 1600 at 20 °C. . . . .	58
4.14	Excitation and emission spectra of $\text{Al}(\text{HBANPF})_3$ at 20 °C. . . . .	59
4.15	Excitation and emission spectra of $\text{Al}(\text{HPhNPF})_3$ at 20 °C. . . . .	60

---

4.16	Deoxygenated emission spectra (exc: 435 nm) of Al(HPhNPF) <sub>3</sub> in Hyflon® AD 60 at 5 °C, 20 °C and 35 °C. . . . .	61
4.17	Bleaching curves of BF <sub>2</sub> HPhN, BF <sub>2</sub> HBAN, Al(HPhNPF) <sub>3</sub> and Al(HBANPF) <sub>3</sub> under intense irradiation of a blue power LED. . . . .	64
4.18	Saturation curves of BF <sub>2</sub> HBANPF, Al(HPhNPF) <sub>3</sub> and Al(HBANPF) <sub>3</sub> in Teflon® AF 1600. The luminescence intensity is plotted against the corrected excitation intensity $cR$ together with a linear fit of the lower ( $cR < 0.5$ ) measurement points. . . . .	66
4.19	Exemplary mono-exponential decay fits for BF <sub>2</sub> HBANPF, Al(HPhNPF) <sub>3</sub> and Al(HBANPF) <sub>3</sub> in Teflon® AF 1600. . . . .	69
4.20	Mono-exponentially fitted decay curves of Al(HBANPF) <sub>3</sub> in Teflon® AF 1600 with two different intensities. . . . .	70
4.21	Mono-exponentially fitted decay curves of Al(HBANPF) <sub>3</sub> in Teflon® AF 1600 at three different intensities with traces of oxygen. . . . .	73
4.22	Single photon counting measurements of the lifetimes of BF <sub>2</sub> HBANPF, Al(HPhNPF) <sub>3</sub> and Al(HBANPF) <sub>3</sub> with 0.05 wt% in Teflon® AF 1600. Recorded at room temperature. . . . .	74
4.23	Measurement curve of the Pd benzoporphyrine in Teflon® AF 1600 sensor during the ascorbate oxygen consumption. . . . .	77
4.24	Example of the standard addition calibration. Al(HBANPF) <sub>3</sub> in Hyflon® AD 60 at 20 °C. . . . .	79
4.25	Measured calibration curves at 20 °C . . . . .	80
4.26	Temperature dependency of the Al(HPhNPF) <sub>3</sub> in Hyflon® AD 60 calibration. . . . .	82
4.27	Excitation intensity dependency of the Al(HPhNPF) <sub>3</sub> in Hyflon® AD 60 calibration. . . . .	83
4.28	Kinetic measurements and calibration curves of the failed Al(HBANPF) <sub>3</sub> in Cytop® CTL-107MK calibration. . . . .	84
4.29	Measurement curves of three used sensors during the oxygen consumption by glucose oxidase and a mono-exponential fit of the Al(HPhNPF) <sub>3</sub> in Hyflon® AD 60 sensor from 150 min (insert). . . . .	87
9.1	NMR spectrum of HPhNPF. . . . .	103
9.2	Mass spectrum of HPhNPF. . . . .	104
9.3	NMR spectrum of HBANPF . . . . .	105
9.4	Mass spectrum of HBANPF . . . . .	106
9.5	NMR spectrum of BF <sub>2</sub> HBANPF. . . . .	107
9.6	Mass spectrum of BF <sub>2</sub> HBANPF. . . . .	108
9.7	NMR spectrum of Al(HPhNPF) <sub>3</sub> . . . . .	109
9.8	Mass spectrum of Al(HPhNPF) <sub>3</sub> . . . . .	110
9.9	NMR spectrum of Al(HBANPF) <sub>3</sub> . . . . .	111
9.10	Mass spectrum of Al(HPhNPF) <sub>3</sub> . . . . .	112

---

9.11	BF <sub>2</sub> HPhN in polystyrene. Emission spectra used for determination of the quantum yields. . . . .	117
9.12	BF <sub>2</sub> HBAN in polystyrene. Emission spectra used for determination of the quantum yields. . . . .	117
9.13	BF <sub>2</sub> HBANPF in Teflon® AF 1600. Emission spectra used for determination of the quantum yields. . . . .	117
9.14	Al(HPhNPF) <sub>3</sub> in Teflon® AF 1600. Emission spectra used for determination of the quantum yields. . . . .	118
9.15	Al(HBANPF) <sub>3</sub> in Teflon® AF 1600. Emission spectra used for determination of the quantum yields. . . . .	118
9.16	Bleaching curves of BF <sub>2</sub> HPhN, BF <sub>2</sub> HBAN, Al(HPhNPF) <sub>3</sub> and Al(HBANPF) <sub>3</sub> with multiple tracked wavelengths. . . . .	119
9.17	Absorption spectra of BF <sub>2</sub> HPhN, BF <sub>2</sub> HBAN, Al(HPhNPF) <sub>3</sub> and Al(HBANPF) <sub>3</sub> during the photobleaching experiments. . . . .	120
9.18	Normalized absorption spectra of BF <sub>2</sub> HPhN, BF <sub>2</sub> HBAN, Al(HPhNPF) <sub>3</sub> and Al(HBANPF) <sub>3</sub> before and after the bleaching experiments (120 min of illumination with a blue power LED). . . . .	121

---

## 8 List of Tables

2.1	Oxygen permeabilities of selected polymers. . . . .	12
3.1	Used Ligands and Dyes. . . . .	21
3.2	Used polymer matrices. . . . .	21
3.3	Used gases. . . . .	22
3.4	Used Solvents. . . . .	22
3.5	Other used chemicals. . . . .	23
3.6	Measurement settings for the emission spectra. . . . .	28
3.7	Settings for the measurements of the oxygenated quantum yields . . . . .	29
3.8	Measurement settings for the oxygenated and deoxygenated emission spectra. . . . .	30
3.9	FluoroLog® 3 settings for the intensity dependency measurements. . . . .	31
3.10	Settings for the measurements of the deoxygenated lifetimes. . . . .	33
3.11	FluoroLog® 3 settings for the deoxygenated lifetime intensity dependency measurements . . . . .	33
3.12	Single photon counting emission monochromator settings . . . . .	34
3.13	Fitting parameters and results of the single photon counting lifetime measurements . . . . .	34
4.1	Molar absorption coefficients of the dyes measured in dichloromethane. . . . .	55
4.2	Quantum yields of the unmodified and perfluoroalkylated dyes in polystyrene and Teflon® AF 1600, respectively. . . . .	62
4.3	Anoxic lifetimes of the dyes at 20 °C in sodium sulfite solution. For all measured values see table 9.3 on page 122. . . . .	68
4.4	Anoxic lifetimes of the dyes in Teflon® AF 1600 at 20 °C in sodium sulfite solution with different excitation intensities. For all measured values see table 9.4 on page 123. . . . .	71
4.5	Phosphorescence Lifetimes of Al(HBANPF) <sub>3</sub> (0.05 wt% in Teflon® AF 1600) with ≈ 1.5 ppmv O <sub>2</sub> with multiple excitation light intensities. For all measured values see table 9.5 on page 124. . . . .	72
4.6	Lifetimes and relative amplitudes of the dyes (0.05 wt% in Teflon® AF 1600). Measured with time correlated single photon counting. . . . .	75
4.7	Important unit conversions. . . . .	77

---

4.8	Measured $K_{SV}$ values of the calibrated dyes at 20 °C. . . . .	81
4.9	$K_{SV}$ -values and calculated quenching constants $k_q$ for Al(HPhNPF) <sub>3</sub> in Teflon® AF 1600 at 5 °C, 20 °C and 35 °C . . . . .	82
4.10	$K_{SV}$ -values at different excitation intensities for Al(HPhNPF) <sub>3</sub> in Teflon® AF 1600 . . . . .	83
4.11	Measured lifetimes and $\tau_0/\tau - 1$ values of the lifetime calibration. The $cR$ value was 0.041. For all measured values see table 9.7 on page 125. . . . .	85
4.12	Measured lifetimes and calculated O <sub>2</sub> concentrations of the gas bottles. . . . .	86
9.1	Measured areas in the integration sphere and oxygenated prompt fluorescence quantum yields. . . . .	115
9.2	Areas, integration ranges and quantum yields of prompt fluorescence ( $pF$ ) (oxygenated), fluorescence and phosphorescence ( $pF + dF + P$ ), phosphorescence ( $P$ ) and delayed fluorescence ( $dF$ ). . . . .	116
9.3	Anoxic lifetimes of the dyes at 20 °C in sodium sulfite solution. . . . .	122
9.4	Anoxic lifetimes of the dyes in Teflon® AF 1600 at 20 °C in sodium sulfite solution with different excitation intensities . . . . .	123
9.5	Phosphorescence Lifetimes of Al(HBANPF) <sub>3</sub> (0.05 wt% in Teflon® AF 1600) with $\approx 1.5$ ppmv O <sub>2</sub> with multiple excitation light intensities. . . . .	124
9.6	Intensities of the luminescence intensity dependency measurements. . . . .	125
9.7	Measured lifetimes and $\tau_0/\tau - 1$ values of the lifetime calibration . . . . .	125



# 9 Appendix

## 9.1 NMR and Mass Spectra

### 9.1.1 HPhNPF

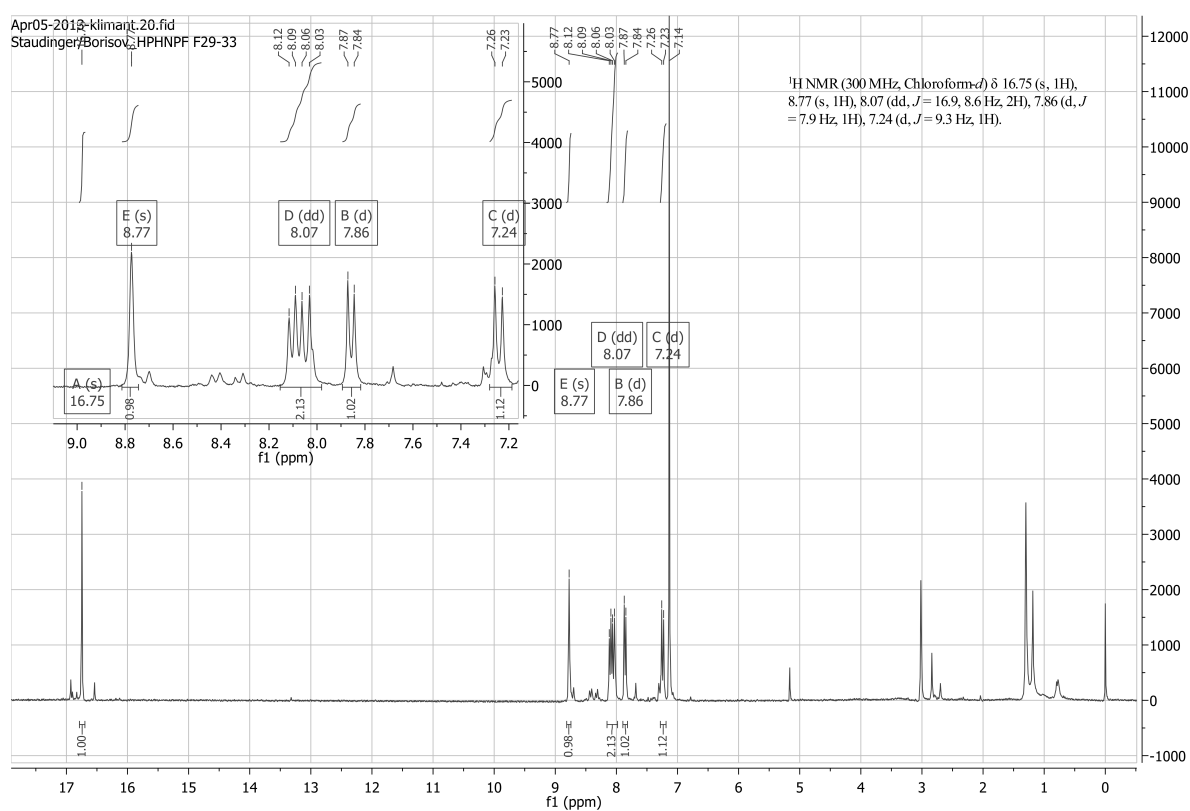
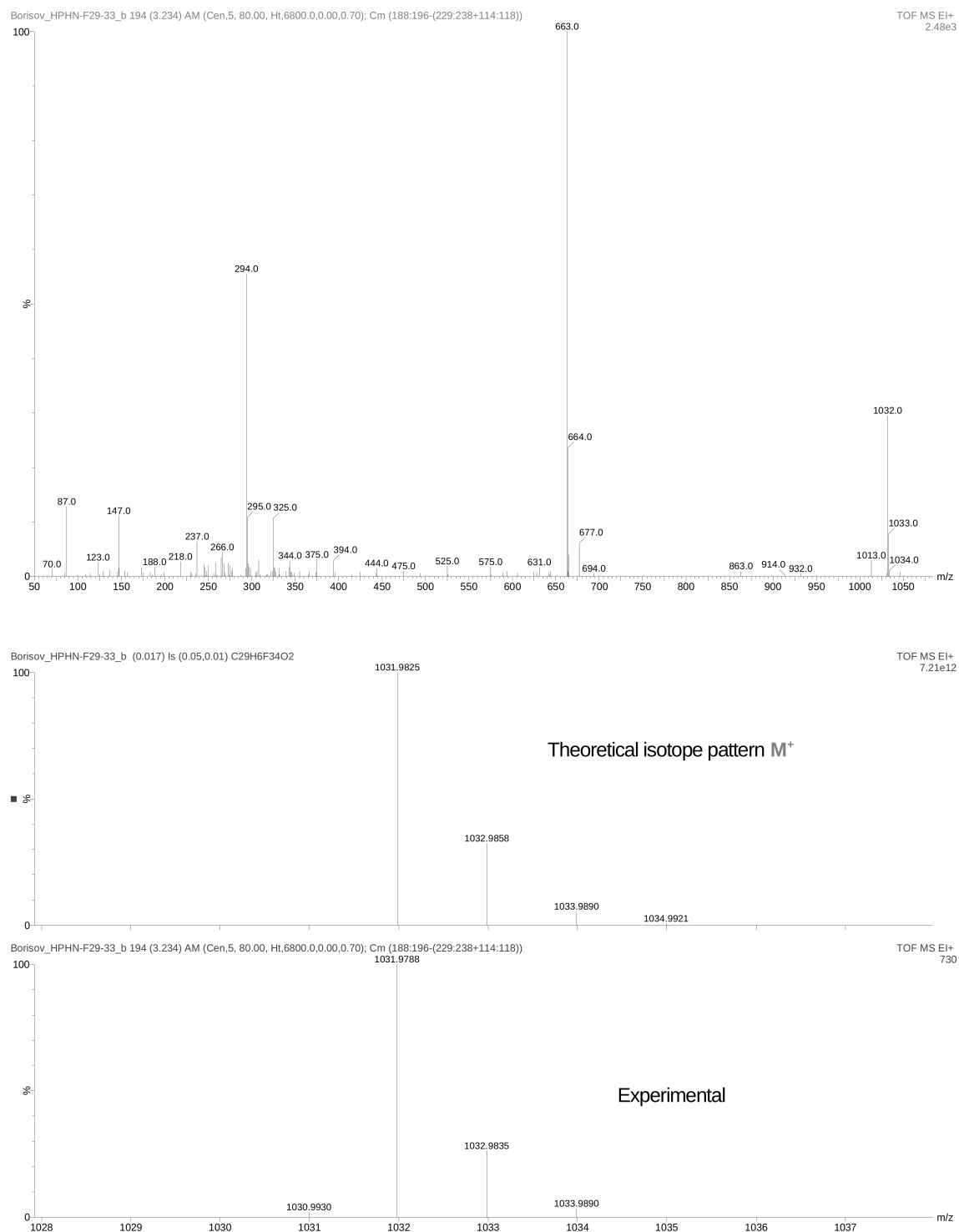


Figure 9.1: NMR spectrum of HPhNPF.



**Figure 9.2:** Mass spectrum of HPhNPF.

## 9.1.2 HBANPF

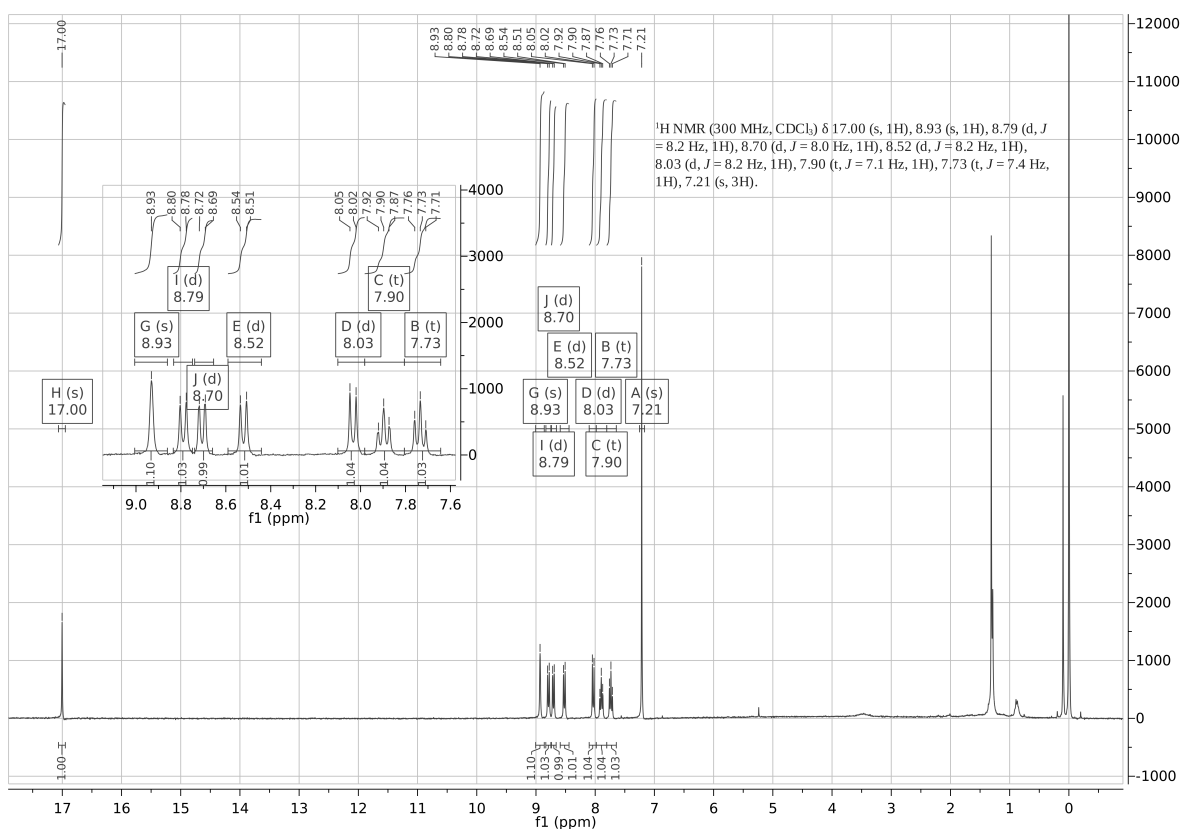
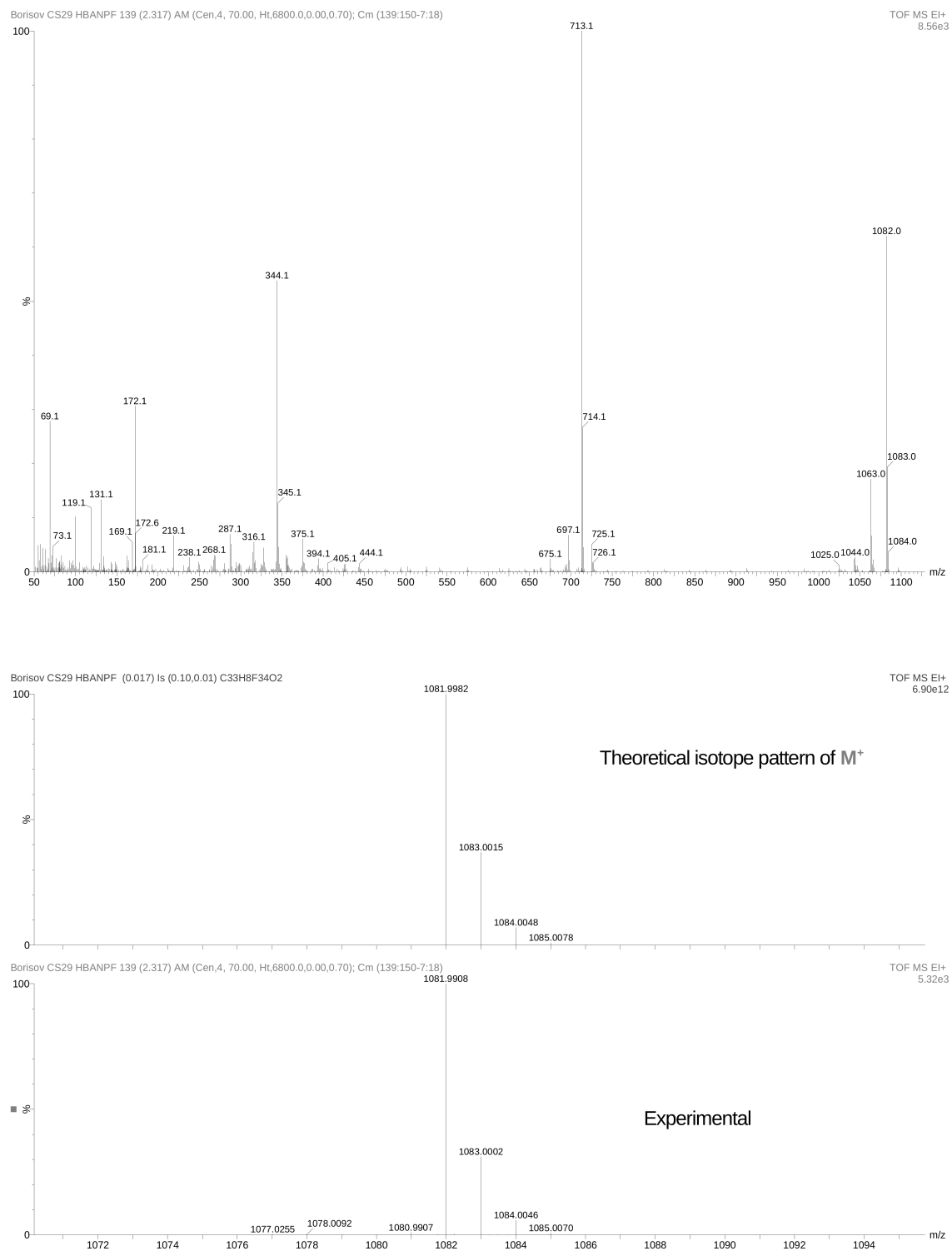
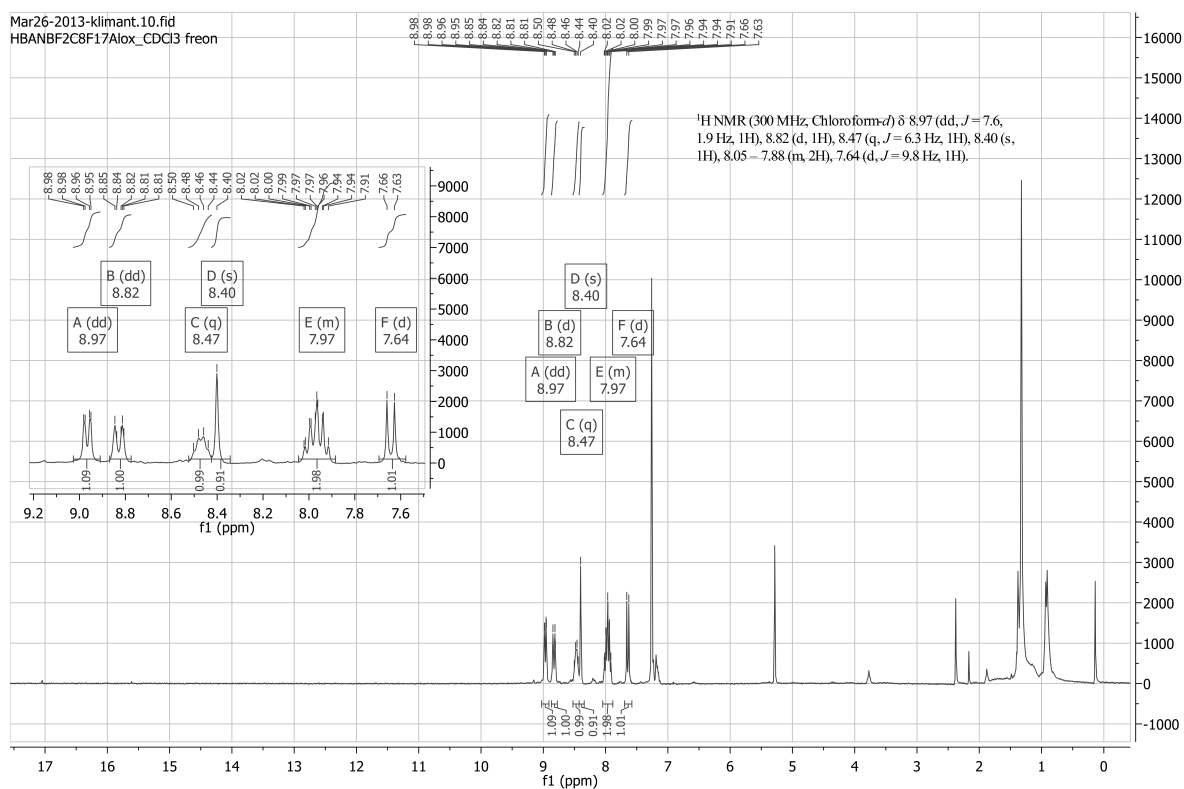
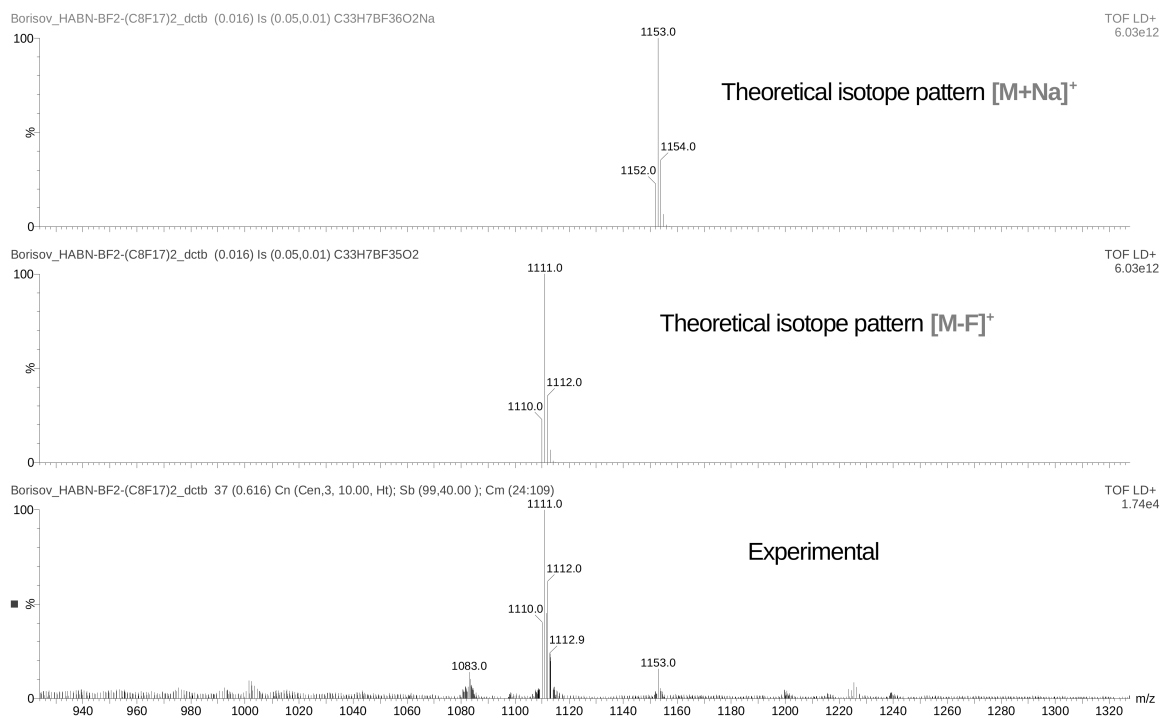


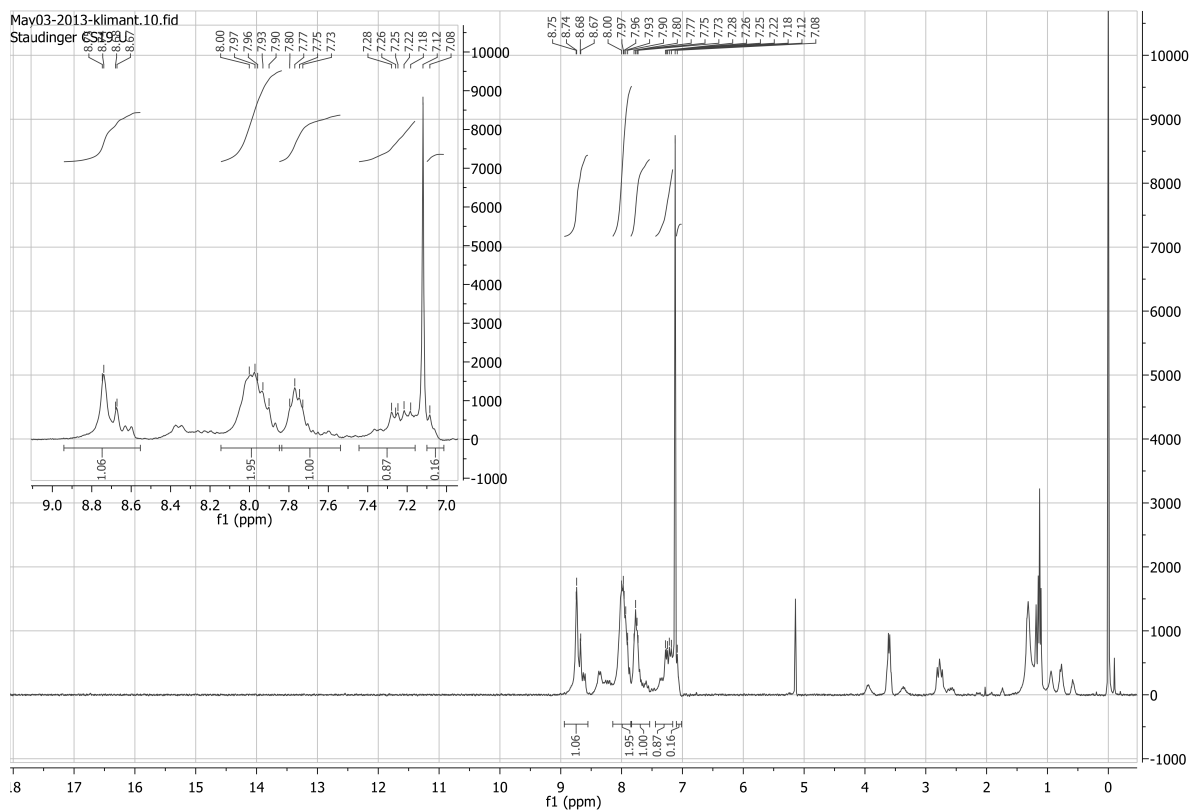
Figure 9.3: NMR spectrum of HBANPF

**Figure 9.4:** Mass spectrum of HBANPF

9.1.3 BF<sub>2</sub>HBANPFFigure 9.5: NMR spectrum of BF<sub>2</sub>HBANPF.



**Figure 9.6:** Mass spectrum of  $BF_2HBANPF$ .

9.1.4 Al(HPhNPF)<sub>3</sub>Figure 9.7: NMR spectrum of Al(HPhNPF)<sub>3</sub>.

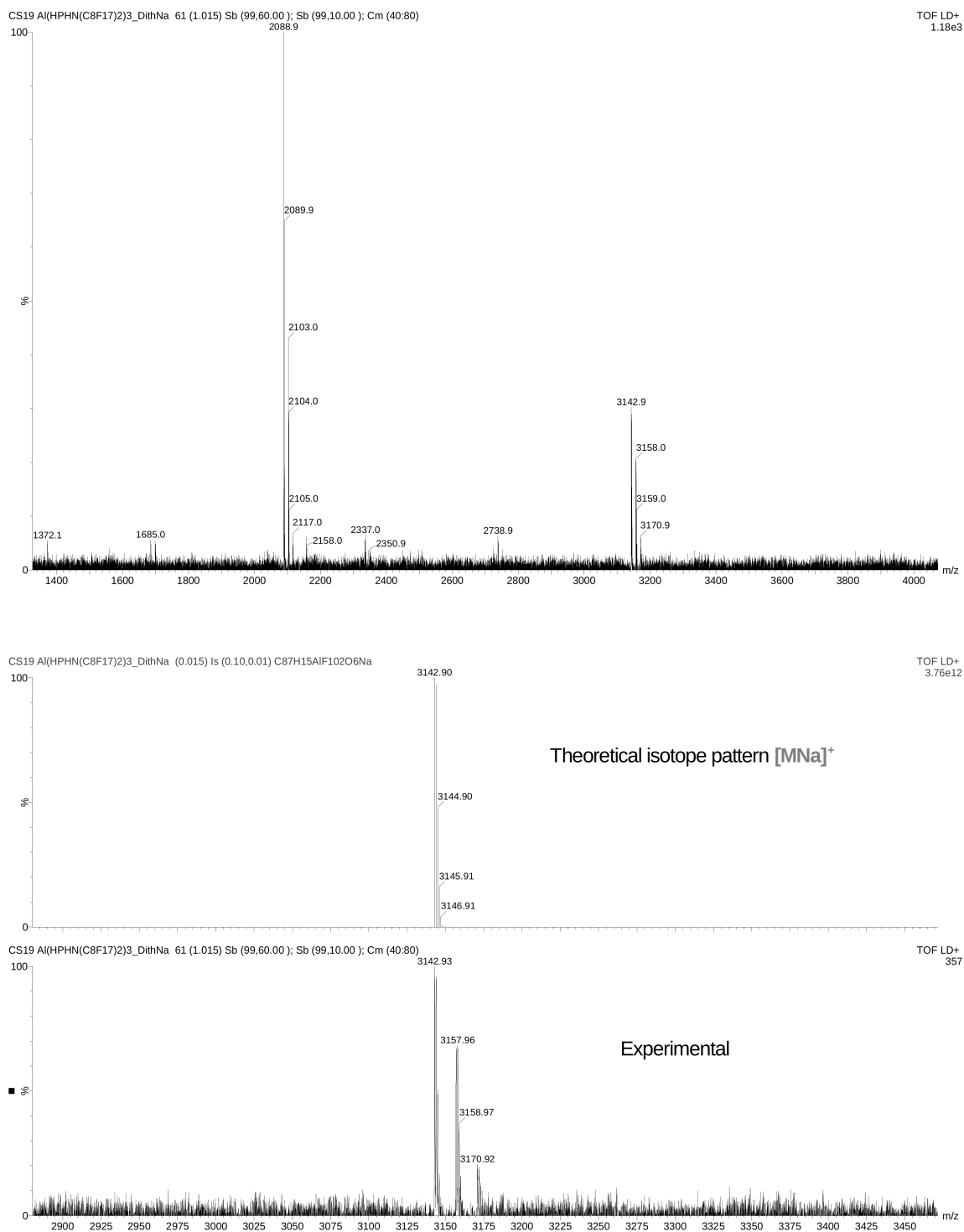


Figure 9.8: Mass spectrum of Al(HPhNPF)<sub>3</sub>.

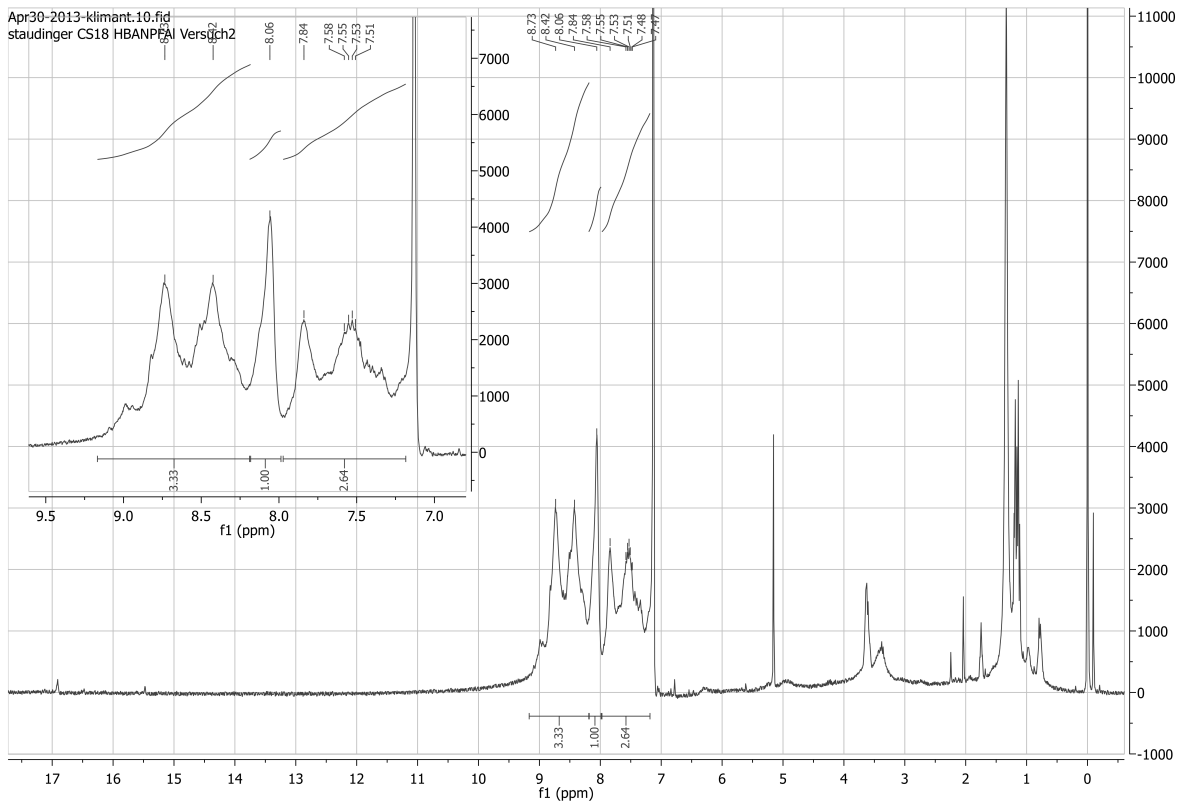
9.1.5 Al(HBANPF)<sub>3</sub>

Figure 9.9: NMR spectrum of Al(HBANPF)<sub>3</sub>.

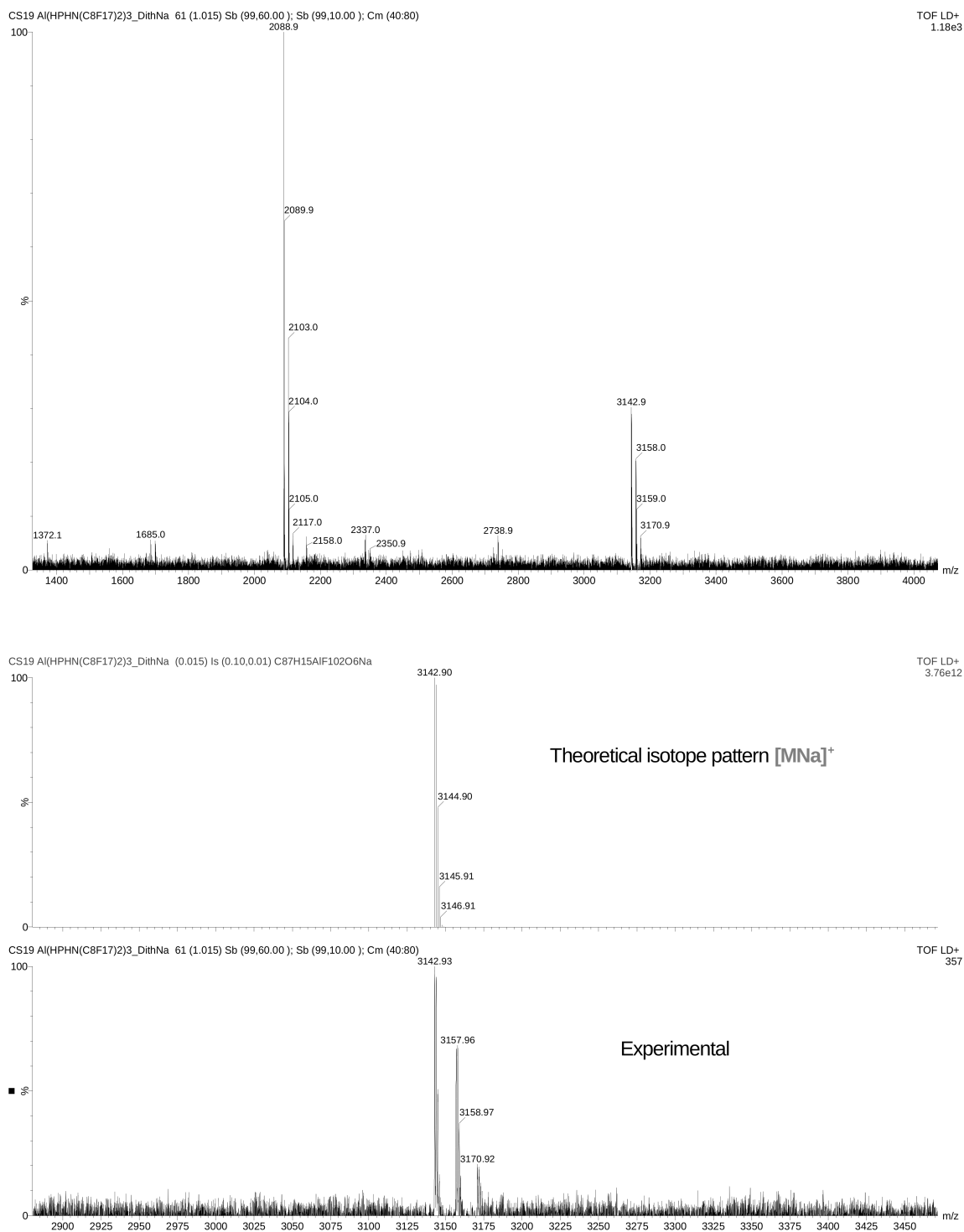


Figure 9.10: Mass spectrum of  $Al(HPnNPF)_3$ .

## 9.2 Model Equations

$$\begin{aligned}
S_0 = & (Ik_{isc}^2 k_{rO_2} k_E + Ik_{isc-1} k_{rO_2} k_r P k_E + k_{isc}^2 k_{rO_2} k_F + k_{isc-1} k_{rO_2} k_r P k_F + \quad (9.1) \\
& Ik_{isc-1} k_{rO_2} k_E k_F + Ik_{rO_2} k_r P k_E k_F + k_{isc-1} k_{rO_2} k_F^2 + k_{rO_2} k_r P k_F^2 + \\
& k_{isc-1} k_{rO_2} k_r P k_{isc} + 2Ik_{isc-1} k_{rO_2} k_E k_{isc} + Ik_{rO_2} k_r P k_E k_{isc} + k_{isc-1} k_{rO_2} k_F k_{isc} + \\
& 2k_{rO_2} k_r P k_F k_{isc} + Ik_{rO_2} k_E k_F k_{isc} + k_{rO_2} k_r P k_{isc}^2 + Ik_{rO_2} k_E k_{isc}^2 + Ik_{isc-1} k_{rO_2} k_E k_P + \\
& k_{isc-1} k_{rO_2} k_F k_P + Ik_{rO_2} k_E k_F k_P + k_{rO_2} k_F^2 k_P + k_{isc-1} k_{rO_2} k_{isc} k_P + Ik_{rO_2} k_E k_{isc} k_P + \\
& 2k_{rO_2} k_F k_{isc} k_P + k_{rO_2} k_{isc}^2 k_P + 2CIk_{isc-1} k_E k_F k_q + 2CIk_r P k_E k_F k_q + \\
& 2Ck_{isc-1} k_F^2 k_q + 2Ck_r P k_F^2 k_q + CIk_{isc-1} k_E k_{isc} k_q + 2CIk_r P k_E k_{isc} k_q + \\
& 2Ck_{isc-1} k_F k_{isc} k_q + 4Ck_r P k_F k_{isc} k_q + CIk_E k_F k_{isc} k_q + 2Ck_r P k_{isc}^2 k_q + \\
& CIk_E k_{isc}^2 k_q + 2CIk_E k_F k_P k_q + 2Ck_F^2 k_P k_q + 2CIk_E k_{isc} k_P k_q + 4Ck_F k_{isc} k_P k_q + \\
& 2Ck_{isc}^2 k_P k_q + Ik_{isc-1} k_{rO_2} k_E k_q O_2 + k_{isc-1} k_{rO_2} k_F k_q O_2 + Ik_{rO_2} k_E k_F k_q O_2 + \\
& k_{rO_2} k_F^2 k_q O_2 + k_{isc-1} k_{rO_2} k_{isc} k_q O_2 + Ik_{rO_2} k_E k_{isc} k_q O_2 + 2k_{rO_2} k_F k_{isc} k_q O_2 + \\
& k_{rO_2} k_{isc}^2 k_q O_2 + k_r^2 ((k_{isc-1} + k_r P + k_P)(k_{rO_2} + 2Ck_q) + k_{rO_2} k_q O_2) - \\
& k_{isc-1} X - k_r F X - k_F X - k_{isc} X + \\
& k_r F (k_{isc}^2 k_{rO_2} + 2(k_F + k_{isc})((k_r P + k_P)(k_{rO_2} + 2Ck_q) + k_{rO_2} k_q O_2) + \\
& Ik_E (C(2k_r P + k_{isc} + 2k_P)k_q + k_{rO_2} (k_r P + k_{isc} + k_P + k_q O_2))) + \\
& k_{isc-1} (2C(Ik_E + 2k_F + k_{isc})k_q + k_{rO_2} (k_r P + Ik_E + 2k_F + k_{isc} + k_P + k_q O_2)))/ \\
& (2(k_r F + Ik_E + k_F + k_{isc})(k_r F k_r P + Ik_r P k_E + k_r P k_F + k_{isc-1} (k_r F + Ik_E + k_F) + \\
& k_r P k_{isc} + Ik_E k_{isc} + (k_r F + Ik_E + k_F + k_{isc})k_P)k_q)
\end{aligned}$$

$$\begin{aligned}
S_1 = & (Ik_r F k_{rO_2} k_r P k_E + I^2 k_{rO_2} k_r P k_E^2 + Ik_{rO_2} k_r P k_E k_F - k_{isc}^2 k_{rO_2} (k_r F + Ik_E + k_F) + \quad (9.2) \\
& Ik_{rO_2} k_r P k_E k_{isc} + I^2 k_{rO_2} k_E^2 k_{isc} + Ik_r F k_{rO_2} k_E k_P + I^2 k_{rO_2} k_E^2 k_P + Ik_{rO_2} k_E k_F k_P + \\
& Ik_{rO_2} k_E k_{isc} k_P + 2CIk_r F k_r P k_E k_q + 2CI^2 k_r P k_E^2 k_q + 2CIk_r P k_E k_F k_q + \\
& 2CIk_r P k_E k_{isc} k_q + CI^2 k_E^2 k_{isc} k_q + 2CIk_r F k_E k_P k_q + 2CI^2 k_E^2 k_P k_q + \\
& 2CIk_E k_F k_P k_q + 2CIk_E k_{isc} k_P k_q + Ik_r F k_{rO_2} k_E k_q O_2 + I^2 k_{rO_2} k_E^2 k_q O_2 + \\
& Ik_{rO_2} k_E k_F k_q O_2 + Ik_{rO_2} k_E k_{isc} k_q O_2 + \\
& k_{isc-1} (-k_{rO_2} (-I^2 k_E^2 + (k_F + k_{isc})(k_r P + k_P) + k_r F (k_r P - Ik_E + k_P) + \\
& Ik_E (k_r P - k_F + k_{isc} + k_P)) + CIk_E (2(k_r F + Ik_E + k_F) + k_{isc})k_q - \\
& k_{rO_2} (k_r F + Ik_E + k_F + k_{isc})k_q O_2) + k_{isc-1} X - Ik_E X)/ \\
& (2(k_r F + Ik_E + k_F + k_{isc})(k_r F k_r P + Ik_r P k_E + k_r P k_F + k_{isc-1} (k_r F + Ik_E + k_F) + \\
& k_r P k_{isc} + Ik_E k_{isc} + (k_r F + Ik_E + k_F + k_{isc})k_P)k_q)
\end{aligned}$$

$$\begin{aligned}
T_1 = & (-k_{isc-1}k_{rO_2}(k_{rF} + k_F) - k_{rO_2}(k_{rF} + k_F + k_{isc})(k_{rP} + k_P + k_qO_2) - \\
& Ik_E(k_{isc-1}k_{rO_2} - Ck_{isc}k_q + k_{rO_2}(k_{rP} + k_{isc} + k_P + k_qO_2)) + X) / \\
& (2(k_{rF}k_{rP} + Ik_{rP}k_E + k_{rP}k_F + k_{isc-1}(k_{rF} + Ik_E + k_F) + k_{rP}k_{isc} + \\
& Ik_Ek_{isc} + (k_{rF} + Ik_E + k_F + k_{isc})k_P)k_q)
\end{aligned} \tag{9.3}$$

$$\begin{aligned}
O_{2T} = & - (1/(2k_{rO_2}(k_{rF} + Ik_E + k_F + k_{isc})k_q))(k_{isc-1}k_{rO_2}(k_{rF} + k_F) + \\
& k_{rO_2}(k_{rF} + k_F + k_{isc})(k_{rP} + k_P - k_qO_2) + Ik_E(k_{isc-1}k_{rO_2} + Ck_{isc}k_q + \\
& k_{rO_2}(k_{rP} + k_{isc} + k_P - k_qO_2)) - X);
\end{aligned} \tag{9.4}$$

$$\begin{aligned}
O_{2S} = & 1/(2k_{rO_2}(k_{rF} + Ik_E + k_F + k_{isc})k_q)(k_{rO_2}(k_{isc-1}(k_{rF} + k_F) + \\
& (k_{rF} + k_F + k_{isc})(k_{rP} + k_P + k_qO_2)) + Ik_E(k_{isc-1}k_{rO_2} + Ck_{isc}k_q + \\
& k_{rO_2}(k_{rP} + k_{isc} + k_P + k_qO_2)) - X);
\end{aligned} \tag{9.5}$$

with (9.6)

$$\begin{aligned}
X = & \sqrt{\frac{4CIk_{rO_2}k_Ek_{isc}(k_{rF}k_{rP} + Ik_{rP}k_E + k_{rP}k_F + k_{isc-1}(k_{rF} + Ik_E + k_F) + \\
& k_{rP}k_{isc} + Ik_Ek_{isc} + (k_{rF} + Ik_E + k_F + k_{isc})k_P)k_q + (Ik_{rO_2}k_{rP}k_E + \\
& k_{rO_2}k_{rP}k_F + k_{isc-1}k_{rO_2}(k_{rF} + Ik_E + k_F) + k_{rO_2}k_{rP}k_{isc} + Ik_{rO_2}k_Ek_{isc} + \\
& Ik_{rO_2}k_Ek_P + k_{rO_2}k_Fk_P + k_{rO_2}k_{isc}k_P - CIk_Ek_{isc}k_q + \\
& k_{rO_2}(Ik_E + k_F + k_{isc})k_qO_2 + k_{rF}k_{rO_2}(k_{rP} + k_P + k_qO_2))^2}
\end{aligned}$$

## 9.3 Quantum Yields

**Table 9.1:** Measured areas in the integration sphere and oxygenated prompt fluorescence quantum yields.

Dye		Integ. Range [nm]	Area	FF <sup>a</sup>	Oxygenated QY [%]
BF <sub>2</sub> HPhN	trans <sub>bg</sub>	395.2–425.1	$4.98 \cdot 10^7$	37.8	1.35
	trans <sub>dye</sub>	395.2–425.1	$2.21 \cdot 10^7$		
	emi <sub>bg</sub>	437.7–566.7	$3.09 \cdot 10^6$		
	emi <sub>dye</sub>	437.7–566.7	$1.68 \cdot 10^7$		
BF <sub>2</sub> HBAN	trans <sub>bg</sub>	396.0–426.0	$4.98 \cdot 10^7$	37.8	5.45
	trans <sub>dye</sub>	396.0–426.0	$2.75 \cdot 10^7$		
	emi <sub>bg</sub>	448.2–610.0	$3.40 \cdot 10^6$		
	emi <sub>dye</sub>	448.2–610.0	$4.88 \cdot 10^7$		
BF <sub>2</sub> HBANPF	trans <sub>bg</sub>	394.5–424.4	$2.68 \cdot 10^7$	148	1.45
	trans <sub>dye</sub>	394.5–424.4	$9.70 \cdot 10^6$		
	emi <sub>bg</sub>	437.1–670.4	$6.29 \cdot 10^6$		
	emi <sub>dye</sub>	437.1–670.4	$4.32 \cdot 10^7$		
Al(HPhNPF) <sub>3</sub>	trans <sub>bg</sub>	392.0–422.0	$2.68 \cdot 10^7$	148	0.87
	trans <sub>dye</sub>	392.0–422.0	$1.69 \cdot 10^7$		
	emi <sub>bg</sub>	424.3–698.7	$7.17 \cdot 10^6$		
	emi <sub>dye</sub>	424.3–698.7	$1.99 \cdot 10^7$		
Al(HBANPF) <sub>3</sub>	trans <sub>bg</sub>	394.3–424.3	$2.68 \cdot 10^7$	148	1.97
	trans <sub>dye</sub>	394.3–424.3	$1.44 \cdot 10^7$		
	emi <sub>bg</sub>	427.0–700.0	$7.04 \cdot 10^6$		
	emi <sub>dye</sub>	427.0–700.0	$4.31 \cdot 10^7$		

<sup>a</sup> Filter factor, calculated with the filter transmittances at 410 nm. (2.64 % and 25.4 % for the 5 % and 25 % filters, respectively)

**Table 9.2:** Areas, integration ranges and quantum yields of prompt fluorescence ( $pF$ ) (oxygenated), fluorescence and phosphorescence ( $pF + dF + P$ ), phosphorescence ( $P$ ) and delayed fluorescence ( $dF$ ).

Dye	Lum.	Integ. Range [nm]	C	Area	QY [%]
BF <sub>2</sub> HPhN	$pF$	438.4–603.3	1.84	$1.30 \cdot 10^8$	1.35 <sup>a</sup>
	$pF + dF + P$	440.7–696.5		$6.87 \cdot 10^8$	7.1
	$P$	495.5–695.1		$4.43 \cdot 10^8$	4.6
	$dF$				1.19
BF <sub>2</sub> HBAN	$pF$	450.2–634.9	1.86	$2.59 \cdot 10^8$	5.45 <sup>a</sup>
	$pF + dF + P$	450.1–698.6		$9.12 \cdot 10^8$	19.2
	$P$	471.4–699.6		$4.33 \cdot 10^8$	9.1
	$dF$				4.6
BF <sub>2</sub> HBANPF	$pF$	439.9–687.8	1.16	$7.76 \cdot 10^7$	1.45 <sup>a</sup>
	$pF + dF + P$	432.7–709.4		$1.77 \cdot 10^8$	3.3
	$P$	523.2–711.5		$8.77 \cdot 10^7$	1.6
	$dF$				0.2
Al(HPhNPF) <sub>3</sub>	$pF$	453.0–700.1	2.43	$3.22 \cdot 10^7$	0.87 <sup>a</sup>
	$pF + dF + P$	452.0–703.6		$2.79 \cdot 10^8$	7.5
	$P$	533.0–703.3		$2.00 \cdot 10^8$	5.4
	$dF$				1.3
Al(HBANPF) <sub>3</sub>	$pF$	445.8–696.8	1.37	$7.25 \cdot 10^7$	1.97 <sup>a</sup>
	$pF + dF + P$	445.1–703.3		$2.19 \cdot 10^8$	6.0
	$P$	520.2–703.3		$1.19 \cdot 10^8$	3.2
	$dF$				0.8

<sup>a</sup> Values from the oxygenated integration sphere experiments (see section 3.5.4)

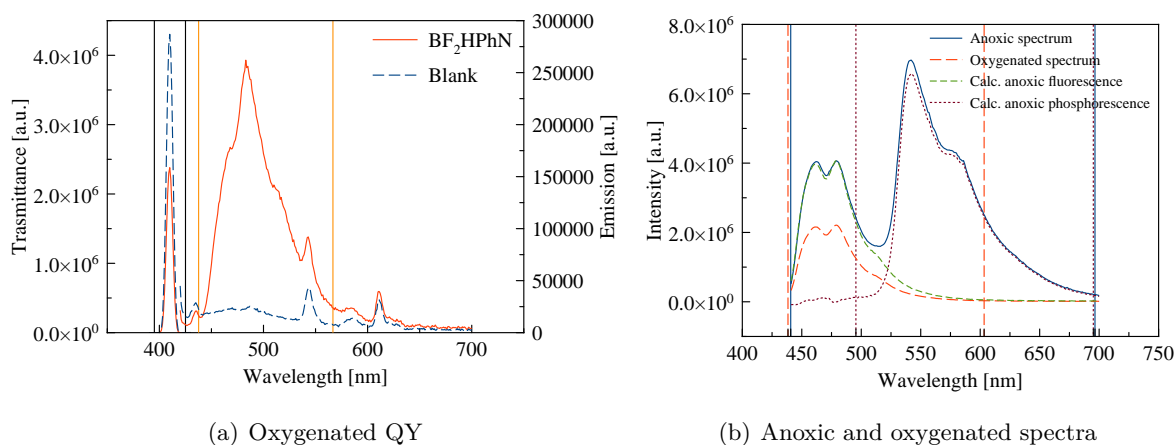


**Figure 9.11:** BF<sub>2</sub>HPhN in polystyrene. Emission spectra used for determination of the quantum yields.

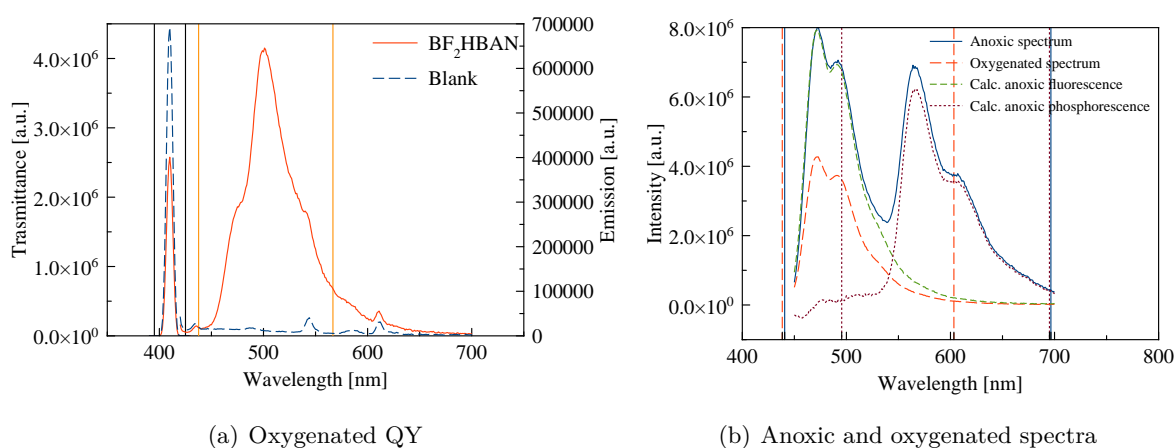


**Figure 9.12:** BF<sub>2</sub>HBAN in polystyrene. Emission spectra used for determination of the quantum yields.

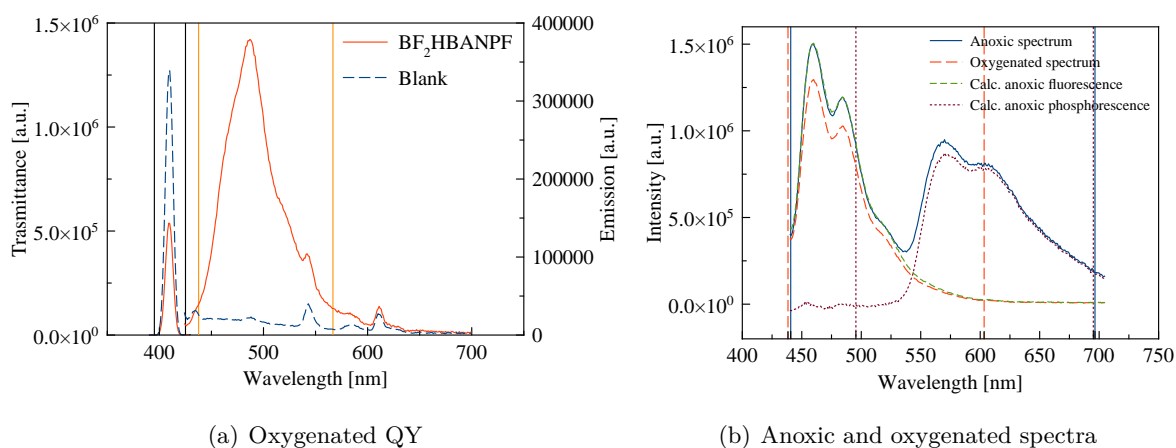


**Figure 9.13:** BF<sub>2</sub>HBANPF in Teflon® AF 1600. Emission spectra used for determination of the quantum yields.

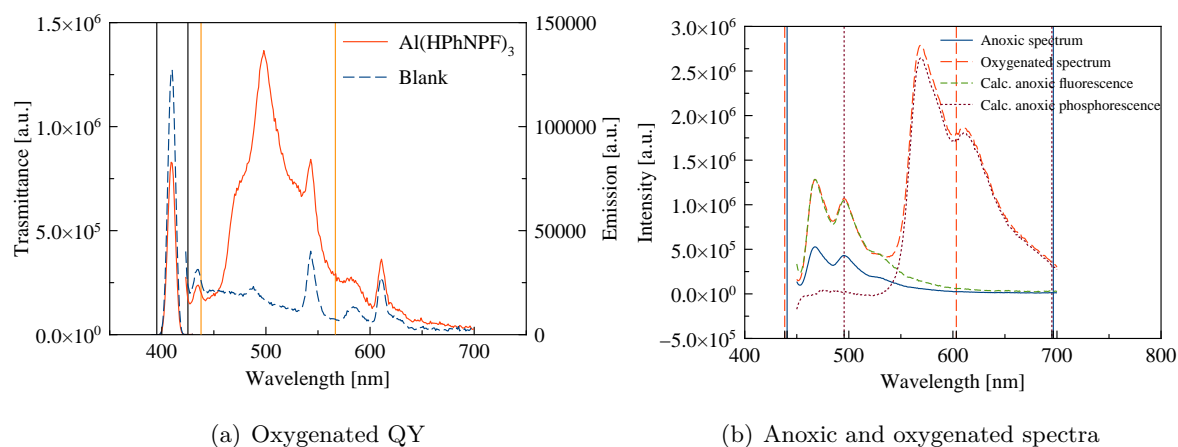


**Figure 9.14:** Al(HPhNPF)<sub>3</sub> in Teflon® AF 1600. Emission spectra used for determination of the quantum yields.

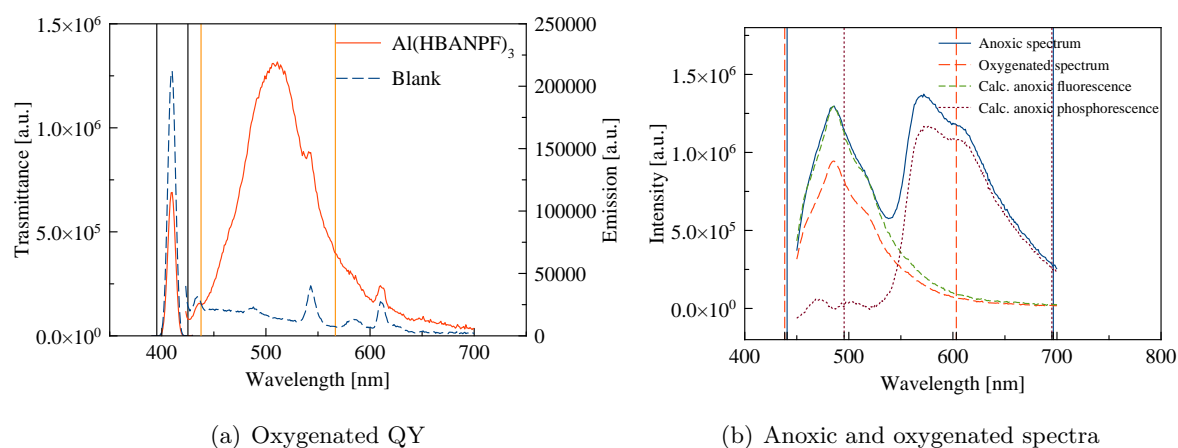


**Figure 9.15:** Al(HBANPF)<sub>3</sub> in Teflon® AF 1600. Emission spectra used for determination of the quantum yields.

## 9.4 Photochemical Stability

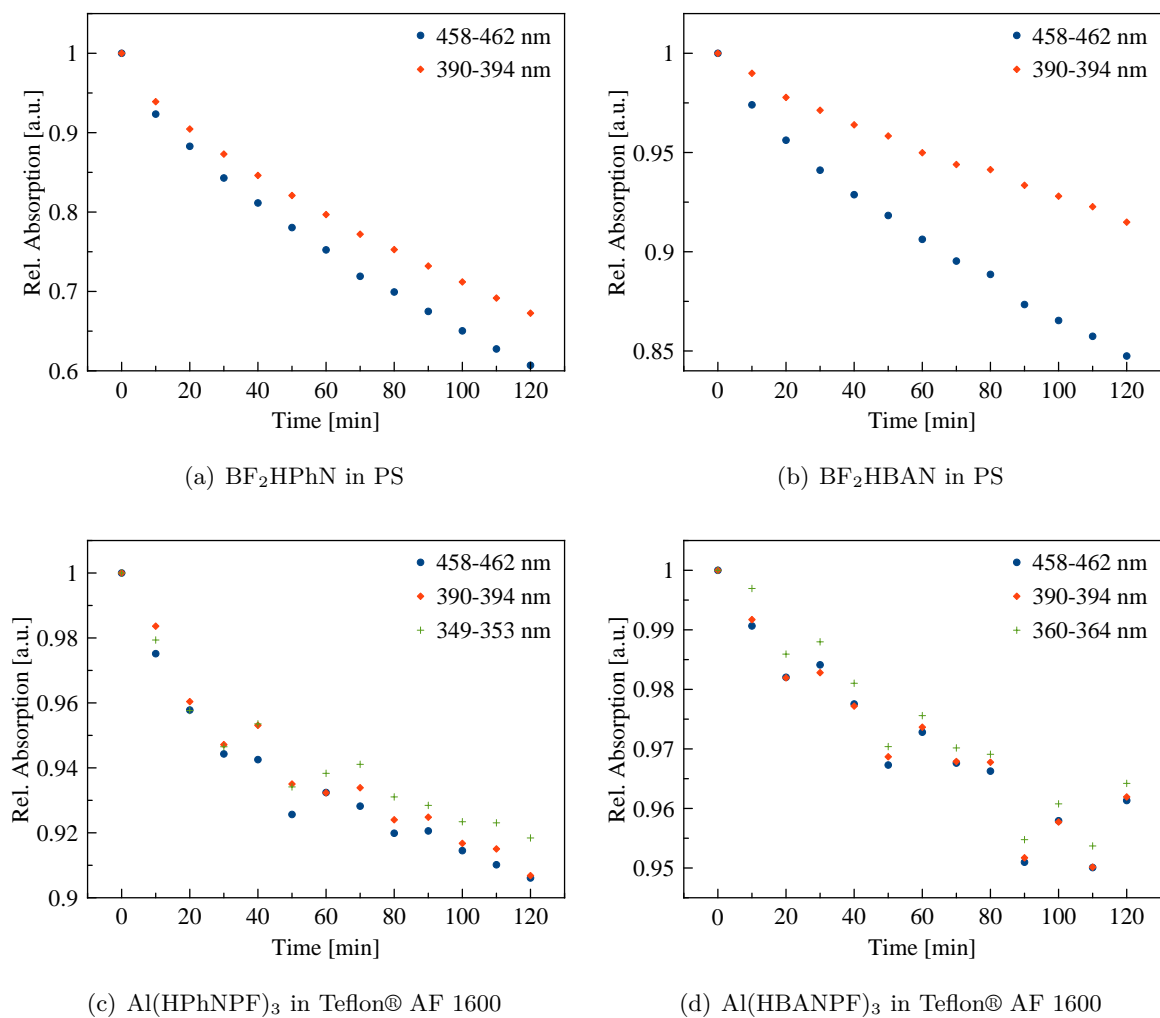


**Figure 9.16:** Bleaching curves of  $\text{BF}_2\text{HPhN}$ ,  $\text{BF}_2\text{HBAN}$ ,  $\text{Al}(\text{HPhNPF})_3$  and  $\text{Al}(\text{HBANPF})_3$  with multiple tracked wavelengths.

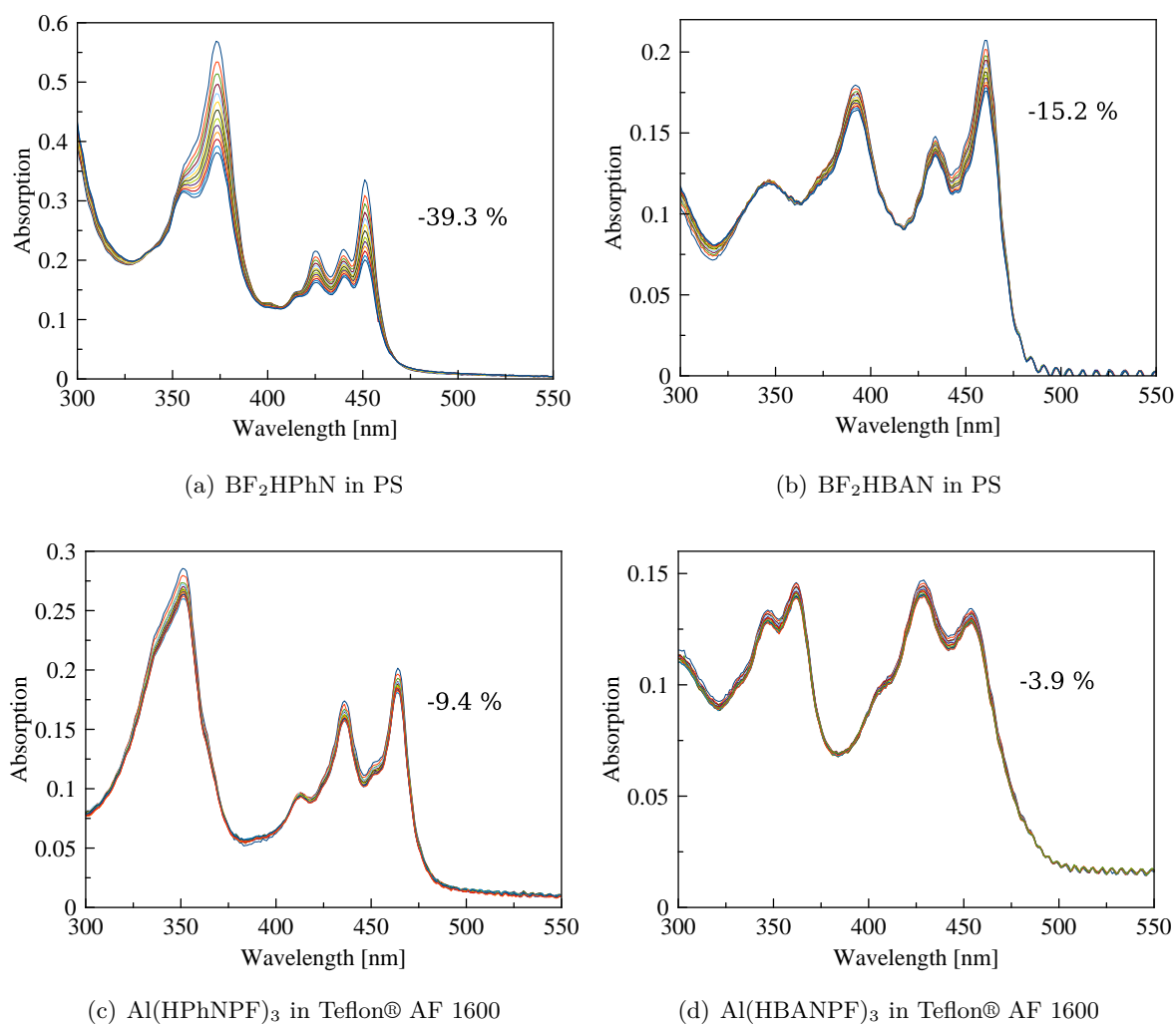


**Figure 9.17:** Absorption spectra of  $\text{BF}_2\text{HPhN}$ ,  $\text{BF}_2\text{HBAN}$ ,  $\text{Al}(\text{HPhNPF})_3$  and  $\text{Al}(\text{HBANPF})_3$  during the photobleaching experiments.

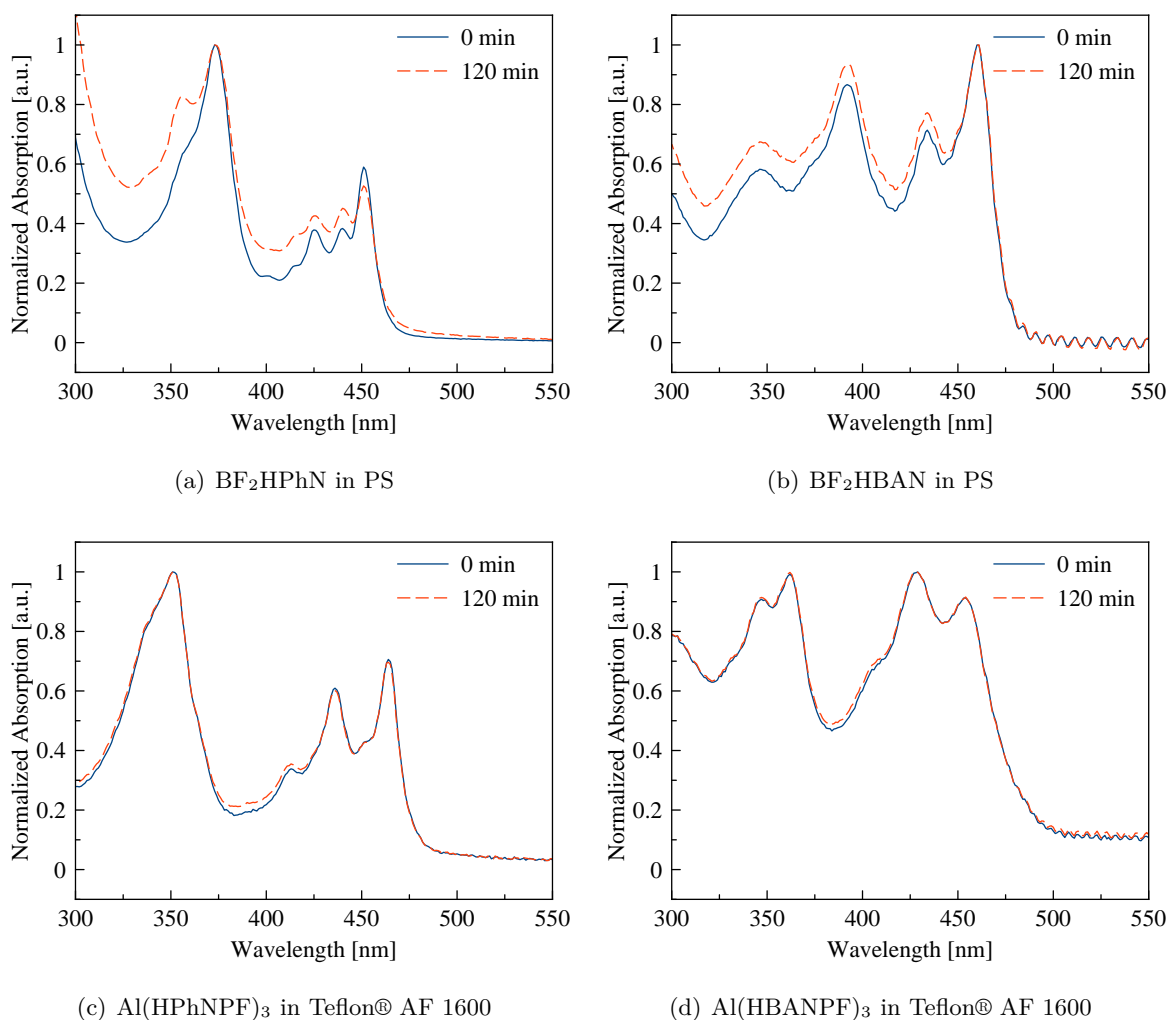


**Figure 9.18:** Normalized absorption spectra of  $\text{BF}_2\text{HPhN}$ ,  $\text{BF}_2\text{HBAN}$ ,  $\text{Al}(\text{HPhNPF})_3$  and  $\text{Al}(\text{HBANPF})_3$  before and after the bleaching experiments (120 min of illumination with a blue power LED).

## 9.5 Lifetime Measurements

**Table 9.3:** Anoxic lifetimes of the dyes at 20 °C in sodium sulfite solution.

Dye	Matrix	Lifetime [ms]							Mean
		1	2	3	4	5	6		
BF <sub>2</sub> HPhN	PS	352	350	356	352	354	362	354 ± 5	
BF <sub>2</sub> HBAN	PS	734	733	735	–	–	–	734 ± 1	
BF <sub>2</sub> HBANPF	Teflon® AF 1600	439	439	445	445	440	447	443 ± 4	
Al(HPhNPF) <sub>3</sub>	Teflon® AF 1600	244	244	244	245	–	–	244 ± 1	
Al(HPhNPF) <sub>3</sub>	Hyflon® AD 60	249	253	254	250	259	–	253 ± 4	
Al(HPhNPF) <sub>3</sub> <sup>a</sup>	Hyflon® AD 60	282	284	284	284	–	–	284 ± 1	
Al(HPhNPF) <sub>3</sub> <sup>b</sup>	Hyflon® AD 60	215	219	220	217	218	–	218 ± 2	
Al(HPhNPF) <sub>3</sub>	Cytop® CTL-809A	343	342	347	343	343	344	344 ± 2	
Al(HBANPF) <sub>3</sub>	Teflon® AF 1600	342	345	346	340	–	–	343 ± 3	
Al(HBANPF) <sub>3</sub>	Teflon® AF 2400	308	317	314	–	–	–	313 ± 5	
Al(HBANPF) <sub>3</sub>	Hyflon® AD 60	391	386	396	399	387	409	395 ± 9	
Al(HBANPF) <sub>3</sub>	Cytop® CTL-809A	463	468	470	467	471	460	467 ± 4	
Al(HBANPF) <sub>3</sub> <sup>c</sup>	Cytop® CTL-107MK	365	357	355	–	–	–	359 ± 6	

<sup>a</sup> 5 °C

<sup>b</sup> 35 °C

<sup>c</sup> Measured in N<sub>2</sub>-atmosphere (purged 1 h). Completely deoxygenated due to the strong chemical oxygen consumption.

**Table 9.4:** Anoxic lifetimes of the dyes in Teflon® AF 1600 at 20 °C in sodium sulfite solution with different excitation intensities

	Filter	$cR^a$	Messung [ms]						Mean
			1	2	3	4	5	6	
BF <sub>2</sub> HBANPF	–	5.6	428	430	440	432	430	431	432 ± 5
	50	2.5	433	433	442	–	–	–	436 ± 6
	10	0.43	452	441	447	–	–	–	447 ± 6
	5	0.19	448	446	448	–	–	–	447 ± 2
	5 + 25	0.049	429	475	454	–	–	–	453 ± 23
Al(HPhNPF) <sub>3</sub>	–	5.4	245	243	243	243	241	245	243 ± 2
	50	2.5	247	250	248	–	–	–	248 ± 2
	10	0.44	252	251	251	–	–	–	251 ± 1
	5	0.19	252	249	250	–	–	–	250 ± 2
	5 + 25	0.053	250	243	244	–	–	–	246 ± 4
Al(HBANPF) <sub>3</sub>	–	5.5	312	311	309	306	306	305	308 ± 3
	50	2.5	319	314	317	–	–	–	317 ± 3
	10	0.43	325	328	332	–	–	–	328 ± 4
	5	0.18	327	328	328	–	–	–	328 ± 1
	5 + 25	0.049	335	334	335	–	–	–	335 ± 1
Al(HPhNPF) <sub>3</sub> <sup>b</sup>	–	0.50	267	273	271	272	273	273	272 ± 3
	50	0.23	273	273	272	274	273	277	274 ± 2
	25	0.14	266	269	272	270	270	271	270 ± 3
	10	0.041	265	269	268	271	269	272	269 ± 3

<sup>a</sup> Value for intensity comparison purposes calculated from the measured  $R$ -intensity value and the actual filter transmittances.

<sup>b</sup> in Hyflon® AD 60.

**Table 9.5:** Phosphorescence Lifetimes of Al(HBANPF)<sub>3</sub> (0.05 wt% in Teflon® AF 1600) with  $\approx 1.5$  ppmv O<sub>2</sub> with multiple excitation light intensities.

Filter [%]	$cR^a$	Measurement [ms]			
		1	2	3	Mean
None	4.9	173	178	180	177 ± 4
None	1.6	151	153	151	152 ± 2
50	0.73	145	141	150	145 ± 5
25	0.43	147	144	146	146 ± 2
10	0.13	143	138	144	142 ± 4
5	0.056	147	153	138	146 ± 8

<sup>a</sup> Value for intensity comparison purposes calculated from the measured  $R$ -intensity value and the actual filter transmittances.

## 9.6 Measurement of the Luminescence Intensity Dependency on Excitation Light

**Table 9.6:** Intensities of the luminescence intensity dependency measurements.

Filter [%]	<i>cR</i> -Values		
	BF <sub>2</sub> HBANPF	Al(HPhNPF) <sub>3</sub>	Al(HBANPF) <sub>3</sub>
–	4.70	4.70	4.70
75	3.05	3.04	3.04
50	2.14	2.13	2.12
25	1.27	1.28	1.25
10	0.372	0.383	0.367
10 + 75	0.241	0.248	0.237
10 + 50	0.169	0.174	0.166
5	0.161	0.167	0.158
5 + 75	0.104	0.108	0.102
10 + 25	0.100	0.105	0.098
5 + 50	0.0732	0.0760	0.0716
5 + 25	0.0434	0.0457	0.0423
10 + 5	0.0127	0.0137	0.0124

## 9.7 Lifetime Calibration of Al(HPhNPF)<sub>3</sub> in Hyflon® AD 60

**Table 9.7:** Measured lifetimes and  $\tau_0/\tau - 1$  values of the lifetime calibration

O <sub>2</sub> [ppmv]	Measurements [ms]						Mean	$\tau_0/\tau - 1$
	1	2	3	4	5	6		
0	206	207	207	203	207	204	206 ± 2	1.23
1.015	156	159	158	158	159	156	158 ± 2	1.61
2.030	122	123	124	132	128	128	126 ± 4	2.00
3.045	107	111	111	111	112	111	111 ± 2	2.29
4.060	93	94	108	95	90	100	97 ± 7	2.62
5.075	83	90	80	81	80	79	82 ± 5	3.08